THÈSE

présentée à

L'UNIVERSITE DES SCIENCES ET TECHNIQUES DE LILLE

(U.E.R. DE PHYSIQUE FONDAMENTALE)

pour obtenir le grade de

DOCTEUR ES SCIENCES PHYSIQUES

par

Brigitte POUILLY

PERTURBATIONS, PHENOMENES RADIATIFS ET PROCESSUS COLLISIONNELS DANS LES MOLECULES DIATOMIQUES

Soutenue le 24 Juin 1983 devant la Commission d'Examen

M.	MACKE B.	Président
Mme	ROUEFF E.	Rapporteur
M.	ALEXANDER M.	Rapporteur
M.	SCHAMPS J.	Rapporteur
M.	ROBBE J.M.	Rapporteur
M.	RICHARDS W.G.	Examinateur
M.	BESWICK A.	Examinateur

A mes parents

Ce travail a été réalisé à l'Université de LILLE I dans le Laboratoire de Spectroscopie des Molécules Diatomiques, Equipe de Recherche Associée au C.N.R.S.

Son Directeur, Monsieur J. SCHAMPS, m'a initiée aux méthodes de traitement théoriques des systèmes diatomiques et m'a prodigué aide et encouragements depuis mon entrée dans le Laboratoire, qu'il trouve ici l'expression de toute ma reconnaissance.

Je tiens à exprimer mes plus vifs remerciements à Madame E. ROUEFF initiatrice de l'étude sur C_2 pour le soutien et l'intérêt qu'elle a accordés à cette étude et pour avoir accepté de rapporter sur ce travail.

L'étude de la collision MgO + N_2O a été réalisée en partie au Département de Chimie de l'Université de MARYLAND dans le Laboratoire de Monsieur M. ALEXANDER. Qu'il reçoive ici le témoignage de ma sincère reconnaissance pour l'aide et le soutien constants qu'il m'a apportés et pour m'avoir communiqué une grande part de sa passion pour la dynamique collisionnelle.

Je remercie également Monsieur le Professeur W.G. RICHARDS de l'Université d'OXFORD, Monsieur le Professeur A. BESWICK de l'Université d'ORSAY et Monsieur le Professeur B. MACKE de l'Université de LILLE I qui ont accepté de juger cette thèse.

Les résultats présentés dans ce travail sont le fruit d'une étroite collaboration avec Monsieur J.M. ROBBE qu'il trouve ici l'expression de ma profonde gratitude pour l'aide efficace et enthousiaste et pour la part active qu'il a apportées aux différentes phases de cette étude.

Enfin, je remercie vivement ceux qui ont contribué à la réalisation matérielle de ce mémoire : Mlle WALASIAK pour le soin qu'elle a apporté à la dactylographie, M. RAFFAUD pour l'illustration et Messieurs FAUQUEMBERGUE et VILAIN pour le tirage.

TABLE DES MATIERES

INTRODUCTION

Depuis quelques années s'est développée au sein du laboratoire une série de travaux théoriques sur les molécules à 8, 9 et 10 électrons de valence de la première et de la deuxième ligne de la classification périodique des éléments. Si pour toutes ces études le dialogue théorie-expérience apparaissait déjà comme fondamental dans l'interprétation des faits expérimentaux, les résultats des calculs restaient plus particulièrement destinés à la recherche de la connaissance de la structure électronique des composés mis en jeu et à l'interprétation des phénomènes de perturbations observés dans ces molécules. Profitant de l'expérience acquise par l'équipe dans ce type de calculs, nous avons dans une première étape interprété les perturbations observées dans le système $A^1\Pi$-$X^1\Sigma^+$ de la molécule BeS. Mais ne souhaitant pas limiter l'intervention de la théorie à ce domaine étroit de la Spectroscopie Moléculaire, nous avons étendu les calculs ab-initio à un aspect maintenant plus dynamique : dynamique intra-moléculaire dans le cas de la photodissociation et des processus radiatifs qui affectent les populations de l'état fondamental de la molécule C_2, dynamique inter-moléculaire dans le cas des transferts d'énergie lors de la collision de la molécule MgO avec le partenaire polaire N_2O.

Puisque les moyens d'approche des problèmes exposés dans les trois parties qui constituent ce travail reposent sur l'utilisation de calculs ab-initio, il nous a paru indiqué de consacrer le premier chapître à un bref rappel sur les techniques des calculs SCF et d'interaction de configurations conduisant à la détermination des énergies et des fonctions d'onde des états électroniques. Notons que grâce au développement d'ordinateurs puissants et à la mise au point de méthodes théoriques sophistiquées les calculs de chimie quantique ont atteint à présent un degré de précision suffisant pour que leur utilité dans l'interprétation des phénomènes de spectroscopie moderne ne soit plus contestée.

Le deuxième chapître est un exemple concret de l'importance décisive de l'interaction théorie-expérience puisque les calculs ab-initio ont fourni dans la déperturbation du système $A^1\Pi$-$X^1\Sigma^+$ de la molécule BeS les informations indispensables à l'interprétation des données expérimentales. En effet, la

localisation de l'état $a^3\Pi$ isoconfigurationnel à l'état $A^1\Pi$ et spectroscopiquement inobservé a permis de conclure que cet état était responsable des perturbations décelées dans le spectre par CHEETHAM, GISSANE et BARROW et initialement attribuées par ces auteurs à un état $^1\Delta$. Les calculs ab-initio des paramètres d'interaction diagonaux et non diagonaux (spin-orbite et orbite-rotation) et plus encore la détermination du signe relatif des éléments non diagonaux nous ont permis de mener à bien la déperturbation et de caractériser complètement l'état $a^3\Pi$ perturbateur.

La procédure de déperturbation développée dans ce chapître vient d'ailleurs d'être appliquée avec succès au système $^1\Pi$-$^1\Sigma$ de la molécule BeO

Le troisième chapître de ce travail concerne la molécule C_2. Récemment découverte dans les nuages interstellaires diffus, la molécule C_2 présente un intérêt astrophysique incontestable puisque cette molécule constitue un maillon de la chaine de réactions permettant de comprendre la formation des molécules interstellaires. Les informations expérimentales sur cette molécule sont très fragmentaires et de l'avis même des astrophysiciens, la connaissance de données théoriques est fondamentale. Nous avons déterminé dans cette étude les paramètres permettant d'atteindre les données nécessaires à l'établissement d'un bilan complet des divers mécanismes non collisonnels susceptibles d'affecter les populations de l'état fondamental $X^1\Sigma_g^+$ et qui pourrait servir à déterminer les conditions physiques dans les nuages diffus où la molécule C_2 est observée. Le problème de la transition d'intercombinaison entre l'état $X^1\Sigma_g^+$ et l'état métastable $a^3\Pi_u$ très proche de l'état fondamental est particulièrement interessant puisque cette transition est une des voies permettant d'expliquer le rapport d'intensité entre les systèmes singulets $A^1\Pi_u$-$X^1\Sigma_g^+$ et triplets $d^3\Pi_g$-$a^3\Pi_u$ observés dans les spectres des comètes.

Grâce au développement des techniques lasers qui permettent la préparation et la caractérisation des états moléculaires mis en jeu, la dynamique collisionnelle connait actuellement un grand succès. Le dernier chapître de ce travail illustre un des aspects de ce vaste domaine en faisant apparaître comment les collisions inélastiques consécutives à une réaction peuvent modifier les populations d'un des produits formés.

Dans la réaction Mg (^3P) + N_2O, la molécule MgO est formée principalement dans l'état fondamental $X^1\Sigma^+$ et les deux premiers états excités de

symétrie Π ($a^3\Pi$ et $A^1\Pi$). Les interactions non BORN-OPPENHEIMER (spin-orbite $a^3\Pi$-$X^1\Sigma^+$ et Coriolis $A^1\Pi$-$X^1\Sigma^+$) et le couplage collisionnel dipole-dipole entre le produit MgO et l'oxydant moléculaire N_2O conduisent dans MgO à des transferts entre les niveaux rovibrationnels de deux états de caractère électronique différent. Les sections efficaces correspondantes calculées dans l'approximation de Born du premier ordre montrent d'une part que les transferts inter états sont privilégiés là où les perturbations entre les états concernés sont maximales et d'autre part confirment la règle de tendance de la conservation de la parité annoncée par ALEXANDER dans les transferts collisionnels inter-états.

CHAPITRE I

GENERALITES SUR LES CALCULS SCF ET L'INTERACTION DE CONFIGURATIONS

I - ORBITALES MOLECULAIRES : APPROXIMATION LCAO-MO

L'utilisation de l'approximation de Born-Oppenheimer, c'est-à-dire la séparation des fonctions d'onde nucléaires et électroniques conduit à l'équation de SCHRÖDINGER électronique :

$$H_e \psi_e = E_e \psi_e \qquad (I.1)$$

où ψ_e est une fonction d'onde électronique, E_e l'énergie électronique correspondante.

Le but des calculs ab-initio est de résoudre l'équation I.1 pour toutes les positions possibles des N noyaux de la molécule.

Dans le cas d'une molécule diatomique isolée et si on néglige les effets relativistes, le hamiltonien H_e s'écrit :

$$H_e = - \sum_{i=1}^{n} \frac{\Delta_i}{2} - \sum_{i=1}^{n} \left(\frac{Z_A}{r_{iA}} + \frac{Z_B}{r_{iB}} \right) + \frac{1}{2} \sum_{i,j}^{n} \frac{1}{r_{ij}} + \frac{Z_A Z_B}{R} \qquad (I.2)$$

r_{iA} et r_{iB} sont les distances qui séparent chaque électron i des deux noyaux A et B de charges respectives Z_A et Z_B.

r_{ij} est la distance entre les électrons i et j, R la distance internucléaire, et n le nombre total d'électrons.

Les termes qui apparaissent dans l'équation (I.2) correspondent respectivement aux opérateurs d'énergie cinétique, l'attraction nucléaire, de répulsion électronique et de répulsion nucléaire.

En première approximation, ce hamiltonien peut être remplacé par un hamiltonien à particules indépendantes [1]. Chaque électron est soumis à un potentiel à symétrie axiale créé par les noyaux et le terme d'interaction entre électrons $\sum_{i,j} \frac{1}{r_{ij}}$ est remplacé par un effet d'écran moyen agissant sur chaque électron et dû aux autres électrons. On appelle spin-orbitales les vecteurs propres monoélectroniques définis dans cette approximation ; ces spin-orbitales sont le produit d'une orbitale $|n, |\lambda|, R>$ (notée ϕ_i) solution de l'équation de SCHRÖDINGER monoélectronique, par un vecteur propre de spin.

Les fonctions d'onde moléculaires ψ_e s'écrivent alors sous la forme de combinaisons linéaires de déterminants de SLATER antisymétriques par rapport aux permutations des électrons. Chaque déterminant est repéré par la donnée des spin-orbitales occupées des couches externes.

L'approximation LCAO-MO consiste à écrire chaque orbitale moléculaire ϕ_i sous la forme d'une combinaison linéaire d'orbitales atomiques de même symétrie :

$$\phi_i = \sum_p C_{ip} \chi_p \qquad (I.3)$$

C_{ip} est le coefficient de l'orbitale p dans l'orbitale moléculaire i.

Les orbitales atomiques que nous utiliserons sont du type orbitales de SLATER [2] centrées sur l'un ou l'autre des atomes.

$$\chi_p\ (n,\ell,m) = (2\zeta)^{n+1/2}\ \{(2n)!\}^{-1/2}\ r^{n-1}\ e^{-\zeta r}\ Y_\ell^m\ (\theta\ ,\ \varphi) \qquad (I.4)$$

II - FONCTION D'ONDE HARTREE-FOCK : CALCULS SCF

La première étape des calculs consiste à obtenir pour chaque état une fonction d'onde dans l'approximation à une seule configuration. Si on accepte cette représentation qui, à chaque état moléculaire, fait correspondre une configuration unique, on ne peut obtenir pour chaque état que l'énergie HARTREE-FOCK qui diffère de l'énergie électronique expérimentale par la somme de l'énergie relativiste et de l'énergie de corrélation entre électrons. C'est pratiquement l'énergie HARTREE-FOCK qui est calculée par la méthode SCF-LCAO-MO.

La méthode du champ auto-cohérent (SCF) adaptée par ROOTHAAN [3,4] aux calculs d'énergie moléculaire repose sur l'utilisation du principe variationnel basé sur le fait que l'énergie E_e calculée pour chaque fonction d'onde normalisée ψ_e :

$$E_e = \int \psi_e^* H \psi_e \, d\tau \qquad (I.5)$$

est une limite supérieure de l'énergie vraie.

Dans l'approximation LCAO-MO, la méthode SCF consiste à faire varier les coefficients C_{ip} de manière à minimiser cette énergie.

III - CALCULS D'INTERACTION DE CONFIGURATIONS (CI)

Dans l'approximation HARTREE-FOCK, nous l'avons déjà indiqué, chaque électron est soumis au potentiel moyen créé par les (n-1) électrons restants ; en d'autres termes, cette approximation néglige les répulsions instantanées entre les électrons dont la contribution à l'énergie totale représente l'énergie de corrélation. Bien qu'elle ne soit qu'un faible pourcentage de l'énergie totale, l'énergie de corrélation est généralement du même ordre de grandeur que les énergies d'excitation électroniques et est souvent plus importante que les quantités d'énergie nécessaires à la rupture de liaisons chimiques ; elle représente donc une grandeur de première importance.

La méthode la plus courante pour tenir compte de l'énergie de corrélation est un calcul d'interaction de configurations (CI). La fonction d'onde moléculaire est alors représentée par une somme de fonctions multiparticules Φ_i, appelées "configuration state functions" (CSF), qui sont toutes fonctions propres de l'opérateur S^2

$$\psi_e = \sum_i C_i \Phi_i \qquad (I.6)$$

où les coefficients C_i sont déterminés par diagonalisation de la matrice énergie dans la base des fonctions ϕ_i. Si toutes les excitations sont permises le nombre de CSF's devient très vite important (5.10^8 pour un système à 10 e^-) et on se trouve devant l'impossibilité de résoudre exactement le problème. Il a donc fallu trouver des méthodes pour contourner cette difficulté d'ordre technique. Un certain nombre de recettes différentes d'interaction de confirations ont été proposées au cours des dix dernières années, toutes respectant les mêmes principes essentiels :

- premier principe : La base d'orbitales atomiques doit être au moins du type double ou triple-zéta et posséder des fonctions de polari-

sation qui permettent la déformation des orbitales atomiques de base

- deuxième principe : On définit un espace de référence de dimension n réduite ($10 \sim 100$ maximum) consistant en un choix particulier des CSF's

- troisième principe : On augmente la taille de la matrice CI, en ajoutant des configurations obtenues par excitation d'un ou plusieurs électrons dans les fonctions monoélectroniques non occupées dans l'espace de référence. Ainsi par exemple, si on limite aux doubles substitutions on obtient de 10^4 à 10^6 CSF's.

Il est important dès lors de préciser la nomenclature couramment admise pour caractériser les différents types d'excitation qui apparaissent dans les calculs CI et que nous retrouverons dans les chapîtres III et IV de ce travail.

Cette nomenclature est basée sur une partition des orbitales moléculaires en :

a) orbitales de coeur dont l'énergie d'excitation serait trop importante pour qu'elles jouent un rôle dans les transitions que l'on considère ;

b) orbitales de valence qui correspondent aux électrons participant effectivement aux transitions ;

c) orbitales virtuelles, non occupées dans les plus bas états électroniques de la molécule, mais qui donnent naissance à des configurations dont le rôle est capital à grande distance internucléaire et pour rendre compte des états plus excités.

- Dans les calculs d'interaction de configurations "Full Valence" (FVCI) sont inclus tous les CSF's construits en distribuant les électrons de valence dans les différentes orbitales de valence obtenues pour chaque état par un calcul SCF préalable. En général 50 à 200 CSF's sont générés à ce stade. Les plus importants d'entre eux servent à construire l'espace de référence indiqué plus haut.

- Un calcul FVCI peut être suivi d'un calcul d'interaction de configuration du premier ordre (First Order CI) dans lequel l'espace des configurations "Full Valence" est étendu par l'adjonction de configurations obtenues en permettant l'excitation d'un électron de valence dans une orbitale virtuelle en parallèle avec un éventuel réarrangement des électrons de valence restants dans les spin-orbitales de valence avec toutefois la restriction que chaque CSF ainsi construit ne doit différer du ou des CSF's de référence que par deux électrons au maximum (10^4 à 10^5 CSF's à ce stade). L'étape ultime consiste à considérer les CSF's obtenus par excitation de deux électrons (SDCI = single-double CI) dans l'espace des orbitales virtuelles ce qui amène couramment la taille de la matrice CI à environ 10^6 éléments.

Quelles sont les méthodes qui permettent de traiter de telles matrices, étant entendu qu'une diagonalisation complète reste impossible ?

La plus utilisée est une méthode de perturbation permettant de déterminer la contribution à l'énergie totale de chaque configuration et d'éliminer les configurations les moins importantes (procédure SHAVITT [5], GERSHGORN et SHAVITT [6]).

Une autre méthode développée essentiellement par PEYERIMHOFF et BUENKER [7] consiste en une diagonalisation d'un grand nombre de matrices de petite taille caractéristiques de différents types d'excitation suivie de la reconstruction d'une matrice CI de plus petite dimension.

Le désavantage de ces deux méthodes est qu'en chaque point de la surface de potentiel on sélectionne un nombre différent de configurations ; la contribution des configurations ignorées peut être importante et varie en chaque point. Parmi d'autres BUENKER et PEYERIMHOFF [8] ont proposé une procédure d'extrapolation basée sur la théorie de perturbation du premier ordre pour tenter de tenir compte de ces configurations ignorées, mais cette procédure qui mélange un calcul exact et un calcul de perturbations peut conduire à une énergie qui ne sera pas une limite supérieure de l'énergie vraie.

Sans prétendre établir un catalogue des méthodes CI, on peut signaler aussi la méthode CIPSI développéepar le groupe de MALRIEU à Toulouse et celui de LEVY à Montrouge. Cette méthode est basée sur une partition des CSF's en trois classes :

- les générateurs ($10 \sim 100$) qui représentent l'espace de référence
- la classe moyenne (10^3) qui est traitée variationnellement
- tous les autres (10^5) sont traités par théorie de perturbation au 2° ordre

Nous avons choisi pour nos calculs d'interaction de configurations la méthode de la "matrice creuse" (NEM Nearly empty matrix) développée par RASEEV.[9] La première étape consiste à sélectionner par un calcul FVCI les configurations importantes pour décrire correctement la courbe de potentiel d'un état donné à grande et à courte distance ; toutes ces configurations forment l'espace de référence.

Les excitations de type FOCI par rapport à tous les CSF's de l'espace de référence conduisent souvent à un nombre important de configurations. La méthode NEM consiste à réduire l'espace des configurations en diagonalisant la matrice construite sur les termes diagonaux et sur les éléments non diagonaux correspondant aux CSF's de l'espace de référence. Seules les configurations dont la contribution à l'énergie est supérieure à un certain seuil ($\simeq 10^{-4}$ Hartree) sont conservées ; enfin, on diagonalise la matrice totale reconstruite sur ces configurations.

Cette méthode qui permet de travailler avec un nombre restreint de configurations (de l'ordre de 300) a l'avantage de ne pas mélanger des techniques exactes et des approximations par théorie de perturbations. Elle permet des suivis sans discontinuité sur les surfaces de potentiel. Les résultats présentés dans la suite de ce travail peuvent apparaître comme justification de la fiabilité de cette technique.

IV - PARAMETRES D'INTERACTION

Nous verrons dans les chapîtres II et IV, qu'il existe dans les molécules BeS et MgO des perturbations entre les niveaux vibrationnels des états $^3\Pi$ et $^1\Sigma^+$ d'une part et $^1\Pi$ et $^1\Sigma^+$ d'autre part. Ces perturbations sont dues à des interactions de type spin-orbite et électronique-rotation (Coriolis) respectivement. Les paramètres de perturbation correspondants peuvent être calculés dès que l'on connait les fonctions d'onde des états concernés.

a - Perturbation d'origine spin-orbite

Dans le cadre de l'approximation de BORN-OPPENHEIMER, nous avons

négligé les effets relativistes c'est-à-dire les interactions dues au spin. Tant que l'énergie d'interaction spin-axe moléculaire est grande vis-à-vis des différences d'énergie entre niveaux de rotation, on peut calculer l'énergie d'interaction spin-orbite par perturbation dans la base des fonctions du cas a) de HUND.

A partir de l'équation relativiste de DIRAC, on peut déduire l'expression du hamiltonien spin-orbite :

$$H_{SO} = \frac{\alpha^2}{2} \sum_{i=1}^{n} \left(\frac{Z_A}{r_{iA}^3} \vec{l_{iA}} \cdot \vec{s_i} + \frac{Z_B}{r_{iB}^3} \vec{l_{iB}} \cdot \vec{s_i} \right) - \frac{\alpha^2}{2} \sum_{i \neq j}^{n} \frac{(\vec{r_{ij}} \wedge \vec{p_i})(\vec{s_i} + 2\vec{s_j})}{r_{ij}^3} \qquad (I.7)$$

(où α est la constante de structure fine).

Le premier terme de ce hamiltonien est un opérateur monoélectronique, (spin-orbite direct) alors que le second est un opérateur biélectronique (spin-autre orbite) qui a pour effet de contrebalancer le champ dû aux noyaux et qui est la plupart du temps introduit dans le premier terme. En effet, si on néglige les interactions spin-autre orbite entre électrons impairs, le reste de l'interaction spin-autre orbite est proportionnel à $\vec{l_i} \cdot \vec{s_i}$ [10]. On peut alors écrire ce hamiltonien sous la forme d'une somme d'opérateurs monoélectroniques [11] :

$$H_{SO} \simeq \frac{\alpha^2}{2} \sum_i \left(\frac{Z_{A\,eff}}{r_{iA}^3} \vec{l_{iA}} \cdot \vec{s_{iA}} + \frac{Z_{B\,eff}}{r_{iB}^3} \vec{l_{iB}} \cdot \vec{s_{iB}} \right) \qquad (I.8)$$

En repérant les électrons par rapport au centre de masse de la molécule, on peut écrire H_{SO} sous la forme simplifiée :

$$H_{SO} \simeq \sum_i a_i \vec{l_i} \cdot \vec{s_i} \qquad (I.9)$$

En développant les produits scalaires $\vec{l_i} \cdot \vec{s_i}$ on obtient finalement :

$$H_{SO} \simeq \sum_i a_i \left(l_{zi} s_{zi} + \frac{1}{2} l_i^+ s_i^- + \frac{1}{2} l_i^- s_i^+ \right) \qquad (I.10)$$

Ainsi il apparaît clairement que l'opérateur spin-orbite est la cause des perturbations homogènes ($\Delta\Omega = 0$ selon la classification de HOUGEN [12]) et qu'il peut avoir des éléments de matrice non diagonaux différents de zéro entre :

deux états tels que $\Delta\Lambda = \Delta\Sigma = 0$ et $\Delta S = 0, \pm 1$;
ou deux états tels que $\Delta\Lambda = -\Delta\Sigma = \pm 1$ et $\Delta S = 0, \pm 1$;

b - Perturbations dues au Hamiltonien de rotation

Le hamiltonien de rotation s'écrit simplement sous la forme :

$$H_{rot} = |\vec{R}|^2 \, B \qquad (I.11)$$

où $\vec{R}$ est le moment cinétique de rotation des noyaux en unité $\hbar$ et B est la constante de rotation

$$B = \frac{\hbar^2}{2\mu R^2} \quad \text{avec} \quad \mu = \frac{M_A M_B}{M_A + M_B} \text{ , masse réduite de la molécule.}$$

Si $\vec{L}$ est le moment cinétique orbital et $\vec{S}$ le moment de spin des électrons, $\vec{J}$ le moment cinétique total de la molécule, alors $\vec{R} = \vec{J} - \vec{L} - \vec{S}$

H_{rot} se transforme en $H_{rot} = B(J^2 - J_z^2) + B(L^2 - L_z^2) + B(S^2 - S_z^2)$

$$+ B(L^+S^- + L^-S^+) - B(J^+L^- + J^-L^+) - B(J^+S^- + J^-S^+) \qquad (I.12)$$

Les perturbations causées par le hamiltonien de rotation sont dues aux trois termes faisant intervenir les opérateurs échelles $J^{\pm}$, $L^{\pm}$, $S^{\pm}$.

Le terme $B(L^+S^- + L^-S^+)$ produit des perturbations qu'il est parfois difficile de distinguer des perturbations spin-orbite qu'elles accompagnent. Elles obéissent à la règle $\Delta\Omega = 0$ avec $\Delta S = 0$, $\Delta\Sigma = -\Delta\Lambda = \pm 1$.

Les termes $B(J^+L^- + J^-L^+)$ et $B(J^+S^- + J^-S^+)$ donnent lieu à des perturbations hétérogènes ($\Delta\Omega = \pm 1$ selon HOUGEN [12]) mais seul le premier terme joue un rôle dans les perturbations des molécules étudiées dans le cadre de ce travail. Il est responsable du découplage du moment orbital avec la rotation et l'intensité des perturbations qu'il induit est proportionnelle à $\sqrt{J(J+1)}$ et au facteur vibrationnel $\langle v \mid \frac{1}{2\mu R^2} \mid v' \rangle = B_{vv'}$.

Les règles de sélection supplémentaires sont $\Delta S = 0$, $\Delta\Sigma = 0$, $\Delta\Lambda = \pm 1$.

V - MOYENS DE CALCULS

Tous les calculs de fonctions d'onde ont été effectués au CIRCE (ORSAY) à l'aide du programme ALCHEMY écrit par BAGUS, LIU, Mc LEAN et YOSHIMINE [13].

Nous nous sommes servis d'un programme écrit par HALL [14] pour calculer au CITI (LILLE) les paramètres de perturbation. Ce programme permet de calculer les éléments de matrice des opérateurs entre deux déterminants de SLATER batis à partir des orbitales moléculaires LCAO-MO.

REFERENCES

1 - F. HUND et R.S. MULLIKEN, *Phys. Rev.* **32**, *186 (1928)*

2 - J.S. SLATER, *Quantum Theory of Atomic Structure*, Mc GRAW-HILL, *New-York (1960)*

3 - C.C.J. ROOTHAAN, *Rev. Mod. Phys.* **23**, *69 (1951)*

4 - C.C.J. ROOTHAAN, *Phys. Rev.* **32**, *179 (1960)*

5 - I. SHAVITT, "*Energy Structure and Reactivity*", *D.W. SMITH et W.B. Mc RAE (Wiley, New-York) (1973) p. 188*

6 - Z. GERSHGORN et I. SHAVITT, *Intern. J. Quant. Chem.* **2**, *751 (1968)*

7 - S.D. PEYERIMHOFF et R.J. BUENKER, *Chem. Phys. Lett.* **16**, *235 (1972)*

8 - R.J. BUENKER et S.D. PEYERIMHOFF, *Theor. Chim. Act.* **35**, *33 (1974)*

9 - G. RASEEV, *Chem. Phys. Lett.* **47**, *36 (1977)*

10 - M. BLUME et R.E. WATSON, *Proc. Roy. Soc. A* **270**, *127 (1962)*

11 - H. LEFEBVRE-BRION et N. BESSIS, *Canad. J. Phys.* **47**, *2727 (1969)*

12 - J.T. HOUGEN, *Monograph 115, National Bureau of Standards, Washington (1970)*

13 - P.S. BAGUS, B. LIU, A.D. Mc LEAN et M. YOSHIMINE, *Alchemy, I.B.M. Research Lab. San-José, CA 95114 (1972)*

14 - J.A. HALL, J. SCHAMPS J.M. ROBBE et H. LEFEBVRE-BRION, *J. Chem. Phys.* **59**, *3271 (1973)*

CHAPITRE II

SYSTEME $A^1\Pi$-$X^1\Sigma^+$

DE LA MOLECULE BeS

INTRODUCTION

Peu d'études expérimentales ont été consacrées aux molécules diatomiques du groupe IIA/VIB, qui mettent en jeu l'atome de BERYLLIUM, en raison de la toxicité de ce produit. En particulier la molécule BeS n'a été étudiée expérimentalement à notre connaissance que par CHEETHAM, GISSANE et BARROW. L'étude spectroscopique faite par ces auteurs du système $A^1\Pi$-$X^1\Sigma^+$ a révélé la présence de perturbations attribuées par CHEETHAM et coll. à un état $^1\Delta$. Cette attribution a longtemps fait penser que la structure électronique de BeS était plus proche des molécules des groupes IIIB/VB ou IVB/IVB que de celle de molécules du groupe IIA/VIB telles que MgO.

Nos calculs ab-initio présentés dans ce travail ont montré que l'état $A^1\Pi$ ne pouvait en aucun cas être perturbé par un état $^1\Delta$ mais que les perturbations observées étaient dues à l'état $a^3\Pi$ de même configuration que l'état $A^1\Pi$. La détermination ab-initio des fonctions d'ondes, des paramètres d'interaction non diagonaux (spin-orbite entre les états $a^3\Pi$ et $X^1\Sigma^+$ et Coriolis entre les états $A^1\Pi$-$X^1\Sigma^+$) et de leurs phases relatives et enfin de la constante spin-orbite de l'état $a^3\Pi$ ont été une aide essentielle dans la déperturbation du système $A^1\Pi$-$X^1\Sigma^+$. De plus, une nouvelle méthode basée sur la très grande sensibilité des intégrales de recouvrement à une très faible variation de la distance d'équilibre de l'état perturbant $a^3\Pi$ a permis de déterminer précisement ce paramètre et de connaitre par voie de conséquence la numérotation vibrationnelle de l'état $a^3\Pi$.

PERTURBATIONS DANS LE SYSTEME $A^1\Pi$-$X^1\Sigma^+$ DE LA MOLECULE BeS : L'ETAT $a^3\Pi_i$

JOURNAL OF MOLECULAR SPECTROSCOPY 96, 1–55 (1982)

Perturbations in the $A^1\Pi$–$X^1\Sigma^+$ System of the BeS Molecule. The $a^3\Pi_i$ State

B. POUILLY, J. M. ROBBE, AND J. SCHAMPS

Laboratoire de Spectroscopie des Molécules Diatomiques. ERA 303, Université des Sciences et Techniques de Lille, Bât. P5, 59655 Villeneuve D'Ascq, France

AND

R. W. FIELD AND L. YOUNG[1]

Department of Chemistry, Massachusetts Institute of Technology, Cambridge, Massachusetts 02139

The states responsible for all perturbations observed by Cheetham *et al.* [*Trans. Faraday Soc.* **61**, 1308–1316 (1965)] in the BeS $A^1\Pi$–$X^1\Sigma^+$ system were electronically ($a^3\Pi_2$, $a^3\Pi_1$, and $X^1\Sigma^+$) and vibrationally assigned. Cheetham *et al.* had incorrectly *suggested* that perturbations presently assigned as $A^1\Pi(v_A) \sim a^3\Pi_2(v_a = v_A + 2)$ were $A^1\Pi \sim {}^1\Delta$. Molecular constants for the newly identified $a^3\Pi_i$ state, which is the lowest energy excited state of BeS, as well as electronic parameters for $A \sim X$, $A \sim a$, and $a \sim X$ interactions were determined. Principal constants (in cm^{-1}) for $A^1\Pi$ and $a^3\Pi$ are

	$a^3\Pi$	$A^1\Pi$
T_e	7 100 (75)	7 961.64 (26)
ω_e	737 (5)	762.13 (7)
$\omega_e x_e$	4.1 (2)	4.09 (4)
r_e (Å)	1.9190 (10)	1.9087 (2)

(1σ uncertainties in parentheses). A coherent picture of the perturbations in $A^1\Pi$ could be drawn *only* by combining fragmentary spectroscopic data from Cheetham *et al.* with new *ab initio* calculations of spin–orbit and rotation–electronic perturbation parameters, spin–orbit splittings, and energy separations of isoconfigurational $a^3\Pi$ and $A^1\Pi$ states.

I. INTRODUCTION

The perturbations in the $A^1\Pi$ state of BeS molecule are interesting for two reasons. First, although one would expect the electronic structure of BeS to resemble more closely that of BeO and MgO or other group IIA/VIA diatomics, the tentative assignment of a perturber of $A^1\Pi$ as a low-lying $6\sigma^2 2\pi^2 7\sigma^2\ {}^1\Delta$ state (*1*) made BeS seem more closely related to the IVA/IVA family. This surprising result was "confirmed" by a relatively primitive theoretical study (*2*). Second, information in the spectrum (*1*) from which the perturbing states might be characterized is simultaneously extensive and fragmentary. It seems as if the assigned and reported lines (*1*, *3*) of the BeS $A^1\Pi$–$X^1\Sigma^+$ system were fiendishly selected to permit a definitive

[1] Present address: Department of Chemistry, University of Chicago, Chicago, Illinois 60637.

0022-2852/82/110001-55$02.00/0

characterization of the perturber, provided every scrap of information is used optimally. We have been forced to devise new deperturbation schemes, based on semi-empirical relationships between matrix elements, and to supplement the spectral data with *ab initio* computed perturbation parameters, spin–orbit splittings, and energy separations between $a^3\Pi$ and $A^1\Pi$ states. Some of the *ab initio* results have been independently confirmed by deperturbation of the $A^1\Pi$–$X^1\Sigma^+$ spectrum; the rest probably could be confirmed if the deperturbation procedure were refined further. The important point is that theory provides guidance to experiment by vastly reducing the number of hypotheses which must be tested, by determining relative signs of perturbation parameters, by restricting the reasonable range of least-squares variation for certain spectroscopic and perturbation parameters, and by assigning fixed values to some otherwise undeterminable parameters.

The eight-valence-electron diatomic molecules appear to divide into three groups which display disparate electronic structural properties (*4*). The alkali halides have no significantly bound low-lying valence states, apart from the ground state. The alkaline earth oxides and sulfides have several known or predicted $^1\Sigma^+$, $^3\Sigma^+$ [MgO (*5*), CaO (*6*), BaO (*7*), BaS (*8*)], $^1\Pi$, and $^3\Pi_i$ [MgO (*9*), CaO and SrO (*10*), BaO (*11*), and BaS (*8*)] excited electronic states below 2 eV. The most important feature of the alkaline earth oxides and sulfides is small isoconfigurational $^1\Pi$–$^3\Pi$ and $^1\Sigma$–$^3\Sigma$ energy separations and a $^1\Sigma^+$ ground state. The third group consists of the IIA/VA diatomics, about which little is known experimentally and the IVA/IVA molecules which characteristically have a very low-lying $^3\Pi$ state with a very large isoconfigurational $^1\Pi$–$^3\Pi$ separation and low-lying $^1\Delta$, $^3\Sigma^-$, and $^1\Sigma^+$ states belonging to a $\sigma^2\pi^2\sigma^{*2}$ configuration.

Our interest in BeS was originally stimulated by Brewer (*12*), who, on the basis of experimental (*1*) and theoretical papers (*2*), argued that BeS much more closely resembles the III/V and IV/IV molecules than BeO or MgO. If this is true, then our understanding of the valence electronic structure for II/VI molecules (*10*) is on a rather fragile foundation. In particular, the suggestion of a $6\sigma^2 2\pi^2 7\sigma^2$ $^1\Delta$ perturbation of $A^1\Pi$ (*1*, *2*) led to predictions of a still lower-lying isoconfigurational $^3\Sigma^-$ state analogous to the C_2 $b^3\Sigma_g^-$ state (*4*). This is surprising in light of *ab initio* calculations for BeO (*13*) and MgO (*5*, *14*, *15*), which show the corresponding configuration to be high lying and, at best, weakly bound. It is important to note that Cheetham *et al.* (*1*) did not definitively reject the possibility that the putative $^1\Delta$ perturbations could be due to a component of a $^3\Pi$ state.

Ab initio calculations on BeS have been performed and are discussed in Section II. One result is that the lowest $^1\Delta$ state of BeS lies at such high energy that one can conclude with certainty that the $A^1\Pi$ state is *not* perturbed by a $^1\Delta$ state. The *only* computed low-lying state other than $X^1\Sigma^+$ that could perturb $A^1\Pi v = 5$–11 is the isoconfigurational $a^3\Pi_i$ state. The fact that the J dependence of the matrix element for an intermediate Hund's case '$\mathbf{a} - \mathbf{b}'$ $^3\Pi_2 \sim {}^1\Pi$ perturbation is similar to that for $^1\Delta \sim {}^1\Pi$ explains why Cheetham *et al.* (*1*) made their incorrect suggestion of a $^1\Delta$ assignment.

In Section III we show that all local perturbations of BeS $A^1\Pi$ may be accounted for by mutual interaction between

$A^1\Pi(v_A)$,
$a^3\Pi_2(v_{a2} = v_A + 2)$,
$a^3\Pi_1(v_{a1} = v_A + 2)$,
$a^3\Pi_0(v_{a0} = v_A + 2)$,
$X^1\Sigma^+(v_X = v_A + 7)$

levels. All rotational assignments, the identification of the $X^1\Sigma^+$ perturbations, and the tentative vibrational numbering of the $A^1\Pi$ state from the original experimental study (*1*, *3*) are verified.

The primary purpose of this paper is to characterize the lowest energy excited state of BeS, the $a^3\Pi$ state. Two major tactical problems had to be overcome.

First, the potential energy curves for $a^3\Pi$ and $A^1\Pi$ are nearly identical and the best documented perturbations involve rather high vibrational levels of both states (v_A = 8–11, v_a = 10–13). This means that equilibrium constants for $a^3\Pi$ may be obtained only from dangerously long extrapolations and that calculated $\Delta v \neq 0$ vibrational overlaps between perturbing $a^3\Pi$ and $A^1\Pi$ levels will be extremely sensitive to small changes in these constants. Second, the perturbations provide fragmentary information about $a^3\Pi$.[2] In no band does $A^1\Pi$ cross two spin components of $a^3\Pi$, thus the spin–orbit splitting for $a^3\Pi$ cannot be directly sampled. After *ab initio* calculations predicted that the potential curves for $a^3\Pi$ and $A^1\Pi$ are nearly identical and that $r_e(a^3\Pi)$ is slightly larger than $r_e(A^1\Pi)$, we felt justified in adopting the following model for the G_v and B_v functions of $a^3\Pi$ as solution to the first tactical problem. The $a^3\Pi$ potential was assumed to fit the Morse form and $\omega_e x_e$ was assumed to have the same value as that for $A^1\Pi$. Then ω_e for $a^3\Pi$ was determined from observed vibrational intervals. The final degree of freedom for a Morse potential, r_e, was systematically varied to satisfy internal consistency checks described in Section III. Thus the derived equilibrium constants for $a^3\Pi$ are considerably less certain than our model-dependent standard errors indicate.

The second tactical problem required that *ab initio* computed constants, particularly the $a^3\Pi$ spin–orbit splitting, be used as initial trial values in the deperturbation analysis and that semiempirical matrix element relationships (confirmed by *ab initio* calculations) be exploited as parameter constraints or consistency checks. The most important of these, that the $a^3\Pi$ spin–orbit constant and the electronic part of the isoconfigurational $a^3\Pi \sim A^1\Pi$ spin–orbit perturbation matrix element be equal in magnitude, was the basis for a new method of determining the absolute vibrational numbering of a high-v perturber (Section IIID). The hybrid *ab initio*-experimental deperturbation procedure developed here is considerably more powerful than that used previously for 8 (*9*, *10*) and 10 (*16*, *17*) valence electron molecules.

II. DETAILS OF *AB INITIO* COMPUTATIONS

Only one theoretical study of the electronic structure of the BeS molecule has been reported (*2*). Verhaegen and Richards (*2*) computed self-consistent-field (SCF)

[2] This is not to imply that the perturbation data are incomplete. In view of the fact that some beryllium compounds have dangerous toxic properties, Cheetham *et al.* (*1*) did indeed attempt to obtain the maximum of spectroscopic information from the minimum number of experiments.

energies of the lowest-lying electronic states in order to determine whether the ground state has $^1\Sigma^+$ symmetry. Their work includes no configuration interaction (CI) and relies on semiempirical estimates of correlation energy. For the purpose of understanding the BeS $A^1\Pi$ perturbations, the calculations of Ref. (*2*) are neither sufficiently accurate nor complete; thus new *ab initio* calculations were performed.

The ALCHEMY program (*18*) was used to compute SCF with limited CI wavefunctions. At an early stage, a set of exploratory SCF calculations was performed at a single internuclear separation r = 3.8 Bohrs (2.01 Å), which is slightly larger than typical BeS equilibrium separations [$r_e(X^1\Sigma^+)$ = 1.7415 Å. $r_e(A^1\Pi)$ = 1.9087 Å]. Nine states, belonging to six configurations, were taken into account in these SCF calculations:

$$(1\text{–}5)\sigma^2 1\pi^4 2\pi^4 6\sigma^2 \qquad {}^1\Sigma^+, \tag{1.1}$$

$$(1\text{–}5)\sigma^2 1\pi^4 2\pi^3 6\sigma^2 7\sigma \qquad {}^3\Pi, {}^1\Pi, \tag{1.2}$$

$$(1\text{–}5)\sigma^2 1\pi^4 2\pi^4 6\sigma 7\sigma \qquad {}^3\Sigma^+, {}^1\Sigma^+, \tag{1.3}$$

$$(1\text{–}5)\sigma^2 1\pi^4 2\pi^3 6\sigma^2 \quad 3\pi \qquad {}^3\Delta, {}^1\Delta, \tag{1.4}$$

$$(1\text{–}5)\sigma^2 1\pi^4 2\pi^2 6\sigma^2 7\sigma^2 \qquad {}^1\Delta, \tag{1.5}$$

$$(1\text{–}5)\sigma^2 1\pi^4 2\pi^3 6\sigma^2 \quad 1\delta \qquad {}^3\Pi. \tag{1.6}$$

SCF energies are listed in parentheses in Table II. From these preliminary *ab initio* calculations, it was apparent that the unknown perturber of $A^1\Pi$ is quite likely to be (1.2) $a^3\Pi$. The configuration (1.5) $^1\Delta$ perturber hypothesis suggested by Cheetham *et al.* (*1*) and apparently confirmed by Verhaegen and Richards (*2*) is incorrect. This $^1\Delta$ state lies at much too high energy to perturb $A^1\Pi$. In fact the configuration (1.5) $^1\Delta$ lies above the (1.4) $^1\Delta$ state. The Rydberg states, among which (1.6) $^3\Pi$ is found, lie still higher. The only remaining low-lying state that could account for the perturbations in $A^1\Pi$ is therefore the configuration (1.2) $a^3\Pi_i$ state.

According to these statements, only states belonging to configurations (1.1), (1.2), and (1.3) were retained for further calculations. In the next step, SCF calculations were carried out for the five states of these configurations at eight internuclear separations (Table II), regularly spaced from 3.0 to 4.4 Bohrs, always using the same orbital basis set. The molecular orbitals were built from the atomic Be basis optimized by Huo *et al.* (*19*) for their BeO calculations and the *S* basis of Cade and Huo (*20*). The resultant basis set (listed in Table I) included 20 σ-type and 9 π-type orbitals. Flexibility of the π-orbital representation, which is most important for calculation of spin–orbit parameters, was ensured by the multi-zeta character of the basis. No further optimization of ζ values was judged necessary.

Figure 1 shows the internuclear distance variation of BeS atomic populations for the valence orbitals (6σ, 7σ, 2π) separately optimized for three electronic states, $^1\Sigma^+$, $^3\Pi$, and $^3\Sigma^+$, representative, respectively, of configurations (1.1), (1.2), and (1.3). The 2π orbital is always well-localized on the $S(3p)$ atomic orbital. At small and medium internuclear distance, 7σ is practically identical to Be($2s$). However, at largest distances, significant $S(3p)$ character appears in 7σ. The opposite behavior is observed for 6σ, for which the $S(3p)$ localization at small distance evolves into

THE $a^3\Pi_i$ STATE OF BeS

TABLE I

STO Basis Set for SCF Calculations of BeS

Atomic symmetry		zeta	
Be		σ	π
	1s	3.43700	
	1s	6.22500	
	2s	0.66082	
	2s	1.01187	
	3s	1.776 00	
	2p	0.90000	0.90000
	2p	1.80000	1.80000
	3d	1.50000	1.50000
S	1s	18.01116	
	2s	5.30794	
	2s	15.83751	
	3s	1.62232	
	3s	2.59027	
	3s	9.40187	
	2p	4.81311	4.82431
	2p	7.83720	7.84493
	2p	13.57266	13.58306
	3p	1.31017	1.29270
	3p	2.30113	2.31802
	3d	2.14199	2.15151

an $S(3p)$–Be$(2s)$ mixture at larger distance, especially for the closed-shell $X^1\Sigma^+$ ground state. These features will prove important later in understanding the values of computed perturbation parameters.

Wavefunctions were improved beyond the SCF level by limited CI within the orbital spaces for the lowest states of each symmetry. Every configuration which could be built by allowing one or two excitations out of or into the valence orbitals of the SCF reference states was included in the CI. The numbers of resultant configurations were 169 for $^1\Sigma^+$, 187 for $^3\Pi$, 143 for $^1\Pi$, and 98 for $^3\Sigma^+$.[3] CI calculations (at r = 3.8 Bohrs) were also carried out for 1.4 $^3\Delta$ and $^1\Delta$ to ensure that these relatively low-lying states could not be strongly lowered by configuration interaction. Table II lists CI energies and predominant configurational parentage for the lowest-lying electronic states. Potential energy curves (at the CI level) are shown in Fig. 2. The computed principal molecular constants are reported and compared with corresponding experimental values from Ref. (*1*) and this work in Table III.

The effect of CI is very small for the $a^3\Pi$, $A^1\Pi$, $^3\Sigma^+$(I), $^3\Delta$(I), and $^1\Delta$(I) states. Even the $X^1\Sigma^+$ state is of more than 85% configuration (1.1) character near r_e. CI

[3] Possibly significant omissions from the list of configurations accessible to the CI are those involving an $S(3d)$ 1δ orbital. $2\pi^3 6\sigma^2 1\delta$ gives rise to $^3\Pi$ and $^1\Pi$ states.

TABLE II

CI Energies (SCF in Parentheses) for the Lowest States of BeS (Energy Units: Hartrees)

State	main configuration	R = 3.0	R = 3.2	R = 3.4	R = 3.6	R = 3.8	R = 4.0	R = 4.2	R = 4.4
				(R a.u)					
$X\,^1\Sigma^+$	(1.1) $(2\pi^4\ 6\sigma^2)$	- 412.16949	- 412.18669	- 412.19055	- 412.18631	- 412.17748	- 412.16635	- 412.15444	- 412.14272
		(- 412.13046)	(- 412.14211)	(- 412.13953)	(- 412.12844)	(- 412.11295)	(- 412.09603)	(- 412.07976)	(- 412.06531)
$a\,^3\Pi$	(1.2) $(2\pi^3\ 6\sigma^2 7\sigma)$	- 412.12603	- 412.15694	- 412.17253	- 412.17814	- 412.17737	- 412.17267	- 412.16572	- 412.15768
		(- 412.10567)	(- 412.13619)	(- 412.15104)	(- 412.15564)	(- 412.15363)	(- 412.14744)	(- 412.13871)	(- 412.12851)
$A\,^1\Pi$	(1.2) $(2\pi^3\ 6\pi^2 7\sigma)$	- 412.11912	- 412.15072	- 412.16667	- 412.17233	- 412.17131	- 412.16605	- 412.15820	- 412.14886
		(- 412.09895)	(- 412.13043)	(- 412.14601)	(- 412.15144)	(- 412.14948)	(- 412.14350)	(- 412.13485)	(- 412.12464)
$^3\Sigma^+$	(1.3) $(2\pi^4\ 6\sigma\ 7\sigma)$	- 412.08073	- 412.10385	- 412.11400	- 412.11573	- 412.11208		- 412.09616	- 412.08614
		(- 412.05019)	(- 412.07373)	(- 412.08436)	(- 412.08672)	(- 412.08388)		(- 412.07002)	(- 412.06120)
$B\,^1\Sigma^+$	(1.3) $(2\pi^4\ 6\sigma\ 7\sigma)$	- 412.05944	- 412.07803	- 412.08287	- 412.07913	- 412.07051	- 412.05958	- 412.04814	- 412.03789
		(- 412.04681)	(- 412.07050)	(- 412.08108)	(- 412.08320)	(- 412.07997)	(- 412.07344)	(- 412.06496)	(- 412.05544)

Energies of the (1.4)$(2\pi^3\ 6\sigma^2\ 3\pi)$ $^3\Delta$ and $^1\Delta$ states calculated at R = 3.8 Bohrs : $^1\Delta$ - 412.02341 (- 412.01380) $^3\Delta$ - 412.03245 (- 412.02284)

Energy of the (1.5) $(2\pi^2\ 6\sigma^2\ 7\sigma^2)$ $^1\Delta$ state calculated at R = 3.8 Bohrs : (-411.96402)

Energy of the (1.6) $(2\pi^3\ 6\sigma^2\ 1\delta^1)$ $^3\Pi$ state calculated at R = 3.8 Bohrs : (-411.88711)

1 Hartree = 219474.55 cm^{-1}

1 Bohr = 0.52918 Å

THE $a^3\Pi_i$ STATE OF BeS

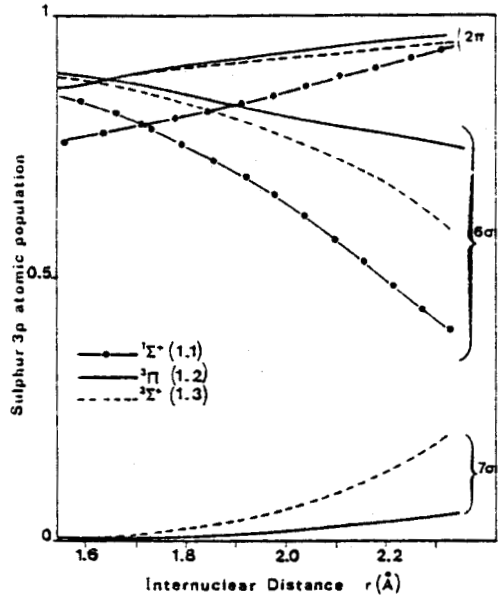

FIG. 1. Sulphur $3p$ atomic population in the SCF valence orbitals for the $2\pi^4 6\sigma^2\ ^1\Sigma^+$ (●), $2\pi^4 6\sigma 7\sigma^3\Sigma^+$ (- - -), and $2\pi^3 6\sigma^2 7\sigma^3\Pi$ (——) electronic states of BeS as function of internuclear separation.

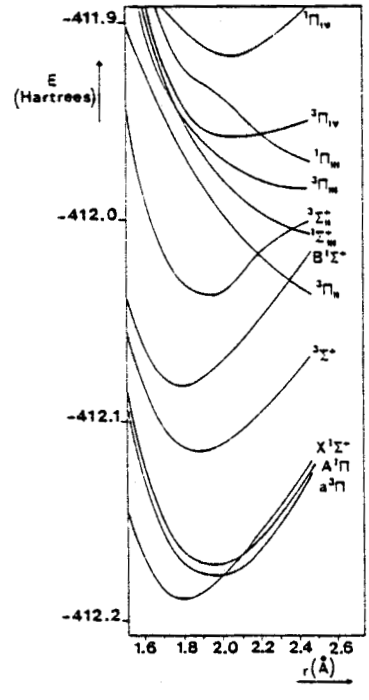

FIG. 2. CI potential energy curves for the lowest-lying electronic states of BeS.

TABLE III

Calculated and Experimental Spectroscopic Constants of BeS (Energy Units: cm^{-1})

	T_e		ω_e		$\omega_e x_e$		B_e	
	CI	exp	CI	exp	CI	exp	CI	exp
$X^1\Sigma^+$	0	0	891	897.94 (a)	7.7	6.137 (a)	0.749	0.79059 (a)
$a^3\Pi$	2650	7100 (b)	723	737 (b)	8.7	4.1 (b)	0.637	0.6511 (b)
$A^1\Pi$	3940	7961.7 (b)	747	762.13 (b)	7.5	4.09 (b)	0.639	0.6581 (b)
$^3\Sigma^+$	16390		760		13.3		0.680	
$B^1\Sigma^+$	23640	25941.6	900	851.3	8.2	4.85	0.742	0.72894
$^3\Delta$	31990	33050 (b)						

a Cheetham et al. (1).
b This work (Section 3).

appears to be very important in the $B^1\Sigma^+$ state; its configuration (1.3) character is predominant at short internuclear separation, decreases to 70% at r_e, and becomes decreasingly important at large r as configuration (1.4) character becomes dominant. It is interesting to compare this behavior to that found in the isoelectronic MgO molecule. In MgO, the $B^1\Sigma^+$ state is strongly affected by CI (*5*, *15*), but the mixing is essentially between configurations (1.3) and (1.1) rather than (1.3) and (1.4) as for BeS. Consequently, CI is important for the MgO $X^1\Sigma^+$ ground state, again contrary to the BeS situation.

Apart from the above conclusion that the unknown perturber is (1.2) $a^3\Pi$, three types of information concerning the perturbations of BeS $A^1\Pi$ may be derived from the *ab initio* calculations: (i) $A^1\Pi$–$a^3\Pi$ energy separation; (ii) properties of the $a^3\Pi$ state; (iii) electronic perturbation matrix elements.

(i) The *ab initio* potential curves for the $A^1\Pi$ and $a^3\Pi$ states are parallel and their energy separation at r_e is 1300 cm^{-1}. Comparable calculations for MgO (*15*) show that computed energy separations between isoconfigurational (relatively free of configuration mixing) states should be reasonably accurate ($\pm$1000 cm^{-1}). This computed separation corresponds to approximately two vibrational quanta ($\sim$700 cm^{-1}) and suggests that the vibrational level of $a^3\Pi$ interacting with a given $A^1\Pi$ level should be $v_a = (v_A + 2) \pm 1$.

(ii) The *ab initio* calculations show that the triply-occupied $a^3\Pi$ 2π orbital is localized on $S(3p)$. This means that the $a^3\Pi$ spin–orbit splitting is governed by the relatively strong sulfur spin–orbit effect rather than the negligibly small beryllium one. An *ab initio* calculation of $A(a^3\Pi)$ gave -170 cm^{-1}. Alternatively, a semiempirical upper bound is given by (*21*)

$$|A(a^3\Pi)| < \frac{1}{2}\zeta_S(3p) = 187.5 \text{ cm}^{-1}.$$

Although this is not a rigorous bound (*17*), it is reasonable to ignore the Be^+-centered

contribution and to assume because $\zeta_S\text{-}(3p) < \zeta_S(3p)$, that the S^--centered contribution is smaller than $\zeta_S(3p)$.

(iii) Perturbation parameters are the final class of *ab initio* generated information. The three most important perturbation parameters are the ones relating to mutual perturbations between the states directly involved in the deperturbation matrix, namely, $X^1\Sigma^+$, $a^3\Pi$, and $A^1\Pi$. The first, **a**, governs the $a^3\Pi_0 \sim X^1\Sigma^+$ spin–orbit interaction and is defined as the matrix element of the one-electron part of the spin–orbit Hamiltonian

$$H^{so} = \sum_i \underline{\mathbf{a}}_i \mathbf{l}_i \cdot \mathbf{s}_i , \tag{2}$$

$$\mathbf{a}(a \sim X) = (2)^{1/2} \langle a^3\Pi_0 | \sum_i (\underline{\mathbf{a}}_i \mathbf{l}_i \cdot \mathbf{s}_i) | X^1\Sigma^+ \rangle. \tag{3}$$

which, in the SCF limit, reduces to

$$|\mathbf{a}(a \sim X)| = |\langle 2\pi | \underline{\mathbf{a}} l^+ | 7\sigma \rangle|.$$

The second, **b**, arises from the $A^1\Pi \sim X^1\Sigma^+$ rotation–electronic interaction and is defined

$$\mathbf{b}(A \sim X) = (2)^{-1/2}[2J(J+1)]^{-1/2} \langle A^1\Pi | (-L^+J^- - L^-J^+) | X^1\Sigma^+ \rangle. \tag{4}$$

In the SCF limit, this definition reduces to

$$|b(A \sim X)| = |\langle 2\pi | l^+ | 7\sigma \rangle|.$$

The third perturbation parameter, $A(^3\Pi \sim {}^1\Pi)$ controls the $a^3\Pi_1 \sim A^1\Pi$ spin–orbit interaction. It is defined as

$$A(a \sim A) = \langle a^3\Pi_1 | \sum_i (\underline{\mathbf{a}}_i \mathbf{l}_i \cdot \mathbf{s}_i) | A^1\Pi \rangle \tag{5}$$

and, in the single-configuration, identical-orbitals-for-isoconfigurational-states limit, it can be shown that (*22*)

$$|A(^3\Pi \sim {}^1\Pi)| = |A(^3\Pi)|. \tag{6}$$

This equality is the basis for a novel strategy employed in Section IIID to determine the absolute vibrational numbering and r_e for the $a^3\Pi$ state.

The *ab initio* wavefunctions also allowed calculation of four secondary electronic perturbation parameters relevant to interactions of the three states in the matrix with the moderately distant (1.3) $b^3\Sigma^+$ and $B^1\Sigma^+$ states.[4] These effects will be included in the deperturbation matrix by means of Van Vleck transformations. The corresponding parameters are

[4] The fifth parameter, $a(A \sim b)$, connecting the $A^1\Pi$ and $b^3\Sigma^+$ states, will not be considered. In contrast to the four other parameters, which are essential because they cause asymetric shifts of *e/f* levels and/or spin–orbit components, this fifth parameter gives rise to a small shift (less than 10 cm^{-1}) which cannot be experimentally separated from the electronic energy of the $A^1\Pi$ state and to a Λ doubling contribution in $A^1\Pi$ which does not appear before the fourth-order and is estimated to contribute much less than 1% in the value of q.

$$\mathbf{a}(a \sim B) = -2\langle a^3\Pi_0|\sum_i \underline{\mathbf{a}}_i\mathbf{l}_i \cdot \mathbf{s}_i|B^1\Sigma^+\rangle,$$

$$\mathbf{a}(a \sim b) = 2\langle a^3\Pi_0|\sum_i \underline{\mathbf{a}}_i\mathbf{l}_i \cdot \mathbf{s}_i|b^3\Sigma_0^+\rangle,$$

$$\mathbf{b}(A \sim B) = -[2J(J+1)]^{-1/2}\langle A^1\Pi|(-L^+J^- - L^-J^+)|B^1\Sigma^+\rangle,$$

$$\mathbf{b}(a \sim b) = [2J(J+1)]^{-1/2}\langle a^3\Pi_1|(-L^+J^- - L^-J^+)|b^3\Sigma_0^+\rangle.$$

In the SCF limits these parameters reduce to

$$|\mathbf{a}(a \sim B)| \simeq |\mathbf{a}(a \sim b)| = |\langle 2\pi|\underline{\mathbf{a}}l^+|6\sigma\rangle|,$$

$$|\mathbf{b}(A \sim B)| \simeq |\mathbf{b}(a \sim b)| = |\langle 2\pi|l^+|6\sigma\rangle|.$$

The **a** and **b** parameters were computed using the SCF and CI wavefunctions. Their internuclear distance dependence is illustrated by Figs. 3 and 4. The shapes of the $\mathbf{a}(r)$ and $\mathbf{b}(r)$ curves are related to the atomic populations of the interacting orbitals. The increase of the $X^1\Sigma^+ \sim a^3\Pi_0$ spin–orbit interaction (Fig. 3) reflects the increase in $S(3p)$ character in the 7σ orbital which enables this orbital to interact more strongly via H^{so} with the $S(3p)$ localized 2π orbital. The increase in the $X^1\Sigma^+ \sim A^1\Pi$ interaction shown in Fig. 4 has a similar explanation. In contrast with

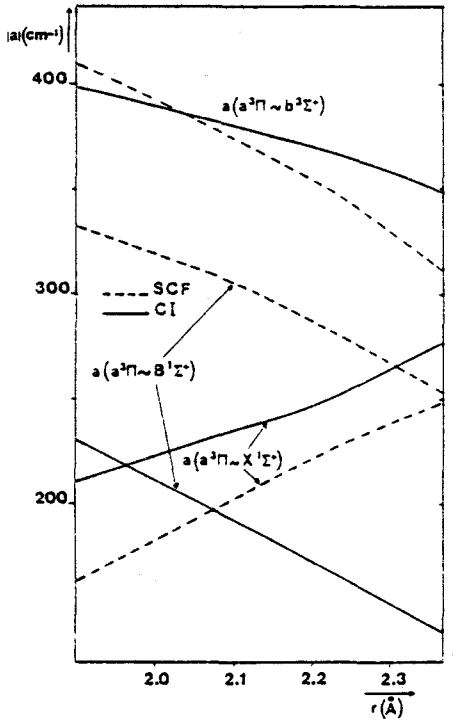

FIG. 3. Internuclear distance dependence of *ab initio* values for the spin–orbit perturbation parameters $a(a \sim X)$, $a(a \sim B)$, $a(a \sim b)$.

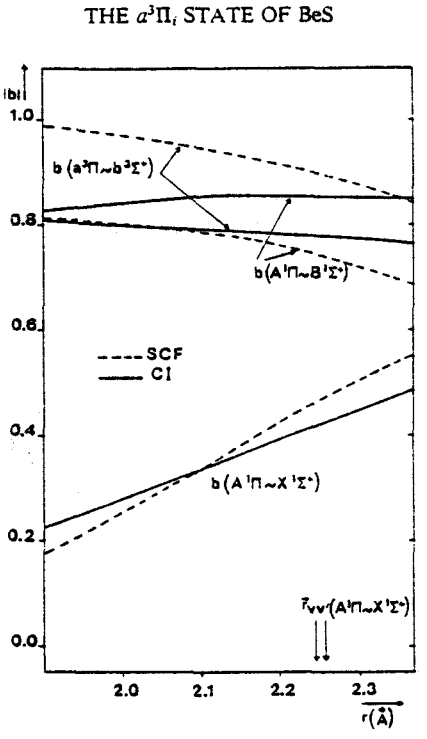

FIG. 4. Internuclear distance dependence of *ab initio* values for the rotation–electronic perturbation parameters $b(A \sim X)$, $b(A \sim B)$, $b(a \sim b)$.

these increasing $2\pi \sim 7\sigma$ interactions, the opposite behavior is observed for the $B^1\Sigma^+ \sim a^3\Pi_0$ and $B^1\Sigma^+ \sim A^1\Pi$ interactions owing to the progressive decrease in $S(3p)$ character in the 6σ orbital.

III. DEPERTURBATION OF $A^1\Pi$

This deperturbation analysis is based on line measurements by Cheetham *et al.* (*1*, *3*) for seven $A^1\Pi$–$X^1\Sigma^+$ vibrational bands: 5–0, 6–0, 7–0, 8–1, 9–1, 10–2, and 11–2. No new spectra were recorded.

In order to form a coherent account of all perturbations in $A^1\Pi$ which Cheetham *et al.* did not attribute to $X^1\Sigma^+$, the following three qualitative questions had to be answered:

1. Are the perturbers $^1\Delta$ and one other state, are they $^3\Pi$, or are they some other exotic possibility?
2. Assuming that the perturber is $^3\Pi$, is it regular or inverted?
3. Although no vibrational level of $A^1\Pi$ is crossed by two Ω components of the perturber within the range of observed rotational levels, several levels, particularly $v_A = 10$ and 11, are affected by two components. Do these two components belong to the same vibrational level of $a^3\Pi$ or to the highest and lowest Ω components of two consecutive levels?

Questions 1 and 2 can be definitively answered by the *ab initio* calculations. Questions 2 and 3 can be definitively and independently answered, while the answer to question 1 is strongly suggested, by experimental data.

Once the qualitative questions are answered, four important quantitative questions must be dealt with:

4. What is the vibrational numbering of the $a^3\Pi$ perturber relative to the $A^1\Pi$ level it perturbs?
5. What is $A(a^3\Pi)$?
6. What is $r_e(a^3\Pi)$?
7. What is the absolute vibrational numbering of $A^1\Pi$?

Experimental data answer questions 6 and 7 definitively and 5 suggestively. *Ab initio* results answer questions 5 to ± 20 cm^{-1} and 4 to ± 1 vibrational quantum. A hybrid *ab initio*-experimental approach answers questions 4, 5, and 6 most convincingly.

A. Qualitative Questions

The locations and pattern of perturbations of the BeS $A^1\Pi$ state are shown in Fig. 5. Perturbations denoted by □ are trivially assigned to a $^1\Sigma^+$ state, because only

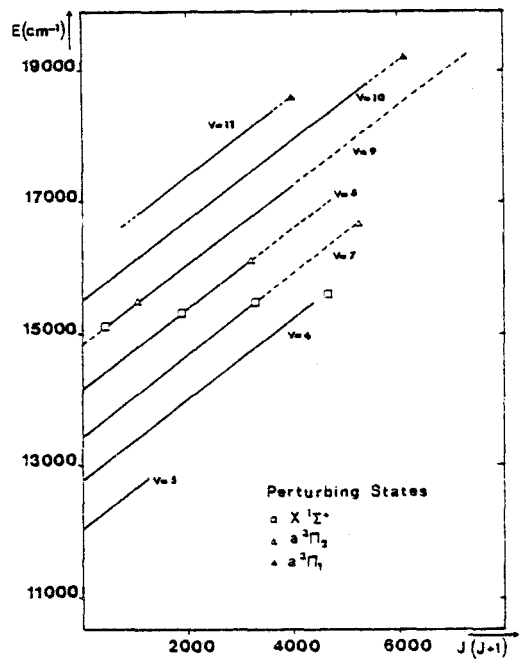

FIG. 5. Locations of perturbations in the BeS $A^1\Pi$ state (v = 5 through 11). The $^1\Pi_e$ and $^1\Pi_f$ Λ components are not resolvable on the energy scale of this figure. Rotational levels are shown by solid and dotted lines, respectively, for those regions of J values for which R or P *and* Q or *only* Q lines are observed. J values where crossings occur by $a^3\Pi_2$ (△), $a^3\Pi_1$ (▲), and $X^1\Sigma^+$ (□) are labeled.

$A^1\Pi$ levels of e symmetry (*23*) are affected.[5] These $^1\Sigma^+$ perturbers must be high vibrational levels of $X^1\Sigma^+$.

The remaining perturbations fall into two groups, denoted by Δ and $\blacktriangle$. In general, the Δ perturbations are weaker than the $\blacktriangle$ ones, even though the latter type of crossing always occurs beyond the highest rotational level sampled. Both e and f levels of $A^1\Pi$ are perturbed, but the maximum level shifts are not exactly equal nor at precisely the same J. The perturbers must have $0 < \Lambda < 2$. On the basis of computational modeling, the different perturbed J values and perturbation strengths at the e/f crossings reflect Λ doubling in $A^1\Pi$ *and* in the perturber and simultaneous admixture of a nearby $X^1\Sigma^+$ vibrational level into both $A^1\Pi$ and the perturber.

The only experimental evidence in favor of the $^3\Pi$ vs the $^1\Delta$ perturber assignment is that the former provides the simplest quantitative account of all details for both Δ and $\blacktriangle$ perturbations. Although the least-squares fitting procedure provides numerous intricate consistency checks of the $^3\Pi$ assignment,[6] the simplest and most convincing is observation of similar magnitudes for the $A^1\Pi \sim a^3\Pi$ perturbation matrix element, A_{11}, determined primarily by the Δ perturbation (nominally $^3\Pi_2$) in $v_A = 7$–9 vs those by the $\blacktriangle$ perturbations (nominally $^3\Pi_1$) in $v_A = 10$ and 11. Since the strength of the $^1\Pi \sim {}^3\Pi$ perturbation is determined by the fractional $^3\Pi_1$ character in the perturber, and there is far less of this in the nominal $^3\Pi_2$ than $^3\Pi_1$ level, the actual interaction strengths are much larger in $\blacktriangle$ than Δ perturbations, in marked constrast to the A_{11} values.

The above argument presupposes answers to questions 2, 3, and 5 and illustrates the value of having such answers from *ab initio* calculations so that one can know how to begin to use the available experimental information. Without a reasonably accurate estimate for the $a^3\Pi$ spin–orbit splitting, no obvious strategy for characterizing the perturber suggests itself. Too many interlocking hypotheses must be examined.

If one assumes that both Δ and $\blacktriangle$ perturbers of a given v_A level belong to the same vibrational level of a $^3\Pi$ state, then this state must be inverted. If $^3\Pi$ were regular, there would be two[7] possibilities:

(a) $\Delta = {}^3\Pi_0$, $\blacktriangle = {}^3\Pi_1$,
(b) $\Delta = 3\Pi_1$, $\blacktriangle = {}^3\Pi_2$.

Hypothesis (a) is impossible because the Λ doubling and $X^1\Sigma^+$ character of the Δ perturber is too small. Hypothesis (b) is ruled out because the Δ perturbations would have to be stronger than the $\blacktriangle$ ones. If $^3\Pi$ is assumed to be inverted, then there are two more possibilities:

[5] These levels are known to have e rather than f symmetry because, in a $^1\Pi$–$^1\Sigma^+$ electronic transition, the $^1\Pi$ levels which participate in R- and P-branch transitions have e symmetry and those which participate in Q branch have f symmetry. Only the upper levels of R- and P-branch $A^1\Pi$–$X^1\Sigma^+$ transitions are shifted at the $\square$ perturbations.

[6] These include: constant electronic factors in A_{11} from the $v_A = 7$–9 vs 10, 11 groups of perturbations, smooth variation of the $^3\Pi$ multiplet (as opposed to single Ω component) origin between these two groups, larger $^1\Sigma^+$ character, and Λ doubling in nominal $^3\Pi_1$ than in $^3\Pi_2$.

[7] There are only two possibilities because the perturber has a smaller B value than the perturbed $A^1\Pi$ level. Thus $A^1\Pi$ overtakes from below and, in the $^3\Pi_i$ hypothesis, crosses $\Omega = 0$, 1, and 2 in that order.

(c) $\Delta = {}^3\Pi_2$, $\blacktriangle = {}^3\Pi_1$,
(d) $\Delta = {}^3\Pi_1$, $\blacktriangle = {}^3\Pi_0$.

Hypothesis (d) is ruled out for the same reason as (b).

Only hypothesis (c) survives. However, we must now test two additional possibilities:

(e) regular ${}^3\Pi$; $\Delta = {}^3\Pi_2(v_a)$, $\blacktriangle = {}^3\Pi_0(v_a + 1)$.
(f) inverted ${}^3\Pi$; $\Delta = {}^3\Pi_0(v_a)$, $\blacktriangle = {}^3\Pi_2(v_a + 1)$.

Both of these require such a large value of $A({}^3\Pi)$ that spin-uncoupling is not sufficient to mix in enough ${}^3\Pi_1$ character to cause the higher-J perturbation to be significantly stronger. In addition, contrary to observations, the higher-J perturber will have a significantly smaller B value. Hypothesis (f) can also be ruled out for the same reason as (a).

Once hypothesis (c) is adopted, it then becomes possible to make quantitative use of the fragmentary perturbation information.

B. Effective Hamiltonian and Fitting Procedure

For each vibrational level of $A^1\Pi v_A = 5$–11 an effective Hamiltonian matrix is set up including one vibrational level each of $A^1\Pi$, $X^1\Sigma^+$, and $a^3\Pi$ (all three Ω components). The v_X and v_a levels included are those which are closest to $A^1\Pi v_A$.

The effective molecular Hamiltonian matrix is presented as Table IV. It is composed of a completely diagonal vibronic part, H^{ev} [for which the eigenvalues are given as $T_v({}^1\Sigma^+)$, $T_v({}^1\Pi)$, and $T_v({}^3\Pi_1)$], a rotational part including centrifugal distortion (*24*),

$$H^R = B(r)(\underline{J} - \underline{L} - \underline{S})^2 \tag{7}$$

and a spin–orbit part, H^{so} [Eq. (2)]. Small and indeterminate effects such as spin–rotation and centrifugal distortions of $A({}^3\Pi)$ are ignored. Contributions to Λ doubling in $A^1\Pi$, *which are not the result of local* perturbations, are included via

$$2pJ(J + 1)$$

on diagonal for ${}^1\Pi^e$ (*22*).

Three main perturbation matrix elements are explicitly included in the matrix: A^+_{01}, A_{11}, and β^+_{10} (*25*). These are products of a vibrational factor [an overlap integral, $S_{vv'}$, or a matrix element of the rotational "constant" $B(r)$ operator, $B_{vv'}$], which is calculable if the potential curves of the interacting states are known, and an electronic factor, **a** or **b**, for which *ab initio* values were presented in Section II. Thus

$$A^+_{01}(a^3\Pi \sim X^1\Sigma^+) = -(2)^{-1}\mathbf{a}(a \sim X)S_{v_a v_X} , \tag{8.1}$$

$$A_{11}(a^3\Pi \sim A^1\Pi) = -A(a \sim A)S_{v_a v_A} , \tag{8.2}$$

$$\beta^+_{10}(A^1\Pi \sim X^1\Sigma^+) = -(2)^{1/2}\mathbf{b}(A \sim X)B_{v_A v_X} . \tag{8.3}$$

Numerous perturbations of the $a^3\Pi$ state also have been taken into account in the matrix. Although the associated perturbation parameters cannot be determined by the fit since they occur only as minor perturbations of the perturber, they slightly

TABLE IV

Hamiltonian Matrix Used in the $A^1\Pi$ State Deperturbations (v = 5 to 11)[a]

	$X^1\Sigma_0^+$ (v+7)	$A^1\Pi_1$ (v)	$a^3\Pi_0$ (v+2)	$a^3\Pi_1$ (v+2)	$a^3\Pi_2$ (v+2)
$X^1\Sigma_0^+$(v+7)	$(T_v(^1\Sigma^+)+B(^1\Sigma^+)\,x^b - D(^1\Sigma^+)\,x^2\,)\,\epsilon$	$-(2x)^{1/2}\beta_{10}^+\,\epsilon$	$(2)^{1/2}\,A_{01}^+\,\epsilon$	0	0
$A^1\Pi_1$(v)		$T_v(^1\Pi)+B(^1\Pi)\,[x-1] - D(^1\Pi)\,[x^2-2x+1] + \epsilon q x$	0	$-A_{11}$	0
$a^3\Pi_0$(v+2)			$T_v(^3\Pi_1)-A(^3\Pi)+B(^3\Pi)\,[x+1] - D(^3\Pi)\,[x^2+4x+1] + B_0^+\,x + 2(1-\epsilon)A_0^+ + 2\epsilon A_{\Sigma}{}^3\Pi$	$(2x)^{1/2}\{B(^3\Pi)+(1-\epsilon)q - 2D(^3\Pi)\,[x+1] + (3-4\epsilon)\,B_1^+\}$	$[2D(^3\Pi)+(1-2\epsilon)B_0^+][x(x-2)]^{1/2}$
$a^3\Pi_1$(v+2)				$T_v(^3\Pi_1)+B(^3\Pi)\,[x+1] - D(^3\Pi)\,[x^2+6x-3] + 2(1-\epsilon)\,B_0^+x + A_0^+ + A_{\Pi}{}^3\Pi$	$(B(^3\Pi)-2D(^3\Pi)\,[(x-1)+B_1^+]\,[2(x-2)]^{1/2}$
$a^3\Pi_2$(v+2)					$T_v(^3\Pi_1)+A(^3\Pi)+B(^3\Pi)\,[x-3] - D(^3\Pi)\,[x^2-4+5] + B_0^+\,(x-2)$

a ϵ=1 for e levels ; ϵ=0 for f levels.

b $x = J(J+1)$

TABLE V

Perturbation Parameters Included in the $a^3\Pi$ Hamiltonian Matrix

$$A_0^+ = p(b^3\Sigma^+) + q(b^3\Sigma^+) + o(b^3\Sigma^+) = \sum_{b^3\Sigma^+, v_b} \frac{|\langle a^3\Pi_0, v_a | \sum_i a_i \vec{\ell}_i \vec{s}_i + B(L^+S^- + L^-S^+) | b^3\Sigma_0^+, v_b \rangle|^2}{E(a^3\Pi_0, v_a) - E(b^3\Sigma_0^+, v_b)}$$

$$B_0^+ = (2)^{-1} q(b^3\Sigma^+) = [2J(J+1)]^{-1} \sum_{b^3\Sigma^+, v_b} \frac{|\langle a^3\Pi_1, v_a | - B(L^+J^- + L^-J^+) | b^3\Sigma_0^+, v_b \rangle|^2}{E(a^3\Pi_1, v_a) - E(b^3\Sigma_0^+, v_b)}$$

$$B_1^+ = (2)^{-1} q(b^3\Sigma^+) + (4)^{-1} p(b^3\Sigma^+) = [2J(J+1)]^{-1/2} \sum_{b^3\Sigma^+, v_a} \frac{\langle a^3\Pi_1, v_a | -B(L^+J^- + L^-J^+) | b^3\Sigma_0^+, v_b \rangle \langle a^3\Pi_0, v_a | \sum_i a_i \vec{\ell}_i \vec{s}_i + B(L^+S^- + L^-S^+) | b^3\Sigma_0^+, v_b \rangle}{E(a^3\Pi, v_a) - E(b^3\Sigma^+, v_b)}$$

$$+ \frac{\langle a^3\Pi_1, v_a | \sum_i a_i \vec{\ell}_i \vec{s}_i + B(L^+S^- + L^-S^+) | b^3\Sigma_1^+, v_b \rangle \langle a^3\Pi_0, v_a | -B(L^+J^- + L^-J^+) | b^3\Sigma_1^+, v_b \rangle}{E(a^3\Pi, v_a) - E(b^3\Sigma^+, v_b)}$$

$$A_{\Sigma}{}^3\Pi = (2)^{-1} o(^1\Sigma^+) = (2)^{-1} \sum_{\substack{n^1\Sigma^+, v_n \\ (n, v_n \neq X, v_a + 5)}} \frac{|\langle a^3\Pi_0, v_a | \sum_i a_i \vec{\ell}_i \vec{s}_i | n^1\Sigma^+, v_n \rangle|^2}{E(a^3\Pi_0, v_a) - E(n^1\Sigma^+, v_n)}$$

$$A_{\Pi}{}^3\Pi = \sum_{A^1\Pi, v_A \neq v_a - 2} \frac{|\langle a^3\Pi_1, v_a | \sum_i a_i \vec{\ell}_i \vec{s}_i | A^1\Pi, v_A \rangle|^2}{E(a^3\Pi_1, v_a) - E(A^1\Pi, v_A)}$$

affect the values of the determinable parameters. Therefore we felt it necessary to include them for the rigor of the model. These perturbations were introduced into the effective Hamiltonian matrix via Van Vleck transformations. The resulting parameters, A_0^+, B_0^+, B_1^+, $A_{\Sigma^3\Pi}$, and $A_{\Pi^3\Pi}$ defined in Table V, were not varied in the fit; they were fixed at their *ab initio* values.

Lastly, the diagonal spin–spin interaction in $a^3\Pi_0$, characterized by Hebb's α parameter (*26*), has been calculated from the *ab-initio* wavefunction and found to be negligible ($\alpha = 0.002\ \text{cm}^{-1}$).

A point that deserves special emphasis is the fact that the results of the fits depend on the relative phases of the six off-diagonal matrix elements appearing in the deperturbation matrix. This is usually called an "interference" effect. If we assume, without loss of generality, that all matrix elements can be taken simultaneously as real, two different though equally acceptable solutions exist depending on the combination of signs imposed (there are 32 equivalent combinations corresponding to one solution and 32 others that correspond to the other solution). It is therefore necessary to have some a priori means of determining a correct combination of signs. In some favorable cases, especially when interaction elements are large, for instance in cases of near pure precession, semiempirical estimates may be sufficient. In the present problem of BeS, the sign of β_{10}^+ cannot be decided using such simple arguments: in a localized orbital model, the 7σ orbital would be purely Be($2s$) and β_{10}^+ would be exactly zero; it is the small $S(3p)$ contribution in 7σ which makes β_{10}^+ nonzero and only *ab initio* calculations are able to reveal the sign of this contribution and therefore that of β_{10}^+. For instance, with the conventions adopted here,[8] all three parameters β_{10}^+, A_{01}^+, and A_{11} are calculated to be negative from *ab initio* wavefunctions and were therefore constrained to remain negative in the fits.

Given a set of initial parameters, the matrix is diagonalized once for each J of e and again for each J of f symmetry. Differences between eigenvalues are compared against observed transitions and corrections to the initial parameters are computed (*27*, *28*). This procedure is iterated until convergence is obtained.

The molecular constants thus obtained for the BeS $A^1\Pi$ state are given in Table VI. These constants differ slightly from those of Cheetham *et al.* (*1*) only because they are deperturbed with respect to the effects of the nearest perturbers and because we define

$$T_v(A^1\Pi) = \nu_{v'v''} + B_{v'}\,, \tag{9}$$

where $\nu_{v'v''}$ is the band origin of Ref. (*1*).

[8] Phase choices of electronic wavefunctions must be clearly defined when off-diagonal elements are involved. We use Freed's RAM phase choices throughout (see especially Eqs. (5.2) and (5.3) of Ref. (*26*)). Electronic wavefunctions are assumed to be defined in terms of Slater determinants. In these determinants, each molecular orbital is assumed to be expanded as a linear combination of conventional Slater-type orbitals in which the only phase-dependent factor is $e^{i\lambda\phi}$. All core orbitals and also the 7σ and 2π orbitals are well localized on their respective atoms [7σ on beryllium ($2s$), and 2π on sulphur ($3p$)]. Their phases will be defined by ascribing a + sign to the main LCAO (real) coefficient. For the 6σ orbital which is sometimes (in $X^1\Sigma^+$ especially) more bonding than the other orbitals in the r-centroid region, we arbitrarily ascribe a + sign to the $S(3p\sigma)$ coefficients. Moreover, the standard order of the valence orbitals in the Slater determinants is chosen to be 2π, 6σ, 7σ, and 3π; for spin-different or projection-different orbitals we use the standard order $n\sigma$, $n\bar{\sigma}$ for σ orbitals and $n\pi^+$, $n\bar{\pi}^+$, $n\pi^-$, $n\bar{\pi}^-$ for ones. There is no supplementary phase factor for each Slater determinant.

TABLE VI

Molecular Constants of the Vibrational Levels of the $A^1\Pi$ State of BeS (Units: cm^{-1})[a]

v	T_v (b)	B_v	D_v 10^6	q 10^4 (c)
5	11 532.249 (5)	0.626455 (11)	1.93 (d)	- 1.06 (5)
6	12 245.341 (4)	0.620762 (16)	1.924 (2)	- 1.22 (3)
7	12 950.197 (6)	0.615048 (6)	1.916 (2)	- 1.02 (2)
8	13 646.796 (7)	0.609445 (8)	1.916 (2)	- 1.38 (2)
9	14 335.304 (14)	0.603759 (5)	1.890 (1)	- 0.92 (2)
10	15 015.639 (60)	0.598241 (6)	1.881 (2)	- 0.98 (3)
11	15 688.350 (45)	0.592862 (19)	1.87 (d)	- 1.08 (3)

a One standard deviation in the last digit is given in parentheses.

b T_v is referred to the $X^1\Sigma^+$ (v=0) energy level.

c For the meaning of the q parameter, see text (section 3).

d fixed values in the fits

The constants in Table VI will *not* reproduce the observed lines unless the full $^1\Pi \sim {}^3\Pi \sim {}^1\Sigma^+$ matrix is set up using the band-by-band constants listed in Appendix 1. If that is done, all unperturbed, perturbed, and extra lines will be reproduced to 0.03-cm^{-1} rms error. Appendix 2 lists all fitted lines, observed minus calculated.

C. $A^1\Pi \sim a^3\Pi$ Perturbations. Equilibrium Constants of the $a^3\Pi$ State

Figure 5 shows that there are only three $^1\Pi \sim {}^3\Pi$ crossings within the range of assigned transitions. Of these, the crossing in $v_A = 7$ occurs at the highest J sampled, and this in only one branch. This leaves only the crossings in $v_A = 8$ and 9 by $a^3\Pi_2 v_a = 10, 11$ (both of which include several extra lines) as the levels from which the most important information about $a^3\Pi$ can be derived. Note, however, that the effects on $v_A = 6$, 7, and 10 by $a^3\Pi_2 v_a = 8$, 9, and 12 and on $v_A = 9$–11 by $a^3\Pi_1 v_a = 11$–13 are nonnegligible and quite informative, at least as a check of the data derived from $v_A = 8$ and 9 deperturbation.

We will concentrate first on the $v_A = 8$ and 9 perturbations because these permit fairly accurate determinations of $T_v(a^3\Pi)$ and $B_v(a^3\Pi)$ values for $v_a = 10$ and 11. These best values provide anchor points for extrapolation of T_v and B_v into higher and lower vibrational levels for which *both* of these quantities cannot be simultaneously fitted.

This extrapolation procedure is illustrated by Table VII which lists T_v, B_v, and D_v values for $a^3\Pi v_a = 9$–12. The absolute vibrational numbering of these levels is discussed in Section IIID. Since only one $a^3\Pi$ vibrational interval $\Delta G(10.5) = 646.77 \pm 0.17$ cm^{-1}, can be determined, it is necessary to assume a value for $\omega_e x_e(a^3\Pi)$ in order to usefully extrapolate to $v_a = 9$ and 12. Setting

$$\omega_e x_e(a^3\Pi) = \omega_e x_e(A^1\Pi) = 4.09 \text{ cm}^{-1}$$

one obtains, assuming arbitrarily an uncertainty of ± 0.2 cm^{-1} on $\omega_e x_e(a^3\Pi)$

$$\omega_e(a^3\Pi) = 737 \pm 5\text{cm}^{-1}.$$

Now, to test this assumption, we fix

$$T_9(a^3\Pi) = 13\,238.2 \pm 0.5 \text{ cm}^{-1}$$

at the extrapolated value and determine a least-squares value of $B_9(a^3\Pi)$. The value given in Table VII agrees satisfactorily with that extrapolated from B_{10} assuming

$$\alpha_e(a^3\Pi) = B_{10} - B_{11} = 0.0068 \pm 0.0001 \text{ cm}^{-1}$$

or even better, with that assuming

$$\alpha_e(a^3\Pi) = \alpha_e(A^1\Pi) = 0.00583 \text{ cm}^{-1}.$$

Since the $v_a = 9 \sim v_A = 7$ crossing occurs near $J = 70$, a 1-cm^{-1} extrapolation error in T_9 results in a change of 0.0002 cm^{-1} in the fitted value of B_9.

It should appear that extrapolating down to $v_a = 9$ using $\omega_e x_e$ and α_e values from $A^1\Pi$ should give T_9 and B_9 to better than ± 1 and ± 0.0005 cm^{-1}. Similar uncertainties should apply extrapolated values for $v_a = 12$. We shall see later that if the $v_A = 10 \sim v_a = 12$ $\Omega = 1$ perturbation is fitted using fixed, extrapolated values for

TABLE VII

Molecular Constants of the BeS $a^3\Pi$ Vibrational Levels (Units: cm^{-1})[a]

v	T_v(b)	B_v	$D_v\ 10^6$
9	12 238 (c)	0.59839 (1)	1.94 (d)
10	13 893.33 (13)	0.59329 (4)	1.93 (d)
11	14 540.10 (4)	0.58701 (8)	1.92 (d)

a One standard deviation in the last digit is given in parentheses.

b T_v is referred to the $X^1\Sigma^+$ (v=0 J=0) energy level.

c Extrapolated from the v=10 - v=11 energy separation assuming $\omega_e x_e(a^3\Pi) = \omega_e x_e(A^1\Pi)$.

d Fixed at the theoretical value : $4B_e^3/\omega_e^2 + \beta_e(v + \frac{1}{2})$ assuming the same β_e constant as in the $A^1\Pi$ state ($\beta_e = -10^{-8}\ cm^{-1}$)

T_{12} and B_{12} but varying $A(a^3\Pi)$, one obtains the following purely experimental estimate

$$A(a^3\Pi) = -180 \pm 20 \text{ cm}^{-1}.$$

The ν_0 and B values given by Cheetham *et al.* (*1*) for their "$^1\Delta$" perturber are quite different from those in Table VII. The reasons for this are: the $^3\Pi_2$ subband origin differs from that of the complete $^3\Pi$ state by

$$\nu_0(^3\Pi_2) = T_v(^3\Pi) + A(^3\Pi) - 3B(^3\Pi); \tag{10}$$

the effective B value for $^3\Pi_2$ is smaller than $B(a^3\Pi)$

$$B_{\text{eff}}(^3\Pi_2) = B(^3\Pi) + 2B(^3\Pi)^2/A(^3\Pi); \tag{11}$$

and the constants in Table VII are locally deperturbed.

To determine the T_e and B_e equilibrium constants of the $a^3\Pi$ state, it seemed tempting to extrapolate the constants from the three now analyzed levels (v = 9, 10, 11). This was indeed done to obtain the value of T_e (T_e = 7103 ± 75 cm^{-1}). The same method could not be used to determine $B_e(a^3\Pi)$ since it only led to the *obvious* result that $B_e(a^3\Pi)$ should be close to $B_e(A^1\Pi)$. A much more accurate determination of $r_e(a^3\Pi)$ is quite necessary in view of the crucial role that the value of r_e, deduced from this B_e parameter, plays in the location of the potential curves and hence in the value of the vibrational overlap integrals, especially when high-lying levels are involved.

Therefore another strategy was used which was based on the following: the *ab initio* calculations have proved that the $^3\Pi$ and $^1\Pi$ states are very well described by a single-configuration ($\pi^3\sigma$) representation; for such a configuration, the electronic part of the A_{11} off-diagonal $^3\Pi \sim {}^1\Pi$ spin–orbit interaction element should be equal to the diagonal spin–orbit A constant of the $a^3\Pi$ state (*10*). Accordingly, we looked for the particular $r_e(a^3\Pi)$ value (close to that of the $A^1\Pi$ state) that leads to overlap integrals $S_{v_a v_A}$ which satisfy the postulated equality of $A_{11}/S_{v_a v_A}$ and $A(^3\Pi)$ in the 8–1 and 9–1 bands.

The following procedure was adopted: fits of the two bands led to A_{11} = −9.3 cm^{-1} in the 8–1 band and A_{11} = −10.4 cm^{-1} in the 9–1 band; since $A(^3\Pi)$ was not determined, we fixed it at several trial values (between −130 and −190 cm^{-1}) and for each of these values of A, we scanned through the range of plausible $r_e(a^3\Pi)$ values, each time calculating the overlap integrals so as to determine the particular r_e value for which the deviation between the $A_{11}/S_{v_a v_A}$ quantity and the fixed $A(^3\Pi)$ constant was the smallest.

Three causes of error limit the precision of this determination of $r_e(a^3\Pi)$: the uncertainty on the $A(^3\Pi)$ spin–orbit constant, the uncertainty on the ω_e and $\omega_e x_e$ constants that serve to calculate the $S_{v_a v_A}$ vibrational overlap integral, and the validity of the postulate on which the method relies, namely, the equality between the electronic perturbation parameter deduced from A_{11} and the spin–orbit constant $A(^3\Pi)$. The quantitative effect of these causes of error was carefully tested. As shown on Fig. 6, where calculations for $A(^3\Pi)$ fixed at −180 and −160 cm^{-1} are presented, the uncertainty on the value of $A(^3\Pi)$ yields a negligible uncertainty (~10^{-4} Å) on the value of r_e. The uncertainties on ω_e (~5 cm^{-1}) and $\omega_e x_e$ (~0.2 cm^{-1}) although

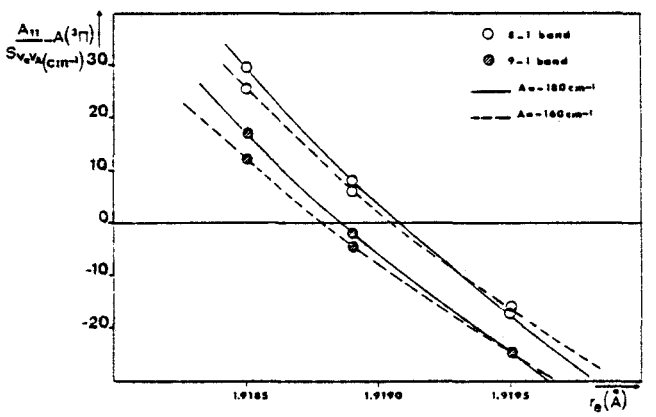

FIG. 6. Optimization of $r_e(a^3\Pi)$ and $A(a^3\Pi)$. Assuming that the correct vibrational assignments are $v = 10$ and 11 for the $a^3\Pi$ levels which perturb $A^1\Pi v = 8$ and 9, two internal consistency requirements are used to determine r_e and A. These are: (i) the quantity $[A_{11}/S_{v_a v_A} - A(^3\Pi)]$ must be zero, (ii) $A_{11}/S_{v_a v_A}$ must be vibration independent. A_{11} is determined by fitting the observed energy levels; the vibrational overlap integral, $S_{v_a v_A}$, is calculated at each r_e value using a Morse curve for $a^3\Pi$ with $\omega_e = 737$ cm^{-1} and $\omega_e x_e = 4.1$ cm^{-1}. The region of the intercept of the r_e axis on the figure shows that the optimum r_e is 1.9190 Å.

they change drastically $S_{v_a v_A}$, only produce a horizontal shift of the curves leading to an uncertainty on r_e of about 15×10^{-4} Å. Lastly, considering that $A(^3\Pi)$ and $A_{11}/S_{v_a v_A}$ actually differ by certainly less than 10% produces a maximum possible vertical shift of the curves of at most 18 cm^{-1} leading to an uncertainty of 3×10^{-4} Å on r_e. On the whole, we estimate the accuracy on the value of $r_e(a^3\Pi)$ to 2×10^{-3} Å. Besides, it is gratifying to note that similar results are obtained for determination of $r_e(a^3\Pi)$ from 8–1 and 9–1 bands.

The equilibrium internuclear separation of the $A^1\Pi$ state, determined from an extrapolation of the B_5 to B_{11} levels and given in Table VIII, is $r_e(A^1\Pi) = 1.9087$ Å. Note that $r_e(a^3\Pi)$ is found to be larger than $r_e(A^1\Pi)$ in BeS. This also occurs for MgO, where the ratio of these equilibrium internuclear separations was 1.0034 compared to 1.0054 for BeS. In both cases, the $a^3\Pi$ and $A^1\Pi$ states have very similar potential curves but with sufficient differences that $\Delta v \neq 0$ vibrational matrix elements allow $\Delta v \neq 0$ perturbations to be detectably large.

From $r_e(a^3\Pi) = 1.9190 \pm 0.0010$ Å, $B_e(a^3\Pi) = 0.6511 \pm 0.0007$ cm^{-1}. If one assumes the α_e and γ_e constants of $(a^3\Pi)$ to be the same as those of the $A^1\Pi$ state (see Table IX), this value of $B_e(a^3\Pi)$ extrapolates to $B_v(v = 10) = 0.5912$ cm^{-1} and $B_v(v = 11) = 0.5856$ cm^{-1}, which are quite close to the experimental values (0.5933 and 0.5870 cm^{-1}; see Table III). This agreement supports a posteriori the deperturbation procedure adopted here based on the initial assumption according to which the $\omega_e x_e$ constants of $a^3\Pi$ and $A^1\Pi$ are equal.

In addition to the diagonal parameters discussed above, the fitting process yields values of the perturbation matrix elements (A^+_{01}, β^+_{10}, A_{11}) and a second-order interaction parameter, q in the $A^1\Pi$ state. The A_{11} parameter already has been discussed in this section in connection with the determination of $r_e(a^3\Pi)$.

TABLE VIII

Molecular Constants of the Lowest States of BeS (cm^{-1}, Except for r_e in Å)

state	T_e	ω_e	$\omega_e x_e$	B_e	$\alpha_e 10^3$	$\gamma_e 10^5$	r_e(Å)
$X^1\Sigma^+$ (a)	0	997.94	6.137	0.79059	6.64	- 1.9	1.7415
$A^1\Pi$	7961.64 (26)	762.13 (7)	4.09 (4)	0.6581 (2)	5.83 (6)	1.2 (4)	1.9087 (2)
$a^3\Pi$	7103 (75)	737 (5)	4.1 (2)(b)	0.6511 (7)	5.8 (3)(b)	1.2 (4)(b)	1.9190 (10)

a Cheetham, Gissane and Barrow, Ref. (1).

b Assumed equal to the corresponding constant in the $A^1\Pi$ state.

TABLE IX

Off-Diagonal Spin–Orbit and Rotation–Electronic Interaction Parameters in BeS

$a^3\Pi \sim A^1\Pi$ interaction

$v(a^3\Pi)$	$v(A^1\Pi)$	A_{11}	$S_{v_a v_A}$	$\lvert A_{11}/S_{v_a v_A}\rvert$ exp	th
10	8	- 9.31 (5)	0.051	182	180
11	9	-10.41 (6)	0.059	176	180

$X^1\Sigma^+ \sim A^1\Pi$ interaction

$v(X^1\Sigma^+)$	$v(A')$	β^+_{10}	$\langle v_A \lvert B(R) \rvert v_X \rangle$	$\lvert b \rvert$ exp	th
14	7	-0.0896 (7)	0.204	0.31	0.41
15	8	-0.0957 (2)	0.211	0.32	0.42
16	9	-0.0985 (10)	0.213	0.33	0.43
17	10	-0.1038 (40)	0.213	0.34	0.44

One standard deviation is given in parentheses.

The β^+_{10} parameters can be determined only in bands involving $A^1\Pi$ vibrational levels crossed by, or at least close to $X^1\Sigma^+$ ones, i.e., in the 7–0, 8–1, 9–1, and 10–2 bands. The fitted values of β^+_{10} are given in Table IX. Dividing these parameters by the corresponding vibrational integrals according to Eq. (8.3), one obtains the electronic part, $\mathbf{b}(X \sim A)$, at the r centroid of each perturbation. Since all observed $X \sim A$ perturbations belong to a single vibrational sequence (shown to be $\Delta v = 7$ in Section IIID), the relevant r centroids are almost identical (they spread over less than 0.05 Å). Therefore the $\mathbf{b}$ $(X \sim A)$ values determined from experimental β^+_{10} are expected to be very similar. As shown by Table IX (fifth column), this approximate constancy of $\mathbf{b}$ $(X \sim A)$ is indeed observed. Furthermore, the experimentally determined values of b $(X \sim A)$ faithfully reproduce the increase of $\mathbf{b}$ $(X \sim A)$ versus $\bar{r}_{v_X v_A}$ found in the *ab initio* calculations: $db/dr = 0.6$ Å^{-1} in the range sampled.

For the same reasons, the two $A_{11}/S_{v_a v_A}$ values deduced from the $a \sim A$ perturbations in the 8–1 and 9–1 bands are also quite similar. Constancy of the electronic parameters from one band to another constitutes the best test of the validity of the deperturbation model. This argument will be used again later in this section to determine the $A(a^3\Pi)$ spin–orbit constant and in Section IIID to decide upon the vibrational numbering of $A^1\Pi$ relative to $X^1\Sigma^+$. Table IX also contains a comparison of the fitted $\mathbf{b}$ $(X \sim A)$ electronic parameter with the *ab initio* value. The agreement between the deperturbed (0.3) and *ab initio* (0.4) values of $\mathbf{b}$ $(X \sim A)$ is adequate to ensure that our theoretical discussion at the end of Section II about the nature of the perturbing configurations applies quantitatively to the actual situation.

Although its effects might seem easy to detect since they are parity dependent and affect only e levels of the $a^3\Pi$ state, the third perturbation parameter, $A_{01}^+(a \sim X)$, is indeterminate. Even setting it to zero or changing its sign does not significantly affect the variances of the fits. This is not surprising, because the perturber of $A^1\Pi$ is the $\Omega = 2$ component of the $a^3\Pi$ state while the A_{01}^+ parameter connects the $X^1\Sigma^+$ state to the $\Omega = 0$ component of $a^3\Pi$. The transfer of $\Omega = 0$ basis function character into the nominal $\Omega = 2$ component of the $a^3\Pi$ state via the $\Omega = 1$ component is a third-order effect and therefore insufficient to allow sensitivity to A_{01}^+.

The next parameter to deal with is the q constant associated with Λ doubling in the $A^1\Pi$ state. Its fitted values, given for the various vibrational levels in Table VI, cluster around an average value of $q = -1.12 \times 10^{-4}$ cm^{-1}. In order to interpret the value of this parameter, one must recall that it results from the interaction of the particular $A^1\Pi(v)$ level with all $X^1\Sigma^+$ vibronic levels of the molecule except one, namely, the closest-lying $X^1\Sigma^+$ $(v + 7)$ level which is already explicitly included in the Hamiltonian matrix. Second-order perturbation theory gives the following expression for q (*22*)

$$q = \sum_{\substack{n^1\Sigma^+, v' \\ (n,v' \neq X, v+7)}} \frac{|\langle A^1\Pi, v|BL^+|n^1\Sigma^+, v'\rangle|^2}{E(A^1\Pi, v) - E(n^1\Sigma^+, v')}.$$

Due to this important restriction in the summation, the value of the parameter appearing in the matrix is only a fraction of the full Λ-doubling parameter; inspection of the structure of the outer orbitals (Fig. 1) indicates that the $B^1\Sigma^+$ state is the state which can be expected to contribute most to the value of the q parameter in $A^1\Pi(v)$. In a crude pure precession model assuming a simple $A^1\Pi \sim B^1\Sigma^+$ interaction between the π and σ components of the $3p$ orbital on sulphur, one gets a value of q equal to -1.0×10^{-4} cm^{-1} which compares well with the experimental value of -1.12×10^{-4} cm^{-1}. However, the spectroscopic constants given in Table III show that potential curves of the $A^1\Pi$ and $B^1\Sigma^+$ states are not at all similar; furthermore Fig. 1 shows that the 2π and 6σ orbitals are not exactly pure atomic orbitals. This means that the prerequisites for pure precession are not fulfilled. Moreover, high vibrational levels of the $X^1\Sigma^+$ state are so close to that of the $A^1\Pi$ state that they could contribute significantly to the value of q, even though the l^+ matrix element involved in this interaction, namely, $b(A \sim X)$ is quite small (Fig. 4). Therefore the correct way to calculate q is to carry out the whole summation which, in principle, involves an infinite number of terms. The summation was truncated to the $v = 0$–19 levels of the $B^1\Sigma^+$ state and $v = 0$–19 of the $X^1\Sigma^+$ state. Using the $b(A \sim X)$ values at the suitable r centroids (Fig. 4), it was found that the $X^1\Sigma^+$ vibrational levels lying below each $A^1\Pi v_A$ level almost exactly compensated the effect of the $X^1\Sigma^+$ vibrational levels lying above it. Hence the overall $X^1\Sigma^+$ contribution to the value of q was negligible for the $v_A = 5$–11 levels of $A^1\Pi$. On the contrary, all $B^1\Sigma^+$ vibrational levels lie above the $A^1\Pi v_A$ levels considered in this study and accumulate their repulsive effects on the e rotational levels of $A^1\Pi v_A$. The final *ab initio* value thus found was $q = -0.4 \times 10^{-4}$ cm^{-1}, which is less than half the experimental value. We have not found any satisfactory interpretation of this dis-

crepancy: rather than suggesting only the possibility of truncation errors we are inclined to believe that the $b(A \sim B)$ parameter is closer to its largest possible value, $\sqrt{2}$, than as calculated in Section II (see Fig. 4), for instance because the 6σ orbital is more purely $3p\sigma(S)$ than suggested by the *ab initio* results.

The last important parameter is the spin–orbit constant. A direct determination was attempted from the 10–2 band, since the $A^1\Pi(v = 10)$ level, which lies just between the $^3\Pi_2$ and $^3\Pi_1$ ($v = 12$) components, is rather strongly affected by both $^3\Pi_2$ (near $J \sim 0$) and $^3\Pi_1$ (just above the highest observed levels), even though no crossings are observed directly. First, we must remember from the discussion of Section II that the absolute value of $A(a^3\Pi)$ cannot exceed 190 cm^{-1} (half the sulphur spin–orbit parameter). To determine a lower bound on $A(a^3\Pi)$ we performed a series of fits where A was held fixed at various values ranging from -190 to -130 cm^{-1}. It was first noticed that, in the 8–1 and 9–1 bands, where $A(a^3\Pi)$ cannot be determined, the fitted A_{11} parameter was found to vary (see Eq. (8.2)) so that it remained practically equal to $A(a^3\Pi)S_{v_a v_A}$. On the contrary, in the 10–2 band, the values obtained for $A_{11}/A(a^3\Pi)$ depended considerably on the fixed value of $A(a^3\Pi)$. Below $|A(a^3\Pi)| = 160$ cm^{-1}, the A_{11} parameter became much too different from its expected value $A(a^3\Pi)S_{v_a v_A}$. Thus, the spin–orbit constant of the $a^3\Pi$ state is bounded between -160 and -190 cm^{-1}. This already had been predicted by *ab initio* calculations and on this point, the deperturbation was unable to yield a more accurate value.

D. Vibrational Numbering

Finally, it should be restated that the deperturbation was performed assuming a relative vibrational numbering of the perturbing levels, namely, v_A in $A^1\Pi$, $v_a = v_A + 2$ in $a^3\Pi$, and $v_X = v_A + 7$ in $X^1\Sigma^+$. In fact, only the absolute vibrational quantum numbers of the $X^1\Sigma^+$ levels involved in the perturbations had been established in Ref. (*1*): the accurate set of constants previously determined (*1*) for $X^1\Sigma^+$ made extrapolation of its energy levels sufficiently reliable to determine unambiguously below $v_X = 20$ which $X^1\Sigma^+$ level is responsible for perturbations observed at a given energy.

Cheetham *et al.* (*1*) state that their vibrational numbering of $A^1\Pi$ is uncertain by ± 1. In our previous discussion we have adopted the numbering of $A^1\Pi$ suggested by Ref. (*1*) and the numbering of $a^3\Pi$ suggested (but also uncertain by ± 1) by the *ab initio* calculation of the intraconfigurational $^1\Pi$–$^3\Pi$ splitting. We will now present the experimental evidence supporting these hitherto tentative vibrational numberings.

D.1. $A^1\Pi$ vibrational numbering. Three trial numberings of $A^1\Pi$ must be evaluated corresponding to whether the perturbing levels of the A and X states differ by 6, 7, or 8 quanta. The $\Delta v = v_X - v_A = 7$ hypothesis has been assumed in the preceding discussion. Since the $\Delta v = 6$ and $\Delta v = 8$ hypotheses are a priori as likely as the $\Delta v = 7$ one, they were carefully tested and as shown here, rejected in favor of $\Delta v = 7$. The test must concern the $X^1\Sigma^+ \sim A^1\Pi$ interaction matrix element. We compared the experimental value $[(2)^{-1/2}\beta_{10}^{+}\langle v_A|B(R)|v_X\rangle]$ of the $b(A \sim X)$ perturbation parameter to the *ab initio* value of this parameter at the r centroid of the interaction. This comparison was done for four bands, 7–0, 8–1, 9–1, and 10–2

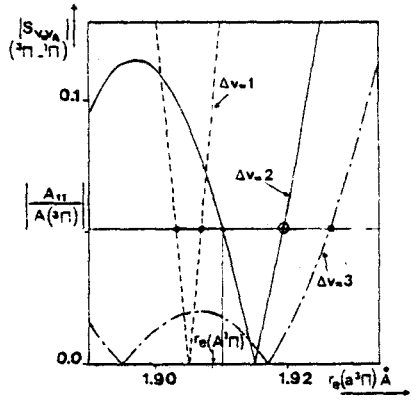

FIG. 7. Use of the $A^1\Pi \sim a^3\Pi$ perturbation matrix element to suggest five most probable trial potential curves for $a^3\Pi$. The *ab initio* $^1\Pi$–$^3\Pi$ energy difference is sufficiently accurate to restrict the trial vibrational numberings of $a^3\Pi$ to three possibilities, $\Delta v = v_a - v_A = 3$, 2, or 1. For each Δv possibility there are two $a^3\Pi$ Morse curves corresponding to two different choices of r_e, chosen such that $|S_{v_a v_A}| = |A_{11}/A(^3\Pi)| = 0.051$. The *two* possibilities reflect the two signs of $S_{v_a v_A}$ and the inability to experimentally determine the sign of an off-diagonal matrix element. One of the $\Delta v = 3$ possible r_e's is unacceptably small and is rejected outright. Nearly identical $S_{v_a v_A}$ vs r_e curves were obtained for the $a^3\Pi$ level which perturbs $A^1\Pi v_A = 8$ and 9. The most probable Δv, r_e possibility is enclosed by O.

ones. Three trial $A^1\Pi$ Morse potentials were generated from the seven observed vibrational levels, one for each of the trial numberings. The $\Delta v = 6$ ($\Delta v = 8$) hypothesis led to trial constants $r_e = 1.9004$ (1.9173) Å, $\omega_e = 770.2$ (754.0) cm^{-1}, $T_e = 7197$ (8719) cm^{-1}. The relevant r centroids were also calculated and found to be shifted by -0.03 Å ($\Delta v = 6$) or $+0.03$ Å ($\Delta v = 8$) from the $\Delta v = 7$ hypothesis.

The criterion that the $b(A \sim X)$ value be nearly the same for the 7–0, 8–1, 9–1, and 10–2 bands, since they correspond to nearly equal r centroids, rules out the $\Delta v = 6$ hypothesis and makes $\Delta v = 7$ preferable to $\Delta v = 8$. The alternative criterion that the experimental and *ab initio* **b** values agree would argue in favor of $\Delta v = 8$. However, we do not consider that our *ab initio* calculations are accurate enough to make this a convincing argument. We are more confident about the calculated small increase of **b** vs r. The $\Delta v = 7$ and $\Delta v = 8$ hypotheses are respectively consistent and inconsistent with the *ab initio* r dependence of **b**; thus we regard the $\Delta v = 7$ hypothesis as proven (Table X).

D.2. $a^3\Pi$ vibrational numbering. We will consider the $v_a - v_A = \Delta v = 1$, 2, and 3 hypotheses. The test utilizes the same method described in Section IIIC by which ω_e and r_e were determined, assuming $\Delta v = 2$. The value $\omega_e x_e$ was fixed at 4.1 cm^{-1} (the value for $A^1\Pi$). Using the fitted term values for the two best sampled $a^3\Pi$ levels (labeled $v_a = 10$ and 11 in Table VII), the $\Delta v = 1$ ($\Delta v = 3$) hypothesis yielded $\omega_e = 728$ (744) cm^{-1} and $T_e = 7850$ (6380) cm^{-1}. Three families of trial Morse potentials were generated from the $\Delta v = 1$, 2, and 3, vibrational constants and r_e values varied over a reasonable range. Overlap integrals, $S_{v_a v_A}$ were calculated and used to find the r_e values within each Δv family which satisfy the criterion $|A_{11}/S_{v_a v_A}| = |A(a^3\Pi)|$ or, for the 8–1 band, $|A_{11}/A(a^3\Pi)| = 0.051$. The method is illustrated by Fig. 7. Identical results are obtained for constants from the 8–1 and 9–1 bands.

TABLE X

Data for Determination of the Relative Numbering of the Perturbing $X^1\Sigma^+$ and $A^1\Pi$ Levels from a Comparison of the Experimental and *ab Initio* Values of the $b(A \sim X)$ Parameter

Band (a)	Numbering hypothesis (b)	Absolute $v(A^1\Pi)$	β^+_{10}	$\langle v_A \lvert B(R) \rvert v_X \rangle$	b_{exp}	$\bar{r}$(Å)	b_{th}
7-0	Δ6	8	-0.0896 (6)	0.206	0.31	2.195	0.39
	Δ7	7	-0.0896 (6)	0.204	0.31	2.228	0.41
	Δ8	6	-0.0896 (6)	0.144	0.44	2.264	0.43
8-1	Δ6	9	-0.0957 (2)	0.186	0.36	2.210	0.40
	Δ7	8	-0.0957 (2)	0.211	0.32	2.242	0.42
	Δ8	7	-0.0957 (2)	0.162	0.42	2.276	0.44
9-1	Δ6	10	-0.0985 (10)	0.162	0.43	2.227	0.41
	Δ7	9	-0.0985 (10)	0.213	0.33	2.258	0.43
	Δ8	8	-0.0985 (10)	0.177	0.39	2.290	0.44
10-2	Δ6	11	-0.1038 (40)	0.135	0.54	2.246	0.42
	Δ7	10	-0.1038 (40)	0.213	0.34	2.276	0.44
	Δ8	9	-0.1038 (40)	0.188	0.39	2.303	0.45

a For the sake of simplicity, a single band designation has been used regardless of the Δv hypothesis. Thus, the 8-1 and 9-1 band designation refers to the notation used in Section II for the two most perturbed bands. This designation corresponds to the Δv = 7 hypothesis ; it must be replaced by 7-1, 8-1 in the Δv = 6 hypothesis or by 9-1, 10-1 in the Δv = 8 one.

b Δv is the difference between the vibrational quantum number v' of an $X^1\Sigma^+$ level and the vibrational quantum number of the $A^1\Pi$ level that it perturbs.

THE $a^3\Pi$, STATE OF BeS

TABLE XI

Data for Determination of the Relative Numberings of the $a^3\Pi$ and $A^1\Pi$ States from Comparison of the B_v Values Extrapolated from $B_e(a^3\Pi)$ vs the Fitted B_v Value (8–1 Band)

	$v(a^3\Pi)$	B_e (cm^{-1})	B_v fitted (cm^{-1})	B_v extr (a) (cm^{-1})
$\Delta v = 1$	9	0.6621	0.5933	0.6081
	9	0.6592	0.5933	0.6052
$\Delta v = 2$	10	0.6572	0.5933	0.5976
	10	0.6511	0.5933	0.5912
$\Delta v = 3$	11	0.6455	0.5933	0.5804

a B_v extr $= B_e - \alpha_e (v + \frac{1}{2}) + \gamma_e (v + \frac{1}{2})^2$ with α_e and γ_e assumed to be the same as in the $A^1\Pi$ state.

As inferred from theoretical discussions in Section II, the range of possible variation of $r_e(a^3\Pi)$ is restricted to a limited region around the equilibrium separation of the $A^1\Pi$ state, say, 1.89–1.94 Å. Figure 7 shows that acceptable values of $r_e(a^3\Pi)$ exist for all three Δv hypotheses. We shall now justify our choice of the solution $r_e(a^3\Pi) = 1.9190$ Å, corresponding to one of the two possibilities of the $\Delta v = 2$ hypothesis. The other possibility for $\Delta v = 2$ ($r_e = 1.910$ Å) and the two possibilities for $\Delta v = 1$ ($r_e = 1.903$ Å and $r_e = 1.907$ Å) are nearly equal to or just smaller than the $A^1\Pi$ equilibrium separation (1.9087 Å), contrary to expectations based on *ab initio* results of Section II or comparison with MgO (*9*, *14*). On the other hand, the single possible r_e value found in the $\Delta v = 3$ hypothesis ($r_e = 1.927$ Å) is much larger than expected on the same basis. Another fact in favor of the $\Delta v = 2$ hypothesis (but for both of its r_e possibilities) is that the singlet–triplet electronic term value separation would be nearly the same in BeS and MgO (*12*) (840 and 934 cm^{-1}, respectively) just as predicted *ab initio* (although slightly larger for both molecules, 1300 cm^{-1} in BeS and 1200 cm^{-1} in MgO (*4*)). In the $\Delta v = 1$ and $\Delta v = 3$ hypotheses, the experimental electronic singlet–triplet splittings would be 110 and 1580 cm^{-1}, respectively. However, neither of these arguments is sufficient to eliminate either the $\Delta v = 1$ or $\Delta v = 3$ hypothesis, thus another test was performed.

In view of the similarity of the $a^3\Pi$ and $A^1\Pi$ potential curves, it was assumed that the α_e and γ_e constants of the $a^3\Pi$ state could be taken equal to those of $A^1\Pi$ (see Table VIII). Using these constants and the B_e values deduced from r_e in the various Δv hypotheses, it was possible to estimate extrapolated values of $B_v(a^3\Pi)$ for the perturbing levels. The results are given in Table XI. They support the second $v = 2$ hypothesis since for the other hypotheses agreement between B_{extr} and B_{fitted} would require an implausible change of α_e by 10 to 25% from $A^1\Pi$ to a $a^3\Pi$.

IV. CONCLUSION

The combination of *ab initio* calculations with experimental data has proved to be essential to carry out the deperturbation of the BeS $A^1\Pi$ state. The *ab initio* results were decisive at several steps of the deperturbation.

First, they clarified the nature and properties of the states that could plausibly be involved in the observed interactions. The earlier suggestion of a $^1\Delta$ perturber could be ruled out and the perturbers of the $A^1\Pi$ state were shown to be the isoconfigurational $a^3\Pi$ state and high-lying vibrational levels of the $X^1\Sigma^+$ state.

Second, the *ab initio* wavefunctions were used in order to calculate interaction parameters. Thus, they provided initial estimates for several electronic parameters required by and eventually refined in the deperturbation procedure, for example the **a** and **b** parameters. Moreover, they permitted a number of second-order parameters characteristic of interactions with the distant $^3\Sigma^+$ state and then undeterminable from a purely experimental deperturbation to be fixed at their *ab initio* values. A point of utmost importance is that the relative signs of perturbation parameters must be known prior to the deperturbation. These signs were unambiguously determined by the *ab initio* calculations.

Lastly, after deperturbation was completed, various pieces of *ab initio* information were used to verify the assumed vibrational numbering of the $A^1\Pi$ and $a^3\Pi$ states. The main tests concerned the near constancy of the $b(A \sim X)$ electronic parameter, the energy difference between the electronic term values of the $A^1\Pi$ and $a^3\Pi$ states and the equality of the $A^1\Pi \sim a^3\Pi$ spin–orbit interaction matrix element to the diagonal value $A(a^3\Pi)$.

This last assumption formed the basis for a new semiempirical method for determining the equilibrium internuclear separation of the perturbing state. Taking advantage of the sensitivity of the vibrational $S_{v_a v_A}$ overlap integral to $r_e(a^3\Pi)$, it was possible to optimize this equilibrium internuclear separation by requiring equality between the fitted value of the vibronic A_{11} parameter and the $S_{v_a v_A} \cdot A(a^3\Pi)$ product.

The BeS perturbations are now clearly understood. From this interpretation, it can be concluded, contrarily to an earlier suggestion (*12*), that the electronic structure of BeS is not peculiar at all. It closely resembles that of BeO, MgO, and more generally that of all IIA–VI molecules.

Thus, by analogy with the situation in these molecules, it can be suggested that the ultraviolet system of BeS is a Be^+ $(2p - 2s)$–triplet–triplet transition similar to the $d^3\Delta$–$a^3\Pi$ one of MgO (*29*, *30*).[9] Application of this hybrid theoretical experimental method to the deperturbation of BeO is presently in progress and is expected to confirm the power of this approach in another case where direct experimental data are partly lacking.

[9] The lower state of the ultraviolet system is almost certainly the $a^3\Pi$ state. The upper state is probably the configuration (1.4) $^3\Delta$ state. If so, the $^3\Delta$ state is inverted with $A(^3\Delta) = -81$ cm^{-1}, $T_{00} = 32932$ cm^{-1} and $B(^3\Delta) < B(a^3\Pi)$. There is a major argument against the original $^3\Pi$–$^3\Pi$ assignment: the *ab initio* energies of the lowest *bound* $^3\Pi$ states above $a^3\Pi i$ ($^3\Pi_{III} = 46\,000$cm^{-1} and $^3\Pi_{IV}$: 48 200 cm^{-1}) are too high lying to be the upper state of the UV system. The arguments in favor of the $^3\Delta$–$a^3\Pi$ assignment are numerous. The *ab initio* $^3\Delta$–$a^3\Pi$ transition frequency and spin–orbit constants are $\lambda_{00} = 31\,806$ cm^{-1} and $A(^3\Delta) = -74$ cm^{-1} compared to the observed 25 940 cm^{-1} and -81 cm^{-1}. In addition, a ligand field theory estimate of the $^3\Delta$–$a^3\Pi$ transition frequency is given by the corresponding $A^2\Pi$–$X^2\Sigma^+$ transition

THE $a^3\Pi_i$ STATE OF BeS

APPENDIX 1. BAND BY BAND CONSTANTS (UNITS: cm^{-1})[a]

bands	5-0	6-0	7-0	8-1
$T_v(X^1\Sigma^+)$	11 028.0 (b)	11 875.64 (1.19)	12 704.61 (40)	13 513.48 (28)
$T_v(A^1\pi)$	11 532.249 (5)	12 245.341 (4)	12 950.197 (6)	13 646.796 (7)
$T_v(a^3\pi)$	11 903.0 (b)	12 575.0 (b)	13 238.0 (b)	13 893.33 (13)
$B_v(X^1\Sigma^+)$	0.7048 (b)	0.6978 (b)	0.6903 (1)	0.6835 (2)
$B_v(A^1\pi)$	0.62645 (1)	0.620762 (16)	0.615048 (6)	0.609445 (8)
$B_v(a^3\pi)$	0.6098 (b)	0.6041 (b)	0.59839 (1)	0.59329 (4)
$D_v(X^1\Sigma^+)$	$2.09\ 10^{-6}$ (b)	$2.09\ 10^{-6}$ (b)	$2.10\ 10^{-6}$ (b)	$2.11\ 10^{-6}$ (b)
$D_v(A^1\pi)$	$1.93\ 10^{-6}$ (b)	$1.924\ 10^{-6}$ (2)	$1.916\ 10^{-6}$ (2)	$1.916\ 10^{-6}$ (2)
$D_v(a^3\pi)$	$1.95\ 10^{-6}$ (b)	$1.95\ 10^{-6}$ (b)	$1.94\ 10^{-6}$ (b)	$1.93\ 10^{-6}$ (b)
$A(a^3\pi)$	- 180.0 (b)	- 180.0 (b)	- 180.0 (b)	- 182.01 (13)
β_{10}^+	- 0.0690 (b)	- 0.0951 (21)	- 0.0896 (7)	- 0.0957 (2)
A_{01}^+	- 9.80 (b)	- 21.0 (b)	- 28.0 (b)	- 34.3 (b)
A_{11}	- 5.0 (b)	- 6.3 (b)	- 8.09 (9)	- 9.31 (5)
A_0^+	- 1.5 (b)	- 1.5 (b)	- 1.5 (b)	- 1.5 (b)
β_0^+	$-\ 2.7\ 10^{-5}$ (b)	$-\ 2.7\ 10^{-5}$ (b)	$-\ 2.7\ 10^{-5}$ (b)	$-\ 2.7\ 10^{-5}$ (b)
β_1^+	$-\ 4.4\ 10^{-3}$ (b)	$-\ 4.4\ 10^{-3}$ (b)	$-\ 4.4\ 10^{-3}$ (b)	$-\ 4.4\ 10^{-3}$ (b)
$A_\Sigma{}^3\pi$	- 1.7 (b)	- 0.1 (b)	- 4.2 (b)	- 3.5 (b)
$A_\pi{}^3\pi$	- 33.0 (b)	- 32.0 (b)	- 28.0 (b)	- 28.0 (b)
q	$-\ 1.06\ 10^{-4}$ (5)	$-\ 1.22\ 10^{-4}$ (3)	$-\ 1.02\ 10^{-4}$ (2)	$-\ 1.29\ 10^{-4}$ (2)
$T_0(X^1\Sigma^+)$	0.0 (b)	0.0 (b)	0.0 (b)	985.674 (2)
$B_0(X^1\Sigma^+)$	0.787271 (5)	0.787309 (16)	0.787270 (6)	0.780593 (2)
$D_0(X^1\Sigma^+)$ (c)	$2.0\ 10^{-6}$ (b)	$2.0\ 10^{-6}$ (b)	$2.0\ 10^{-6}$ (b)	$2.0\ 10^{-6}$ (b)

in BeBr λ_{00} = 26 450 cm^{-1}, where BeBr is the beryllium monohalide with r_e ($X^2\Sigma^+$, 1.95 Å) most similar to that of BeS ($a^3\Pi$, 1.92 Å). The $^3\Delta$–$a^3\Pi$ transition is the largest wavelength fully allowed transition out of the $a^3\Pi$ state and the corresponding transition is prominent in the spectra of MgO and CaO. The $^3\Sigma^+$ and $^3\Sigma^-$ states isoconfigurational with $^3\Delta$ cannot be the upper state of the UV system because the head separations would have to be 180 cm^{-1}; there would be three groups of multiple heads and each head would necessarily be less intense than a nearby $^3\Delta$–$a^3\Pi$ head. Unfortunately, there are several arguments against the $^3\Delta$–$a^3\Pi$ assignment. The appearance of the UV bandheads is decidedly that of a parallel rather than perpendicular transition. Each $\Delta\Lambda = \Delta\Omega$ subband should have a head in the R branch and a head-like feature at the Q-branch origin. They merge into one head only if the R head occurs at low J (large ΔB). In addition, a semiempirical calculation of the Λ doubling in $a^3\Pi_0$ $v = 0$ requires that the $^3\Delta_1$–$a^3\Pi_0$ subband at 25 924.5 cm^{-1} should be doubled by about 7 cm^{-1}. We believe that the evidence in favor of the $^3\Delta_i$–$a^3\Pi_i$ assignment is so compelling that eventually an explanation will be found for the absence of certain features in the low-resolution absorption spectrum.

POUILLY ET AL.

APPENDIX 1—*Continued*

bands	9-1		10-2		11-2	
$T_v(X^1\Sigma^+)$	14 311.27	(37)	15 102.0	(b)	15 880.0	(b)
$T_v(A^1\Pi)$	14 335.304	(14)	15 015.639	(60)	15 688.350	(45)
$T_v(a^3\Pi)$	14 540.10	(4)	15 179.0	(b)	15 810.0	(b)
$B_v(X^1\Sigma^+)$	0.6776	(5)	0.6690	(b)	0.6618	(b)
$B_v(A^1\Pi)$	0.603759	(5)	0.598241	(6)	0.592862	(19)
$B_v(a^3\Pi)$	0.58701	(7)	0.5820	(b)	0.5766	(b)
$D_v(X^1\Sigma^+)$	$2.11\ 10^{-6}$	(b)	$2.12\ 10^{-6}$	(b)	$2.13\ 10^{-6}$	(b)
$D_v(A^1\Pi)$	$1.890\ 10^{-6}$	(1)	$1.881\ 10^{-6}$	(2)	$1.87\ 10^{-6}$	(b)
$D_v(a^3\Pi)$	$1.92\ 10^{-6}$	(b)	$1.91\ 10^{-6}$	(b)	$1.90\ 10^{-6}$	(b)
$A(a^3\Pi)$	- 179.84	(10)	- 180.0	(b)	- 180.0	(b)
β^+_{10}	- 0.0985	(10)	- 0.1038	(43)	- 0.107	(b)
A^+_{01}	- 33.4	(b)	- 30.7	(b)	- 26.1	(b)
A_{11}	- 10.41	(5)	- 11.98	(33)	- 13.25	(20)
A^+_0	- 1.5	(b)	- 1.5	(b)	- 1.5	(b)
B^+_0	$- 2.710^{-5}$	(b)	$- 2.710^{-5}$	(b)	$- 2.710^{-5}$	(b)
B^+_1	$- 4.410^{-3}$	(b)	$- 4.410^{-3}$	(b)	$- 4.410^{-3}$	(b)
$A_{\Sigma 3\Pi}$	- 4.5	(b)	- 4.7	(b)	- 4.7	(b)
$A_{\Pi 3\Pi}$	- 30.0	(b)	- 16.0	(b)	- 30.0	(b)
q	$- 0.92\ 10^{-4}$	(1)	$- 0.98\ 10^{-4}$	(3)	$- 1.08\ 10^{-4}$	(10)
$T_0(X^1\Sigma^+)$	985.664	(20)	1959.014	(6)	1959.056	(30)
$B_0(X^1\Sigma^+)$	0.780590	(10)	0.773916	(19)	0.773910	(10)
$D_0(X^1\Sigma^+)$(c)	$2.0\ 10^{-6}$	(b)	$2.0\ 10^{-6}$	(b)	$2.0\ 10^{-6}$	(b)

(a) One standard deviation is given in parentheses

(b) Fixed values in the fits

(c) Cheetham et al. (1)

ACKNOWLEDGMENTS

This research was supported in part by a NATO International Travel Grant 1177 and computer time supplied by the Laboratory for Computer Science (MIT). R. W. Field is grateful to the National Science Foundation for continuing support. The authors thank R. F. Barrow for supplying complementary spectroscopic data, for his advice throughout the work and for critically reading the manuscript.

RECEIVED: March 29, 1982

REFERENCES

1. C. J. CHEETHAM, W. J. M. GISSANE, AND R. F. BARROW, *Trans. Faraday Soc.* **61**, 1308–1316 (1965).
2. G. VERHAEGEN AND W. G. RICHARDS, *Proc. Phys. Soc.* **90**, 579–581 (1967).
3. Lines for A–X bands were not tabulated in Ref. (*1*). They were provided by R. F. Barrow from the Part II thesis of C. J. Cheetham, Oxford, 1964.
4. K. P. HUBER AND G. HERZBERG, "Constants of Diatomic Molecules," Van Nostrand–Reinhold, New York, 1979.
5. C. W. BAUSCHLICHER, JR., D. M. SILVER, AND D. R. YARKONY, *J. Chem. Phys.* **73**, 2867–2870 (1980); C. W. BAUSCHLICHER, JR., B. H. LENGSFIELD III, D. M. SILVER, AND D. R. YARKONY, *J. Chem. Phys.* **74**, 2379–2383 (1981).
6. W. B. ENGLAND, *Chem. Phys.* **53**, 1–21 (1980); C. W. BAUSCHLICHER, JR., AND D. R. YARKONY, *J. Chem. Phys.* **68**, 3990–3997 (1978).
7. R. A. GOTTSCHO, *J. Chem. Phys.* **70**, 3554–3556 (1979).
8. P. G. CUMMINS, R. W. FIELD AND I. RENHORN, *J. Mol. Spectrosc.* **90**, 327–352 (1981).
9. T. IKEDA, N. B. WONG, D. O. HARRIS, AND R. W. FIELD, *J. Mol. Spectrosc.* **68**, 452–487 (1977).
10. R. W. FIELD, *J. Chem. Phys.* **60**, 2400–2413 (1974).
11. R. A. GOTTSCHO, J. B. KOFFEND, AND R. W. FIELD, *J. Mol. Spectrosc.* **82**, 310–338 (1980).
12. Private communication to R. W. Field from Leo Brewer
13. P. K. PEARSON, S. V. O'NEIL, AND H. F. SCHAEFER III, *J. Chem. Phys.* **56**, 3938–3942 (1972); C. W. BAUSCHLICHER, JR., AND D. R. YARKONY, *J. Chem. Phys.* **72**, 1138–1144 (1980).
14. J. SCHAMPS AND H. LEFEBVRE-BRION, *J. Chem. Phys.* **56**, 573–585 (1972).
15. B. HURON, J. P. MALRIEU, AND P. RANCUREL, *Chem. Phys.* **3**, 277–283 (1974); B. HURON AND P. RANCUREL, *Chem. Phys. Lett.* **13**, 515–520 (1972).
16. R. W. FIELD, B. G. WICKE, J. D. SIMMONS, AND S. G. TILFORD, *J. Mol. Spectrosc.* **44**, 383–399 (1972).
17. R. W. FIELD, A. LAGERQVIST, AND I. RENHORN, *Phys. Scr.* **14**, 298–319 (1976).
18. P. S. BAGUS, B. LIU, A. D. MCLEAN, AND M. YOSHIMINE, "ALCHEMY," IBM Research Laboratories, San Jose, California 95114, 1972.
19. W. M. HUO, K. F. FREED, AND W. KLEMPERER, *J. Chem. Phys.* **46**, 3556–3565 (1967).
20. P. E. CADE AND W. M. HUO, *J. Chem. Phys.* **47**, 649–672 (1967).
21. C. FROESE-FISCHER, "Some Hartree-Fock Results for the Atoms Helium to Radon," Technical Report, Department of Mathematics, University of British Columbia, 1968.
22. I. KOVACS, "Rotational Structure in the Spectra of Diatomic Molecules," Elsevier, New York, 1969.
23. J. M. BROWN, J. T. HOUGEN, K. P. HUBER, J. W. C. JOHNS, I. KOPP, H. LEFEBVRE-BRION, A. J. MERER, D. A. RAMSAY, J. ROSTAS, AND R. N. ZARE, *J. Mol. Spectrosc.* **55**, 500–503 (1975).
24. J. T. HOUGEN, "The Calculation of Rotational Energy Levels and Rotational Line Intensities in Diatomic Molecules," NBS Monograph 115, U. S. Government Printing Office (SD Catalog, No. C13.44:115), Washington, D. C., 1970.
25. K. F. FREED, *J. Chem. Phys.* **45**, 4214–4241 (1966).
26. M. H. HEBB, *Phys. Rev.* **49**, 610–618 (1936).
27. A. J. KOTLAR, R. W. FIELD, J. I. STEINFELD, AND J. A. COXON, *J. Mol. Spectrosc.* **80**, 86–108 (1980).
28. R. A. GOTTSCHO, Ph.D. thesis, Department of Chemistry, Massachusetts Institute of Technology, Cambridge, Mass., 1979.
29. P. J. EVANS AND J. C. MACKIE, *Chem. Phys.* **5**, 277 (1974).
30. J. SCHAMPS AND G. GANDARA, *J. Mol. Spectrosc.* **62**, 80 (1976).

CHAPITRE III

LA MOLECULE C_2 DANS LES NUAGES INTERSTELLAIRES DIFFUS

INTRODUCTION

La présence de la molécule C_2 dans les nuages interstellaires diffus avait été suggérée par DALGARNO et BLACK (1976) comme produit de la recombinaison dissociative de C_2H^+ lui-même issu du processus d'association radiatif $C^+ + H_2$. Effectivement, en 1977, SOUZA et LUTZ détectaient la molécule C_2 dans le spectre de l'étoile Cyg OB2. Depuis cette première observation, SNOW (1978), CHAFFEE et LUTZ (1978), HOBBS (1979), CHAFFEE, LUTZ et BLACK (1980), COSMOVICI et STRAFELLA (1981), HOBBS et CAMPBELL (1982), et DANKS et LAMBERT (1982) ont détecté la présence de cette molécule vers les étoiles ζ-Perseï, 0 Perseï et ζ-Oph.

L'intérêt porté récemment à la molécule interstellaire C_2 tient d'une part au fait qu'elle constitue un test de l'importance des réactions chimiques en phase gazeuse pour la formation des molécules interstellaires, et d'autre part à l'avantage qu'elle a de posséder des raies d'absorption dans le rouge et le proche infra-rouge, donc accessibles aux télescopes terrestres, alors que jusque là, les informations sur la température, les densités et le champ de rayonnement dans les nuages interstellaires étaient déduites essentiellement des observations de la molécule H_2, dont les raies d'absorption situées dans l'ultra-violet lointain, ne sont accessibles qu'au moyen de satellites. D'autre part, les populations relatives des niveaux rotationnels de l'état fondamental $X^1\Sigma_g^+$, dont la durée de vie est très grande, sont mesurables et peuvent fournir des méthodes de diagnostic sensibles des conditions physiques des nuages responsables des raies d'absorption.

La détection vers ζ-Perseï de raies interstellaires du système de PHILLIPS ($A^1\Pi_u - X^1\Sigma_g^+$) provenant de niveaux rotationnels jusque J = 10 (CHAFFEE, LUTZ et BLACK (1980)) a permis la détermination de la densité de colonne de C_2 et a fourni une température du milieu de l'ordre de 97K apparemment en désaccord avec la température cinétique de 45K déduite du modèle de BLACK, HARTQUIST et DALGARNO (1970) construit à partir des raies U.V. de H_2. Un désaccord existe aussi au niveau des températures calculées pour le nuage ζ-Oph entre les mesures de SNOW (1978) à partir des raies de C_2 et celles de BLACK et DALGARNO (1977) obtenues à partir des raies de H_2. Mais la tempéra-

ture rotationnelle déterminée à partir des observations de CHAFFEE, LUTZ et BLACK (1980) n'est une bonne mesure de la température cinétique des gaz que si les collisions inélastiques avec les espèces abondantes du milieu interstellaire (typiquement H et H_2) dominent l'équilibre statistique des populations rotationnelles. Or, un certain nombre de mécanismes non collisionnels sont susceptibles d'affecter ces populations :

a - La photodissociation directe à partir de l'état $X^1\Sigma_g^+$

b - Les processus radiatifs mettant en jeu l'état fondamental

- cascades radiatives dues au moment quadrupolaire ;
- pompage radiatif dans le spectre discret d'absorption (bandes de PHILLIPS $A^1\Pi_u \leftarrow X^1\Sigma_g^+$, transitions vers les niveaux liés des états $^1\Pi_u$ plus excités, bandes de MULLIKEN $D^1\Sigma_u^+ \leftarrow X^1\Sigma_g^+$) suivi de fluorescence dans les différents niveaux vibrationnels de l'état fondamental. La figure III.a présente la position des courbes de potentiel des états qui interviennent dans ces processus.

c - La transition d'intercombinaison $a^3\Pi_u - X^1\Sigma_g^+$ par interaction spin-orbite et mettant en jeu l'état $a^3\Pi_u$ très proche du fondamental (figure III.a).

En raison de la difficulté d'atteindre expérimentalement les paramètres physiques intervenant dans ces processus, les astrophysiciens en ont souvent été réduits à les estimer. Mais pour déterminer les conditions physiques dans les nuages interstellaires, ces estimations se sont révélées trop imprécises. Le besoin d'autres valeurs s'est donc fait sentir et ce travail constitue une approche théorique à l'étude de ces divers phénomènes. Avant de présenter nos résultats théoriques, nous allons résumer l'état actuel des connaissances sur les points précédemment exposés.

Le taux de photodissociation global (point a) à partir de l'état $^1\Sigma_g^+$ a été estimé par BLACK, HARTQUIST et DALGARNO (1979) à 10^{-10} s^{-1} par comparaison avec d'autres molécules interstellaires connues (HD, CO, CN).

Concernant le point b, VAN DISCHOECK et BLACK (1982) ont récemment calculé les cascades quadrupolaires à l'intérieur de l'état $X^1\Sigma_g^+$, et ont trouvé des valeurs typiques de probabilité de transition variant de 10^{-17} à 10^{-11} s^{-1} pour des valeurs du nombre quantique de rotation J comprises entre 2 et 20. La deuxième partie du point b, c'est-à-dire le pompage radiatif

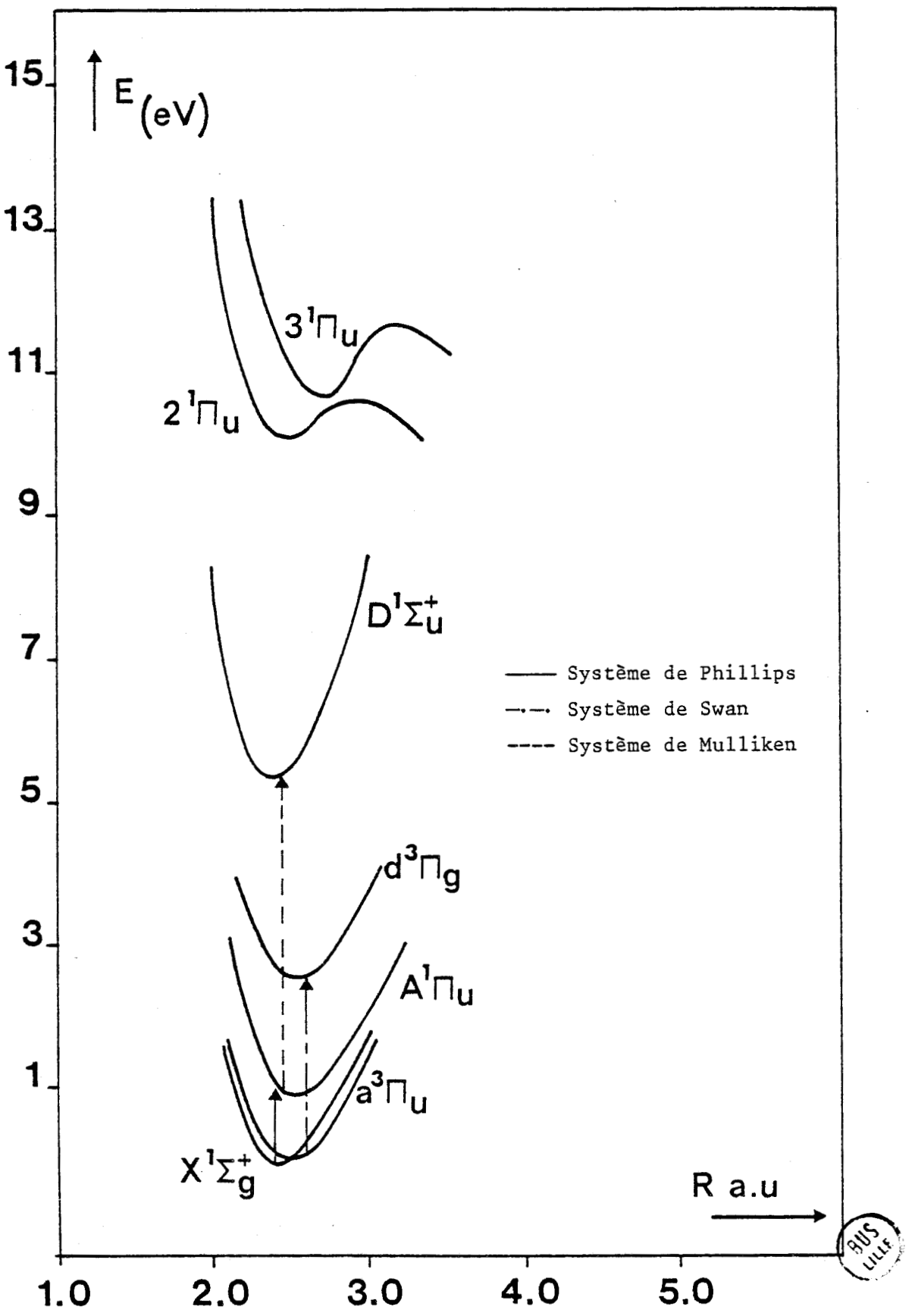

FIGURE III.a

Position des courbes de potentiel des états de C_2.

nécessite la connaissance des moments de transition des differents systèmes concernés. Plusieurs valeurs différentes de la force d'oscillateur f_{00} du système de PHILLIPS $A^1\Pi_u - X^1\Sigma_g^+$ ont été obtenues expérimentalement : 4×10^{-3} par COOPER et NICHOLLS (1975) et 2.5×10^{-3} par ROUX, CERNY et d'INCAN (1976), $2.3 \times 10^{-3} - 1.5 \times 10^{-3}$ par ERMAN, LAMBERT, LARSSON et MANNFORS (1982). Les moments de transition mettant en jeu les états $^1\Pi_u$ plus excités n'ont jamais été déterminés ni expérimentalement ni théoriquement. Enfin, deux mesures indépendantes de durée de vie pour l'état $D^1\Sigma_u^+$ (CURTIS, ENGMAN et ERMAN (1976), SMITH (1969)) donnent des résultats comparables pour le moment de transition $D^1\Sigma_u^+ - X^1\Sigma_g^+$ ($\Sigma|R_e|^2 = 0.34$ a.u. et 0.42 u.a. respectivement), résultats approximativement trois fois plus élevés qu'une troisième mesure due à COOPER et NICHOLLS (1976) $\Sigma|R_e|^2 = 0.13$ a.u.. Toutefois, compte tenu de la dépendance en longueur d'onde λ du champ de radiation interstellaire (LANG 1980) :

$$\phi = 2.44 \times 10^{-16}\ \lambda^{2.7} \text{ photons cm}^{-2}\ \text{s}^{-1}\ \text{Hz}^{-1}.$$

l'absorption dans le système de PHILLIPS ($A^1\Pi_u - X^1\Sigma_g^+$) est nettement supérieure à l'absorption dans les autres systèmes, en particulier le système de MULLIKEN $D^1\Sigma_u^+ - X^1\Sigma_g^+$. En conséquence, une incertitude sur le moment de transition de ce système n'est pas critique ; c'est la raison pour laquelle nous n'avons pas jugé utile de le calculer.

Enfin, les transitions d'intercombinaison (point c) se sont révélées importantes pour expliquer les intensités des systèmes singulets et triplets dans le spectre d'émission des comètes (KRISHNA SWAMY et O'DELL 1979). VAN DISHOECK et BLACK (1982) ont tenté d'évaluer comment ce mécanisme peut affecter les populations rotationnelles de l'état fondamental de C_2. Leur calcul repose sur l'utilisation d'une valeur du carré du moment de transition $\Sigma|R_e|^2_{a-X}$ égale à (1-2) 10^{-5} u.a., suggérée par A'HEARN et FELDMAN (1980). Cette valeur a été déduite à la fois des mesures des forces de bandes relatives des systèmes de MULLIKEN ($D^1\Sigma_u^+ - X^1\Sigma_g^+$) faites par COOPER et NICHOLLS (1976) et du système de SWAN ($d^3\Pi_g - a^3\Pi_u$) (KRISHNA SWAMY et O'DELL (1979)). Or récemment, LAMBERT et DANKS (1982) ont calculé que si on utilisait comme valeur de la force d'oscillateur du système de MULLIKEN celle déduite des mesures de CURTIS, ENGMAN et ERMAN (1976) ou de SMITH (1969), la force d'oscillateur de la transition d'intercombinaison $a^3\Pi_u - X^1\Sigma_g^+$ serait divisée par un facteur 100. Le carré du moment de transition correspondant serait d'environ

10^{-7} u.a. Tout récemment de nouvelles mesures de durée de vie radiatives du système de PHILLIPS (ERMAN, LAMBERT, LARSSON et MANNFORS (1982)) et des résultats de l'analyse des raies solaires du même système (BRAULT, DELBOUILLE, GREVESSE, ROLAND, SAUVAL et TESTERMAN (1982)) viennent d'être publiées. Si l'on utilise ces nouvelles données pour interpréter le rapport d'intensité du système de PHILLIPS au système de SWAN dans les comètes on doit supposer une valeur du carré du moment de transition $a^3\Pi_u - X^1\Sigma_g^+$ égale à $\Sigma|R_e|^2_{a-X} = 10^{-3}$ a.u. Ainsi, il apparaît clairement que ces valeurs extrêmement dispersées (de 10^{-7} à 10^{-3} u.a.) ne peuvent être guère utilisées pour obtenir des valeurs fiables des probabilités de transition entre les états $a^3\Pi_u$ et $X^1\Sigma^+$, et l'on doit envisager une méthode d'approche différente de ce problème.

La première partie de ce travail, qui a déjà fait l'objet d'une publication, présente des calculs ab-initio relatifs aux points a et b (sections efficaces de photodissociation, cascades quadrupolaires, forces d'oscillateur) la seconde partie concerne l'étude de la transition d'intercombinaison en utilisant pour le moment de transition $\Sigma|R_e|^2_{a-X}$ une valeur qui peut être déduite de nos calculs ab initio du moment de transition $\Sigma|R_e|^2_{A-X}$ du système de PHILLIPS en considérant le couplage spin-orbite entre les états $A^1\Pi_u$ et $a^3\Pi_u$. Enfin la dernière partie présente une discussion des résultats obtenus.

I - PHOTODISSOCIATION ET PROCESSUS RADIATIFS DANS LA MOLECULE C_2 INTERSTELLAIRE

J. Phys. B: At. Mol. Phys. **16** (1983) 437–448. Printed in Great Britain

Photodissociation and radiative processes in interstellar C_2

B Pouilly†, J M Robbe†, J Schamps† and E Roueff‡

† Laboratoire de Spectroscopie des Molécules Diatomiques, Equipe de Recherche Associée au CNRS no 303, Université des Sciences et Techniques de Lille, UER de Physique Fondamentale, Bâtiment P5, 59655, Villeneuve D'Ascq Cédex, France

‡ Observatoire de Meudon, Département d'Astrophysique Fondamentale, 92190, Meudon, France

Received 29 July 1982, in final form 4 October 1982

Abstract. *Ab initio* methods are used to compute photodissociation and radiative processes occurring in interstellar C_2 from the $X\,^1\Sigma_g^+$ ground state.

To this end, self-consistent-field + configuration interaction wavefunctions and potential energy curves of the $X\,^1\Sigma_g^+$ and the first four $^1\Pi_u$ states and transition moments between the ground and excited electronic states are computed. Photodissociation cross sections for absorption into the second and third $^1\Pi_u$ states are calculated and the corresponding interstellar photodissociation probability is found to be $0.73\times10^{-10}\,s^{-1}$. Ground-state transition probabilities and absorption oscillator strengths f_{00} of the Phillips ($A\,^1\Pi_u$–$X\,^1\Sigma_g^+$) and $2\,^1\Pi_u$–$X\,^1\Sigma_g^+$ systems are determined.

1. Introduction

Interstellar C_2 molecules have been detected to date in four locations (Hobbs and Campbell 1982). Along each of the light paths towards ζ Perseï, o Perseï and ζ Oph, the detection of interstellar lines arising from levels up to $J = 10$ has provided an accurate total column density of C_2 and has allowed an analysis of the rotational excitation equilibrium. In three directions, the various level populations can be characterised by a single excitation temperature near $T = 100$ K. However, this rotational temperature, experimentally determined, is not a good measure of the kinetic temperature because the photodissociation mechanism and the competition between collisional and radiative processes alter the level populations from those expected in pure thermal equilibrium. The purpose of this paper is to use *ab initio* methods to compute the rate of direct photodissociation from the $X\,^1\Sigma_g^+$ ground state. At the same time different radiative processes relevant to the chemistry of interstellar C_2 are studied. They include radiative cascades inside the electronic ground state by quadrupole transitions and radiative pumping mechanisms from the ground state in the discrete part of the absorption spectrum.

2. Electronic wavefunction calculations

Most calculations on the C_2 molecule have been related to the Swan bands electronic transition moment. Only a few theoretical calculations have been devoted to other valence states.

0022-3700/83/030437+12$02.25

B Pouilly, J M Robbe, J Schamps and E Roueff

The most complete work is that of Kirby and Liu (1979) whose original motivation was the location of dissociative states which can play a role in photodissociation processes from the $X\,^1\Sigma_g^+$ ground state. Then Dupuis and Liu (1980) calculated more accurate potential energy curves of C_2 and C_2^- ground states and very recently Van Dishoeck and Black (1982) (hereafter referred to as VDB) published a work devoted to the excitation of interstellar C_2.

Before undertaking the study of radiative processes in interstellar C_2 from the $X\,^1\Sigma_g^+$ ground state, we have to select the possible final channels. Due to symmetry selection rules, only $^1\Sigma_u^+$ and $^1\Pi_u$ symmetries can be involved in dipole transitions.

With regard to $^1\Sigma_u^+$ symmetry, the potential curves reported by Kirby and Liu (1979) show that there is one bound valence state, $D\,^1\Sigma_u^+$, lying within 13.6 eV (the cut-off in the interstellar medium $\lambda = 912$ Å) of the ground state. This $D\,^1\Sigma_u^+$ state dissociates into $C(2p^2\,^1D) + C(2p^2\,^1S)$ at about 10.18 eV above $X\,^1\Sigma_g^+$, assuming an experimental dissociation energy of 6.23 eV for the $X\,^1\Sigma_g^+$ state. Because the repulsive part of the $D\,^1\Sigma_u^+$ potential curve lies far from the Franck–Condon vertical excitation region, the contribution of the continuum of this state to the total photodissociation processes may be neglected. Except for $C(2p^2\,^1D) + C(2p^2\,^1S)$, there is no dissociation limit within 13.6 eV for $^1\Sigma_u^+$ states. The $C(2p^2\,^3P) + C(2p3s\,^3P)$ limit, where the two $^1\Sigma_u^+$ states dissociate, lies at 13.71 eV. Hence, the $^1\Sigma_u^+$ photodissociation channel can be ruled out.

For the $^1\Pi_u$ symmetry, the problem is more complicated because valence and Rydberg states occur within the limit $\lambda = 912$ Å. Herzberg *et al* (1969) located a $^1\Pi_u$ Rydberg state that they called $F\,^1\Pi_u$ at about 9.24 eV above $X\,^1\Sigma_g^+$. This state does not appear in the calculations of Kirby and Liu (1979) because their orbital basis set contains no diffuse orbitals. Kirby and Liu considered their second $^1\Pi_u$ root as a possible photodissociation channel since the state is dissociative. We expect that interactions between $F\,^1\Pi_u$ and this second calculated root will modify in a sensitive way the shape of the $2\,^1\Pi_u$ state and a mixed valence Rydberg orbital basis set is needed to account for the photodissociation into $^1\Pi_u$ states.

We started from the extended basis set of Slater-type functions of Kirby *et al* (1980a, b) for the carbon atom in their CH^- calculations. It consists of the (5s/4p) basis of Clementi and Roetti (1974) augmented by two 3d polarisation functions and two Rydberg 3s and 3p functions with exponents optimised for the carbon atom Rydberg states ^1P and ^3D respectively. We added to this set two new Rydberg 4s and 4p functions (exponents 0.35). In our calculations, valence orbitals were centred on each carbon atom, while Rydberg orbitals were centred on the centre of charge of the molecule. Preliminary tests of the linear independence of the atomic basis set showed that some eigenvalues of the overlap matrix S were lower than 2×10^{-4}. This value was defined by Bagus and Wahlgreen (1976) as the limit beyond which the basis set is linearly dependent. Following this criterion, we deleted the 3s function (exponent 1.29478) and the 2p function (exponent 0.96499) responsible for such a small eigenvalue. The final basis set is reported in table 1.

The SCF molecular orbitals obtained in this way served as basis orbitals for the configuration interaction (CI) calculations. The first step in the CI wavefunction determination consists in constructing a full valence CI (FVCI) wavefunction, which includes all the valence configuration state functions (CSF) of the appropriate symmetry generated by distributing eight valence electrons among the valence orbitals—$2\sigma_{g,u}$, $3\sigma_{g,u}$, $1\pi_{g,u}$—the core $1\sigma_{g,u}$ orbitals being frozen. Typically 142 CSF for $^1\Sigma_g^+$ symmetry and 176 CSF for $^1\Pi_u$ symmetry were obtained.

Table 1. Slater basis set for C_2 calculations.

nl	zèta
1s	9.250 13
1s	5.538 75
2s	5.305 67
2s	2.041 26
2s	1.305 52
3s	0.583 80
4s	0.35
2p	6.532 86
2p	2.607 86
2p	1.440 37
3p	1.232 10
3p	0.479 60
4p	0.35
3d	2.35
3d	1.24

Following these FVCI calculations, three different first-order CI (FOCI) calculations were performed: one for $^1\Sigma_g^+$ and two for $^1\Pi_u$ symmetry. Let us consider first the $^1\Sigma_g^+$ symmetry case.

Because we are mainly interested by radiative processes from the ground state or radiative cascades inside it, the $^1\Sigma_g^+$ FOCI was constructed to obtain a good representation of the $X\,^1\Sigma_g^+$ wavefunction only. The FVCI $^1\Sigma_g^+$ configuration space was extended by adding all CSF obtained by the removal of one valence electron in the virtual orbitals $4\sigma_{g,u} \rightarrow 6\sigma_{g,u}$ and $2\pi_{g,u} \rightarrow 5\pi_{g,u}$ with the constraint that each CSF must be related to the reference determinant $1\sigma_g^2 2\sigma_g^2 1\sigma_u^2 2\sigma_u^2 1\pi_u^4$ by at most two electron replacements. The total number of CSF is 254.

The $^1\Pi_u$ symmetry case presents quite a different problem since we need good representations in the whole R range not only for the lowest $A\,^1\Pi_u$, but also for all the $^1\Pi_u$ states which dissociate to a limit lower than 13.6 eV above $X\,^1\Sigma_g^+$. A brief study of the correlation between separated-atom limits and molecular states show that there is one $^1\Pi_u$ dissociating into $C(^3P)+C(^3P)$ limit, two into $C(^1D)+C(^1D)$, and one into $C(^1D)+C(^1S)$, where ^3P, ^1D and ^1S are the atomic states arising from the $1s^2 2s^2 2p^2$ configuration. Hence we need, at most, to account for the four lowest $^1\Pi_u$ states. FOCI was constructed starting from the same set of orbitals as for $^1\Sigma_g^+$ symmetry but now several reference determinants have to be considered. The FVCI results have shown that at least twelve reference CSF are needed to account correctly for the potential curves of the lowest $^1\Pi_u$ states. These reference CSF have been shared in two groups: the first one, referred as FOCI I, to describe the potential curves at R lower than 3.5 au, is composed of the following configurations:

$$1\sigma_g^2\ \ 2\sigma_g^2\ \ 3\sigma_g\ \ 1\sigma_u^2\ \ 2\sigma_u^2\ \ 1\pi_u^3$$
$$1\sigma_g^2\ \ 2\sigma_g^2\ \ 4\sigma_g\ \ 1\sigma_u^2\ \ 2\sigma_u^2\ \ 1\pi_u^3$$
$$1\sigma_g^2\ \ 2\sigma_g^2\ \ 3\sigma_g^2\ \ 1\sigma_u^2\ \ 2\sigma_u\ \ 1\pi_u^2\ \ 1\pi_g$$

and the second one called FOCI II to insure a correct dissociation of these lowest $^1\Pi_u$ states. is composed of configurations in which $1\sigma_g$, $2\sigma_g$, $1\sigma_u$ and $2\sigma_u$ molecular orbitals

are fully occupied since they are correlated with the 1s and 2s atomic orbitals. These selected configurations are:

$$1\sigma_g^2\ 2\sigma_g^2\ 3\sigma_g\ 1\sigma_u^2\ 2\sigma_u^2\ \ 1\pi_u^3$$
$$1\sigma_g^2\ 2\sigma_g^2\ \ 1\sigma_u^2\ 2\sigma_u^2\ 3\sigma_u\ \ 1\pi_g^3$$
$$1\sigma_g^2\ 2\sigma_g^2\ 3\sigma_g\ 1\sigma_u^2\ 2\sigma_u^2\ \ 1\pi_u\ 1\pi_g^2$$
$$1\sigma_g^2\ 2\sigma_g^2\ \ 1\sigma_u^2\ 2\sigma_u^2\ 3\sigma_u\ 1\pi_u^2\ 1\pi_g.$$

With the constraint that each CSF must be related to the whole reference determinants by at most two electron replacements, the total number of CFS is 2449 for FOCI I and 2388 for FOCI II. To restrict the $^1\Pi_u$ configuration spaces, we use the method of the 'nearly empty CI matrix' developed by Raseev (1977). It consists in diagonalising a matrix filled only on its diagonal and on a number of lines equal to the number of reference determinants. Then, all CSF with coefficients greater than a threshold (respectively 3×10^{-4} (FOCI I) and 1×10^{-4} (FOCI II)) were kept. In this case 230 and 281 CSF were selected. A complete diagonalisation of the matrix built on these determinants was finally performed.

Using the ALCHEMY programs (Bagus *et al* 1972), we performed calculations of wavefunctions, energies, electronic transition and quadrupole moment functions.

A comparison of our $X\ ^1\Sigma_g^+$ SCF energy at the internuclear equilibrium separation ($R = 2.348$ au) with other published results is given in table 2. It shows that our basis set is reliable for the calculations of the energies of the different states. In the same table, the second column shows CI results obtained with various degrees of configuration interaction. Our CI results differ by only 0.009 au from those of Kirby and Liu (1979) although they have performed MCSCF + CI calculations.

Table 2. Comparison between our $X\ ^1\Sigma_g^+$ (SCF and CI) energy results and other published results (au).

SCF results ($R = 2.348$ Bohr)		CI results ($R = 2.348$ Bohr)	
This work	−75.401 94	This work	−75.603 66
A	−75.405 87	A	−75.716 66
B	−75.405 6	B (INO)	−75.678 1
C	−75.406 20	D	−75.612 20

A, Dupuis and Liu (1980).
B, Van Dishoeck and Black (1982).
C, Cade and Wahl (1974).
D, Kirby and Liu (1979).

The differences are larger between our results and those of Van Dishoek and Black (1982), and especially with those of Dupuis and Liu (1980), differences which are simply explained by the size of the CI used by these authors (1850 CSF in VDB, single double CI in SDCI of Dupuis and Liu (1980)).

The CI energies of $X\ ^1\Sigma_g^+$ and the first four $^1\Pi_u$ states are collected in table 3. We have verified that, at $R = 3.5$ au, the two $^1\Pi_u$ parts are smoothly joined. Potential curves obtained by cubic fits to the energies are given in figure 1.

Table 3. The CI energies for the $X\ ^1\Sigma_g$ state and the lowest $^1\Pi_u$ states of C_2 (au).

States \ R(au)	1.75	2.04	2.24	2.44	2.64	2.74
$X\ ^1\Sigma_g^+$	−75.286 27	−75.536 08	−75.593 34	−75.603 22	−75.588 29	−75.576 00
$A\ ^1\Pi_u$	−75.155 23	−75.460 43	−75.541 83	−75.569 21	−75.566 25	−75.558 07
$F\ ^1\Pi_u$	−74.867 96	−75.146 80	−75.216 30	−75.235 01	−75.226 59	−75.217 31
$3\ ^1\Pi_u$	−74.788 60	−75.057 04	−75.135 95	−75.191 96	−75.213 54	−75.216 24
$4\ ^1\Pi_u$	−74.718 96	−75.019 43	−75.117 54	−75.128 33	−75.152 37	−75.161 65

States \ R(au)	2.84	3.00	3.50	6.00	10.0
$X\ ^1\Sigma_g^+$	−75.562 09	−75.538 51	−75.472 43	−75.387 74	−75.378 69
$A\ ^1\Pi_u$	−75.547 08	−75.525 75	−75.446 78	−75.408 82	−75.405 35
$F\ ^1\Pi_u$	−75.216 97	−75.216 39	−75.252 80	−75.298 86	−75.291 79
$3\ ^1\Pi_u$	−75.205 30	−75.184 96	−75.191 15	−75.292 20	−75.289 34
$4\ ^1\Pi_u$	−75.167 52	−75.171 98	−75.081 71	−75.085 19	−75.238 81

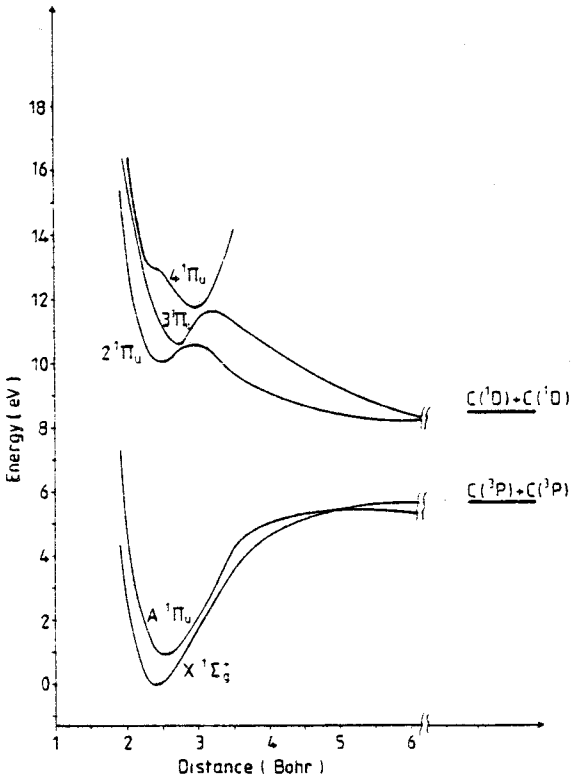

Figure 1. *Ab initio* CI potential energy curves of the $X\ ^1\Sigma_g^+$ and the four lowest $^1\Pi_u$ states of C_2.

The spectroscopic constants deduced from our theoretical potential curves are compared in table 4 with the experimental values and also with other theoretical results. Our values agree well with those of Kirby and Liu (1979). The $F\ ^1\Pi_u$ Rydberg

state is well described in our CI calculations. Its potential shape explains why only a few vibrational levels (0, 1) were observed by Herzberg *et al* (1969) and indicates that the $F\ ^1\Pi_u$ state is a good candidate for the photodissociation process (see § 4).

Table 4. Comparison between our spectroscopic constants and other published results.

States	T_e (eV) Exp	calc	A	ω_e (cm^{-1}) Exp	calc	A	B_e (cm^{-1}) Exp	calc	A
$X\ ^1\Sigma_g^+$	0	0	0	1854.8	1734	1788.6	1.820	1.74	1.76
$A\ ^1\Pi_u$	1.04	0.89	1.14	1608	1670	1507	1.6165	1.59	1.55
$F\ ^1\Pi_u$	9.24[a]	10.03	—	(1557)[b]	1703	—	1.645	1.68	—

A, Kirby and Liu (1979) results.
[a] ν_{00} value.
[b] $\Delta G(1/2)$ value.

3. Quadrupole transitions probabilities in the $X\ ^1\Sigma_g^+$ state

The quadrupole moment (in atomic units) of a linear molecule is defined as

$$Q(R)=\sum_k Z_k R_k^2-\tfrac{1}{2}\left\langle \Psi_{el}\left|\sum_i r_i^2(3\cos^2\theta-1)\right|\Psi_{el}\right\rangle$$

where Z_k is the nuclear charge of atom k, the distance from the coordinate origin for the k atom is R_k and for the ith electron r_i and Ψ_{el} is the electronic wavefunction of the $X\ ^1\Sigma_g^+$ state.

The probability of a quadrupole transition (in s^{-1}) is written as

$$A(v'J', v''J'')=\frac{\alpha^5}{15}\Delta E^5\sum_{M'}\sum_{M''}|\langle v'J'M'|Q(R)|v''J''M''\rangle|^2(2J'+1)^{-1}$$

where α is the fine-structure constant and ΔE is the transition energy in atomic units.

The sum over M' and M'' may be expressed as

$$\left|\int \psi_{v'J'}Q(R)\psi_{v''J''}\,dR\right|^2 S(J', J'')$$

where $S(J', J'')$ is a branching ratio equal to

$$\frac{J'(J'+1)(2J'+1)}{(2J'-1)(2J'+3)} \qquad \text{for } J'=J''$$

$$\frac{3(J'+1)(J'+2)}{2(2J'+3)} \qquad J'=J''-2$$

$$\frac{3J'(J'-1)}{2(2J'-1)} \qquad J'=J''+2.$$

The branching ratios ensure the correct normalisation of the calculated quantities. Note that the factor of $\frac{3}{2}$ which appears in our branching ratios has been directly included by VDB in their proportionality factor.

Processes in interstellar C_2

The rovibrational wavefunctions ψ_{vJ} are solutions of the radial Schrödinger equation in which the potential $V(R)$ is a RKR potential deduced from the spectroscopic constants of Marenin and Johnson (1970).

The CI $Q(R)$ values are given for ten internuclear separations in table 5. Figure 2 compares our SCF and FOCI functions with VDB CI results. At the SCF level, $Q(R)$ is equal to 2.84 au (compared with 2.78 au) at $R = 2.348$ Bohr. This result confirms as previously noted (VDB) that the quadrupole moment is well accounted for in the SCF approximation, provided that sufficient d polarisation orbitals are included in the basis set. This encouraging result gives confidence in our basis set for the transition moment calculations.

The main effect in the variation with R of the quadrupole moment function is due to the CI. The SCF and FOCI functions exhibit about the same behaviour with R, that is a fast increase until a maximum is reached and a decrease towards zero when R

Table 5. Ground-state quadrupole moment $Q(R)$ (au).

R(au)	1.75	2.04	2.24	2.44	2.74	2.84	3.00	3.50	6.00	10.00
$Q(R)$ (au)	0.41	1.19	1.69	2.14	2.70	2.84	3.05	3.42	4.44	4.52

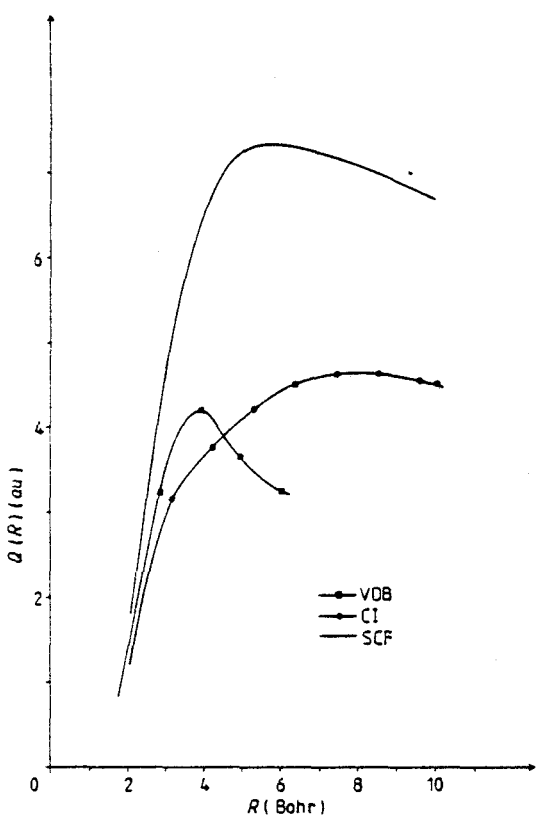

Figure 2. Comparison between our *ab initio* ground-state quadrupole moment function $Q(R)$ and the VDB functions.

becomes infinite. However, the maximum of the SCF function (7.5 au) is about twice that of the FOCI function (4.70) and is reached at a smaller R. The small differences between our FOCI function and the VDB function is ascribed to differences in the CI wavefunctions used. Since our $X\,^1\Sigma_g^+$ potential curve converges towards the good experimental dissociation limit, we think that the behaviour of the quadrupole moment function is correct at large R values. In any case, this difference does not affect the transition probabilities significantly since the $X\,^1\Sigma_g^+$ potential well is very deep and only the part between the turning points (for $v = 10$, $R_{min} = 1.98$, $R_{max} = 3.01$ au) of the $Q(R)$ function is sampled.

Our $Q(R)$ function has been extrapolated smoothly to zero each side of the calculated R range.

In table 6 the emission transition probabilities are given. For the $v = 0$ level, only transitions $J' = J'' + 2$ are to be considered. Since our $Q(R)$ function is always smaller than that of VDB in the range $R = 1.90$ to 3.00 au, our emission probabilities are smaller by a factor of about $\frac{2}{3}$ for transitions inside the $v = 0$ level.

Table 6. Emission quadrupole transition probabilities (s^{-1}). In this table $X(-y)$ stands for $X \times 10^{-y}$.

	$A(0J', 0J'')$			$A_{v'J'}$	
J'	*A*	*B*	v'	*A*	*B*
2	1.294 (−17)	1.763 (−17)	1	0.600 (−7)	0.646 (−7)
4	1.283 (−15)	1.742 (−15)	2	0.125 (−6)	0.130 (−6)
6	1.351 (−14)	1.838 (−14)	3	0.194 (−6)	0.196 (−6)
8	0.668 (−13)	9.065 (−14)	4	0.267 (−6)	0.262 (−6)
10	2.235 (−13)	3.034 (−13)	5	0.344 (−6)	0.327 (−6)
12	5.898 (−12)	8.020 (−13)	6	0.424 (−6)	0.390 (−6)
14	1.332 (−12)	1.808 (−12)	7	0.504 (−6)	0.451 (−6)
16	2.681 (−12)	3.638 (−12)	8	0.584 (−6)	0.508 (−6)
18	4.940 (−12)	6.712 (−12)	9	0.662 (−6)	0.611 (−6)

A, This work.
B, Van Dishoeck and Black (1982).

For other vibrational levels, we have calculated the quantities

$$A_{v'J'} = \sum_{v''J''} A(v'J', v''J'')$$

which are practically J independent as previously noted by VDB. Our results (table 6) are comparable with VDB. Because $A(v'J', v''J'')$ is proportional to the fifth power of ΔE which becomes much more important for $\Delta v \neq 0$ transitions, small changes in $Q(R)$ do not affect the final value of $A_{v'J'}$ significantly.

4. Oscillator strengths—photodissociation cross sections

The band oscillator strength between two different electronic states is defined as

$$f_{v'v''} = \tfrac{2}{3} g |\langle \psi_{v'}(R) | D(R) | \psi_{v''}(R) \rangle|^2 \Delta E$$

where $\psi_{v'}(R)$ and $\psi_{v''}(R)$ are respectively the final and initial vibrational nuclear wavefunctions, ΔE is the transition energy in atomic units and g is a degeneracy factor equal to two in the case of a $\Lambda' = 1$, $\Lambda'' = 0$ transition and equal to one otherwise. The electronic transition moment $D(R)$ in atomic units is given by:

$$D(R) = \left\langle \psi'_{el} \left| \sum_i \frac{1}{\sqrt{2}} (\mu_{x_i} + i\mu_{y_i}) \right| \psi''_{el} \right\rangle \qquad \text{for } \Lambda' - \Lambda'' = +1$$

or

$$D(R) = \left\langle \psi'_{el} \left| \sum_i \mu_{z_i} \right| \psi''_{el} \right\rangle \qquad \text{for } \Lambda' = \Lambda''$$

where the sum is over all electrons.

In the case of absorption into a vibrational continuum, the photodissociation cross section $\sigma_{v''}(E')$ is defined by analogy with the oscillator strength $f_{v'v''}$ as

$$\sigma_{v''}(E') = \tfrac{2}{3} K g |(\psi_{E'}(R)|D(R)|\psi_{v''}(R))|^2 \Delta E$$

where $\psi_{E'}(R)$ is an energy normalised continuum vibrational wavefunction which behaves at large R as

$$\left(\frac{2\mu}{\hbar^2} \frac{1}{\pi^2 E'}\right)^{1/4} \sin\left(\frac{2\mu E'}{\hbar^2}\right)^{1/2} R + \eta(E')$$

where μ is the reduced mass, η the scattering phaseshift and K is a proportionality factor equal to 2.688×10^{-18} in order to express $\sigma_{v''}(E')$ in cm^2 when all other quantities are in atomic units.

Figures 3 to 5 show the variation of the electronic transition moments $D(R)$ between the $X\,^1\Sigma_g^+$ ground state and the different $^1\Pi_u$ states.

In figures 4 and 5, fast changes in $D(R)$ reflect changes in the dominant configuration of the wavefunction of our second and third $^1\Pi_u$ calculated states. There is one change in our second $^1\Pi_u$ state between the Rydberg $1\pi_u^3 4\sigma_g$ and the valence $3\sigma_g^2 2\sigma_u 1\pi_u^2 1\pi_g$ configurations at about $R = 2.7$ au but in the third $^1\Pi_u$ state, the situation is more complicated with changes occurring at $R = 2.0$, 2.7 and 3.1 au.

4.1. Oscillator strengths

With our $D(R)$ functions, a value of $f_{00} = 2.5 \times 10^{-3}$ has been obtained for the $A\,^1\Pi_u$–$X\,^1\Sigma_g^+$ transition. This calculated value confirms recent experimental determinations. The first published value of 4×10^{-3} was that of Cooper and Nicholls (1975). Roux *et al* (1976) obtained $f_{00} = 2.5 \times 10^{-3}$ and recently, Erman *et al* (1982) published new $f_{v'v''}$ values ranging from 2.3×10^{-3} to 1.5×10^{-3} for f_{00}, assuming different variations of the transition moment function with the nuclear separation. Nevertheless, it seems that f_{00} must be closer to 2.5×10^{-3} rather than to 1.5×10^{-3} since this last result was obtained by Erman *et al* (1982) assuming an R dependence for $D(R)$ opposite to that given in our calculations as well as by VDB.

For the $F\,^1\Pi_u$–$X\,^1\Sigma_g^+$ transition a calculated value of $f_{00} = 0.02$ has been obtained, compared with the value of $f_{00} = 0.1$ estimated by Chaffee *et al* (1980).

4.2. Photodissociation cross sections

Using a cubic spline fit to the potential curves and transition moments, we have

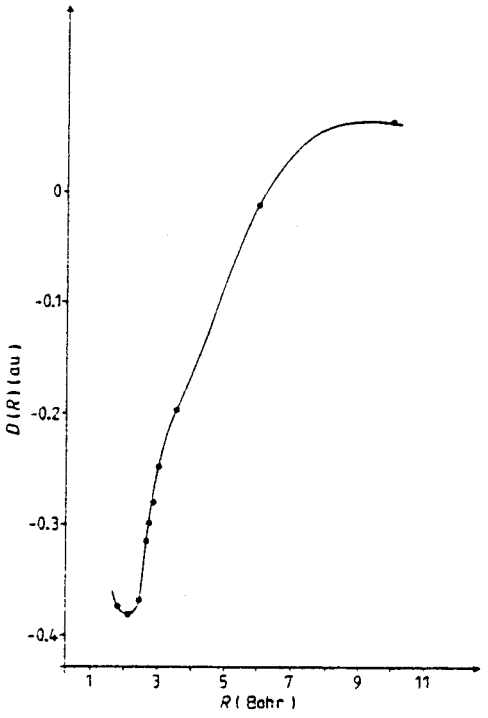

Figure 3. Electronic transition moment

$$\left\langle X\,{}^1\Sigma_g^+ \middle| \sum_i \frac{1}{\sqrt{2}}(\mu_{xi}+\mu_{yi}) \middle| A\,{}^1\Pi_u \right\rangle$$

as a function of internuclear separation.

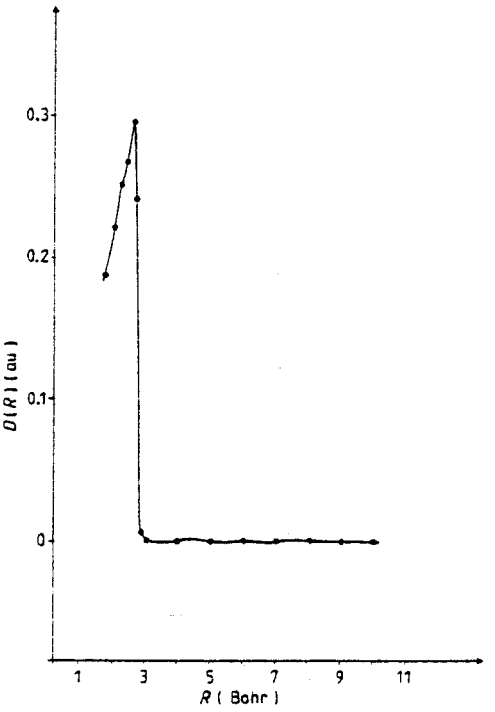

Figure 4. Electronic transition moment

$$\left\langle X\,{}^1\Sigma_g^+ \middle| \sum_i \frac{1}{\sqrt{2}}(\mu_{xi}+\mu_{yi}) \middle| 2\,{}^1\Pi_u \right\rangle$$

as a function of internuclear separation.

computed the photodissociation cross sections for absorption into the second and third $^1\Pi_u$ states from the $X\,^1\Sigma_g^+$ $v=0, J=0$ level. The variations with photon energy are shown in figure 6. The sharp peak at 10.51 eV is probably due to quasi-bound levels in the second $^1\Pi_u$ state.

Except for this peak, figure 6 shows that both the second and third $^1\Pi_u$ states contribute to the photodissociation process. For the first, the cross section reaches its maximum value 0.5×10^{-17} cm^2 at 10.60 eV and for the second a value of 0.77×10^{-17} cm^2 is obtained at 12.2 eV. The photodissociation probability P is defined by

$$P=\frac{1}{h}\int_{912\text{Å}}^{\lambda_T} U_\lambda \sigma_\lambda \lambda \, d\lambda \ (s^{-1})$$

where σ_λ is the photodissociation cross section, λ_T a threshold wavelength lying in the ultraviolet range of wavelengths (1300 Å here) and U_λ the energy density of the radiation field at wavelength λ. In the wavelength range studied U_λ is held constant and equal to 4×10^{-17} erg cm^{-3} Å^{-1} (Lang 1980).

We have found 0.73×10^{-10} s^{-1} for the value of P. Using their own model of the diffuse interstellar cloud in the line of sight to ζ Per and with a value of P estimated at 10^{-10} s^{-1}, Black *et al* (1978) predicted a column density of 1.4×10^{13} cm^{-2}, a prediction confirmed by the study of interstellar C_2 towards ζ Per by Chaffee *et al* (1980). Hence, our calculated P value reinforces the assumptions of Black *et al* (1978).

Processes in interstellar C_2

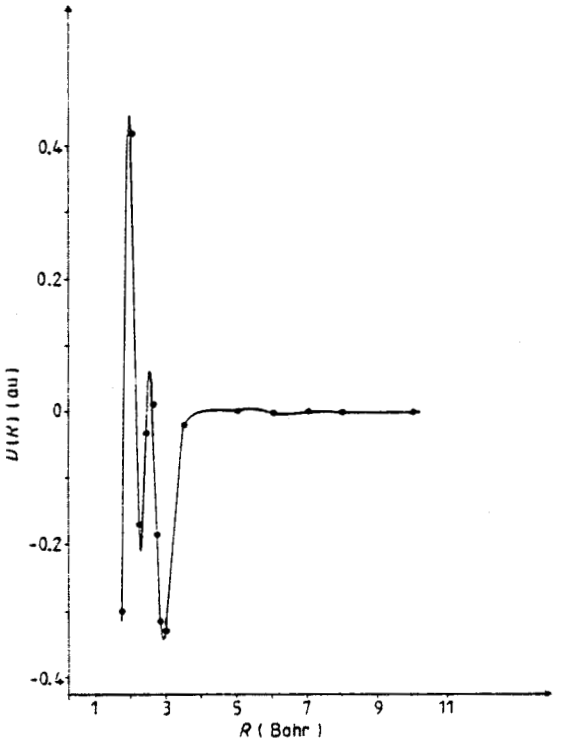

Figure 5. Electronic transition moment

$$\left\langle X\,{}^1\Sigma_g^+ \middle| \sum_i \frac{1}{\sqrt{2}}(\mu_{xi} + \mu_{yi}) \middle| 3\,{}^1\Pi_u \right\rangle$$

as a function of internuclear separation.

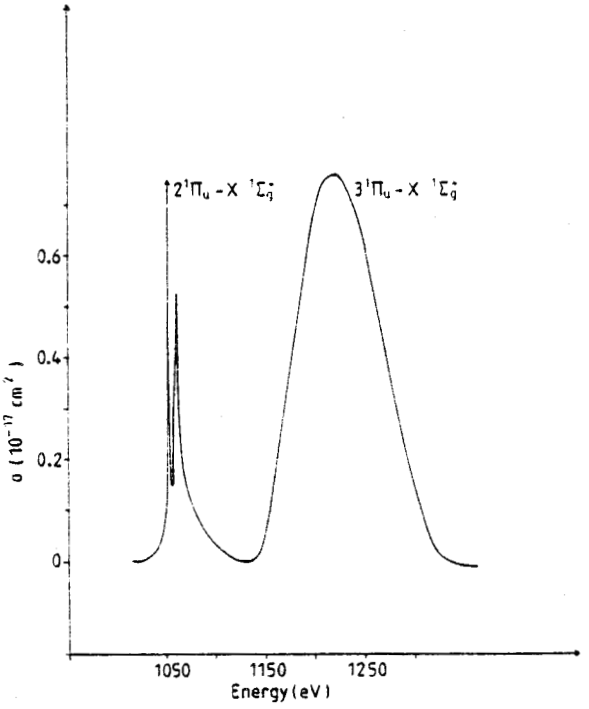

Figure 6. Photodissociation cross section from the $v'' = 0$ level of the $X\,{}^1\Sigma_g^+$ ground state as a function of the photon energy.

5. Concluding remarks

In this work are presented the first *ab initio* calculations of photodissociation and radiative processes occurring in the C_2 molecule from the $X\ ^1\Sigma_g^+$ ground state. Starting from a mixed valence Rydberg basis set of atomic orbitals, we were able to account correctly for the locations and potential shapes of the $X\ ^1\Sigma_g^+$ and $^1\Pi_u$ states lying below the cut-off limit of the H_α Lyman line ($\lambda = 912$ Å). We have shown that the $F\ ^1\Pi_u$ state observed by Herzberg *et al* (1969) is indeed a Rydberg state with main configurations $(1\sigma_g^2 2\sigma_g^2 1\sigma_u^2 2\sigma_u^2 1\pi_u^3)3p\sigma$.

Our transition moments are precise enough to compute correctly the f_{00} value of the $A\ ^1\Pi_u$–$X\ ^1\Sigma_g^+$ transition and to confirm recent experimental measurements. The $D(R)$ functions serve as input in photodissociation processes calculations which show that the interstellar photodissociation probability is about $0.73 \times 10^{-10}\ s^{-1}$, a value in good agreement with assumptions currently made in order to interpret astrophysical data on C_2.

Acknowledgments

The authors thank Helene Lefebvre-Brion for reading the manuscript critically, Georges Raseev for his advice during calculations and the referee for constructive recommendations.

References

Bagus P S, Liu B, McLean A D and Yoshime M 1972 *ALCHEMY* IBM Research Laboratory San Jose, California 95114, USA
Bagus P S and Wahlgren U I 1976 *Comput. Chem.* **1** 95–101
Black C J, Hartqvist T W and Dalgarno A 1978 *Astrophys. J.* **224** 448–52
Cade P E and Wahl A C 1974 *At. Data Nucl. Data Tables* **13** 339
Chaffee F H, Lutz B L and Black J H 1980 *Astrophys. J.* **236** 474–82
Clementi E and Roetti C *At. Data Nucl. Data Tables* 1974 **14** 282
Cooper D M and Nicholls R W 1975 *J. Quant. Spectrosc. Radiat. Transfer* **15** 139–50
Dupuis M and Liu B 1980 *J. Chem. Phys.* **73** 337–42
Erman P, Lambert D L, Larsson M and Mannfors B 1982 *Astrophys. J.* **253** 983–9
Herzberg G, Lagerqvist A and Malmberg C 1969 *Can. J. Phys.* **47** 2735–2743
Hobbs L M and Campbell B 1982 *Astrophys. J.* **254** 108–110
Kirby K and Liu B 1979 *J. Chem. Phys.* **70** 893–900
Kirby K, Roberge W G, Saxon R P and Liu B 1980a *Astrophys. J.* **239** 855–8
Kirby K, Saxon R P and Liu B 1980b *J. Chem. Phys.* **73** 1873–9
Lang K R 1980 *Astrophysical Formulae* (Berlin: Springer) p 167
Marenin I R and Johnson H R 1970 *J. Quant. Spectrosc. Radiat. Transfer* **10** 305–9
Raseev G 1977 *Chem. Phys. Lett.* **47** 36–42
Roux F, Cerny D and D'Incan J 1976 *Astrophys. J.* **204** 940–3
Van Dishoeck E and Black J H *Astrophys. J.* **258** 533–47

II - TRANSITION D'INTERCOMBINAISON $a^3\Pi_u - X^1\Sigma_g^+$

1) Généralités

La probabilité d'émission dipolaire d'EINSTEIN (s^{-1}) entre les niveaux rovibroniques (v' J') et (v" J") de deux états électroniques différents est définie par :

$$A\ (v'\ J',\ v''\ J'') = \frac{64\pi^4}{3h}\ \nu^3 \sum_{M'M''} \frac{\left|< \psi'\ v'\ J'\ M' \left| \sum_i e_i \vec{r}_i \right| \psi''\ v''\ J''M'' >\right|^2}{(2J' + 1)} \qquad (III.1)$$

ν caractérise la fréquence de la transition. Le terme qui apparait sous la somme représente un élément de matrice de l'opérateur moment dipolaire exprimé dans le référentiel fixe du laboratoire et la sommation sur i s'étend à toutes les particules de charge e_i (noyaux et électrons).

Puisque nous sommes concernés dans ce problème par l'intensité d'une émission spontanée, la lumière correspondante n'est pas polarisée, et les trois directions de l'espace X, Y et Z du référentiel fixe sont équivalentes. L'utilisation de la seule composante μ_Z du moment dipolaire conduit à la règle de sélection $\Delta M = 0$ et permet de réduire la double sommation qui apparaît dans l'expression précédente (III.1)

$$A\ (v'\ J',\ v''\ J'') = \frac{64\pi^4}{3h}\ \nu^3\ \frac{\sum_M 3\left|< \psi'\ v'\ J'\ M \left| \sum_i \mu_{Z_i} \right| \psi''\ v''\ J''\ M >\right|^2}{(2J' + 1)} \qquad (III.2)$$

où M varie de - J' à + J'.

La factorisation de la fonction d'onde totale en un terme électronique, un terme vibrationnel et un terme rotationnel permet d'écrire la sommation sous la forme :

$$\sum_{M} 3\left|\langle \psi' v' J' M \left| \sum_{i} \mu_{Z_i} \right| \psi'' v'' J'' M \rangle\right|^2 = \left| \int \psi_{v'} (R)\, D (R)\, \psi_{v''} (R)\, dR \right|^2 \cdot S_{J'J''} \qquad \text{(III.3)}$$

R est la distance internucléaire, D (R) le moment de transition électronique, $\psi_{v'}$ et $\psi_{v''}$ les fonctions d'onde vibrationnelles ; toutes les quantités sont exprimées dans le référentiel de la molécule. Le terme $S_{J'J''}$ est un facteur de force de raie ou facteur de HÖNL-LONDON.

Les facteurs de HÖNL-LONDON tabulés pour les transitions électroniques les plus importantes (KOVACS) obéissent aux règles de sommation (WHITING, SCHADEE, TATUM, HOUGEN, NICHOLLS (1980))

$$\sum_{J''} S_{J'J''} = (2 - \delta_{0,\Lambda'}\, \delta_{0,\Lambda''})\ (2S + 1)\ (2J' + 1) \qquad \text{(III.4)}$$

$$\sum_{J'} S_{J'J''} = (2 - \delta_{0,\Lambda'}\, \delta_{0,\Lambda''})\ (2S + 1)\ (2J'' + 1) \qquad \text{(III.5)}$$

2) Application à la transition d'intercombinaison de C_2

A la température des nuages interstellaires diffus, la molécule C_2 existe essentiellement dans son état fondamental $X\,^1\Sigma_g^+$. Sa présence dans les niveaux vibrationnels et rotationnels excités de cet état provient de l'absorption dans les niveaux liés des états électroniques $A\,^1\Pi_u$, $D\,^1\Sigma_u^+$, $F\,^1\Pi_u$ et $3\,^1\Pi_u$ suivie de fluorescence dans les différents niveaux vibrationnels de l'état fondamental.

L'état métastable $a\,^3\Pi_u$, longtemps considéré comme l'état fondamental n'est situé qu'à 716 cm^{-1} de l'état $X\,^1\Sigma_g^+$ si bien que les composantes vibrationnelles de ces deux états sont très proches. La figure III.b donne la position en énergie des différentes composantes vibrationnelles de ces deux états.

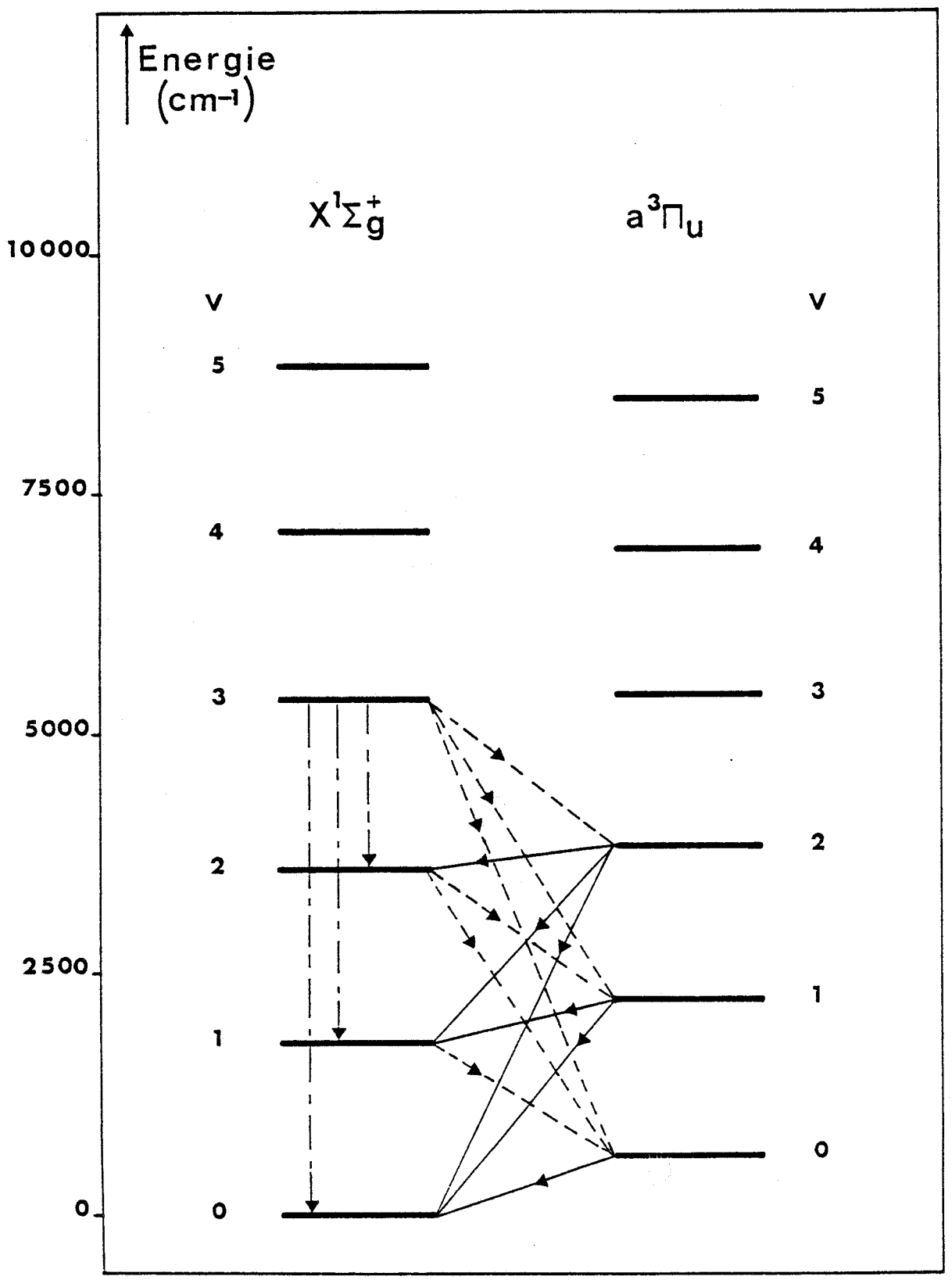

FIGURE III.b

Position relative des premiers niveaux vibrationnels des états $X^1\Sigma_g^+$ et $a^3\Pi_u$ et mécanismes susceptibles d'affecter les populations dans l'état $X^1\Sigma_g^+$: ---- $X^1\Sigma_g^+$ (v') → $a^3\Pi_u$ (v'') ; ——— $a^3\Pi_u$ (v') → $X^1\Sigma_g^+$ (v'') ; —·—·— cascades quadrupolaires.

Puisque la molécule C_2 est une molécule homonucléaire de spin nucléaire nul, seuls les niveaux symétriques existent. Dans l'état $X^1\Sigma_g^+$ les niveaux symétriques sont ceux qui correspondent aux valeurs paires du nombre quantique de rotation J. Dans l'état $a^3\Pi_u$ toutes les valeurs de J existent mais pour chaque J, une seule composante du dédoublement Λ apparaît : celle qui correspond à l'état symétrique. La figure III.c donne les premiers niveaux de rotation existant pour chaque composante vibrationnelle des états $X^1\Sigma_g^+$ et $a^3\Pi_u$.

Considérons des transitions entre deux niveaux de vibration, l'un appartenant à l'état $X^1\Sigma_g^+$, l'autre à l'état $a^3\Pi_u$, il ressort de la figure III.c que lorsque le niveau de l'état $X^1\Sigma_g^+$ est situé au dessus du niveau de l'état $a^3\Pi_u$, pour chaque valeur de $J > 2$ de l'état $X^1\Sigma_g^+$, il existe neuf raies possibles ($\Delta J = 0, \pm 1$), 1 raie P (J"), 1 raie Q (J"), 1 raie R (J") pour chaque composante Ω de l'état $a^3\Pi_u$. Lorsque l'état $a^3\Pi_u$ est l'état supérieur de la transition pour chaque valeur de J pair et pour chaque composante Ω, il existe 1 raie Q (J") alors que pour chaque valeur de J impair, il existe pour chaque composante du niveau $^3\Pi_u$ une raie P (J") et une raie R (J").

En vertu de la règle de sélection générale sur le spin (cas a ou cas b) $\Delta S = 0$ il n'existe pas de transition directe singulet-triplet. La transition d'intercombinaison $a^3\Pi_u - X^1\Sigma_g^+$ n'est permise que grâce à la contamination de l'état triplet $a^3\Pi_u$ par l'état singulet $A^1\Pi_u$ induite par l'interaction spin-orbite et au moment de transition $A^1\Pi_u - X^1\Sigma_g^+$.

Par suite de la règle de sélection $\Delta\Omega = 0$ pour l'opérateur spin-orbite, des trois composantes $a^3\Pi_{u,0}$, $a^3\Pi_{u,1}$, $a^3\Pi_{u,2}$ de l'état $a^3\Pi_u$, seule la composante $\Omega = 1$ est couplée à l'état $A^1\Pi_u$. La fonction d'onde d'un niveau rovibronique de cette composante $a^3\Pi_{u,1}$ s'écrit :

$$|\psi_{a_1}, v_{a_1}, J> = |\psi^0_{a_1}, v_{a_1}, J> + \sum_{v_A} \frac{<\psi^0_{a_1}, v_{a_1}, J \mid H_{SO} \mid \psi^0_A, v_A, J>}{E^0(a^3\Pi_{u,1}, v_{a_1}, J) - E^0(A^1\Pi_u, v_A, J)} \; |\psi^0_A, v_A, J> \qquad \text{(III.6)}$$

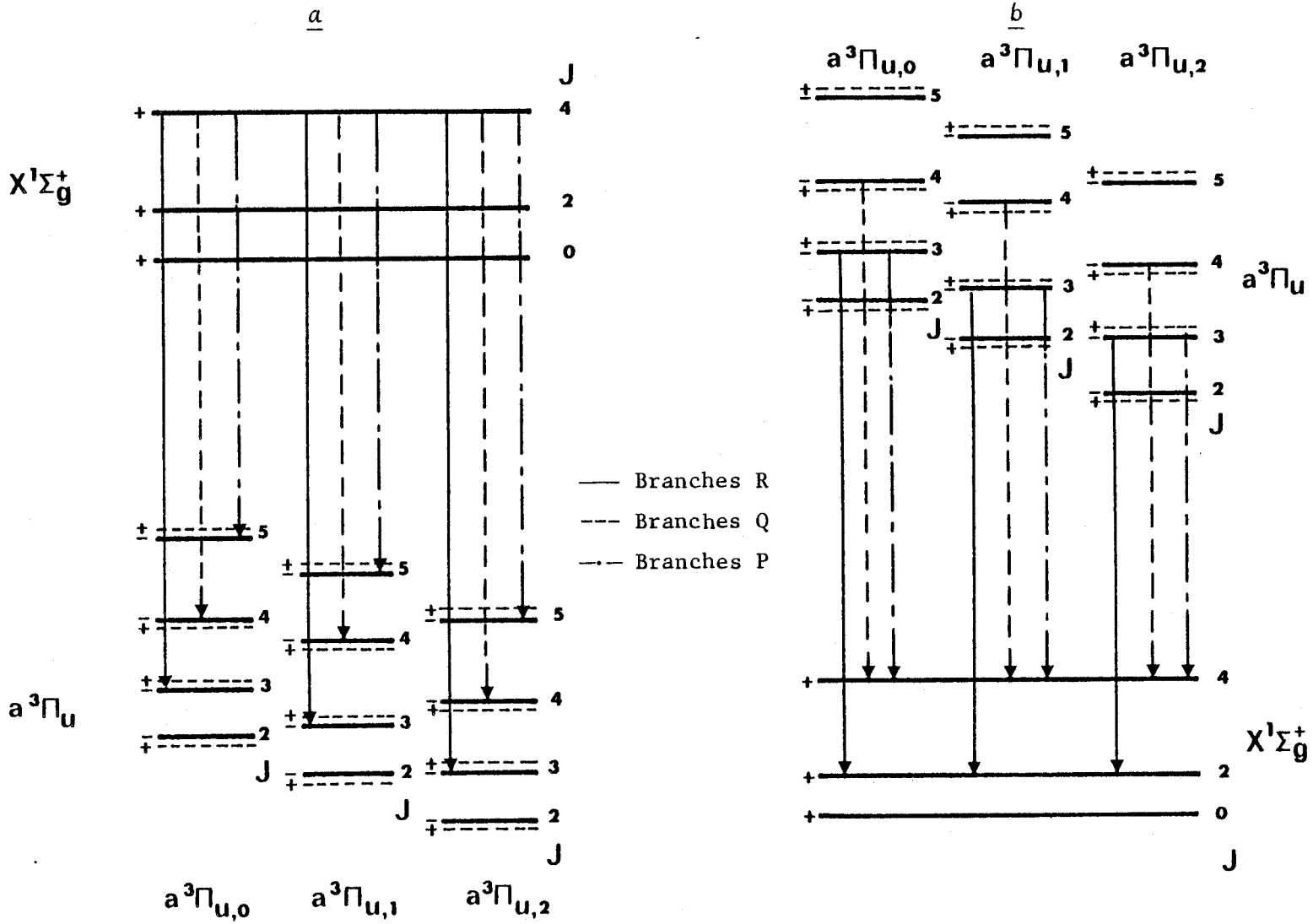

FIGURE III.c

Branches de la transition d'intercombinaison

a - $X^1\Sigma_g^+ \rightarrow a^3\Pi_u$ $\qquad$ b - $a^3\Pi_u \rightarrow X^1\Sigma_g^+$

Dans l'état $X^1\Sigma_g^+$ seuls les niveaux de parité + existent. Dans l'état $a^3\Pi_u$ seuls les niveaux de parité - existent

où ψ^0_α caractérise la fonction d'onde électronique d'ordre zéro de l'état α, H_{SO} est l'opérateur spin-orbite et $E^0(\alpha, v_\alpha, J)$ donne l'énergie d'ordre zéro de l'état électronique α dans son niveau rovibrationnel (v_α, J) ; l'indice 1 de l'expression précédente caractérise la composante $\Omega = 1$ de l'état $a^3\Pi_u$ et la sommation s'étend à tous les niveaux vibrationnels de l'état $A^1\Pi_u$. L'expression ci-dessus se simplifie quand les états $^1\Pi$ et $^3\Pi$ couplés, peuvent être représentés par une seule et même configuration. Nos calculs, ab initio, ont montré que les états $A^1\Pi_u$ et $a^3\Pi_u$ sont bien de cette catégorie (configuration principale à 97 % $1\sigma_g^2\ 2\sigma_g^2\ 3\sigma_g\ 1\sigma_u^2\ 2\sigma_u^2\ 1\pi_u^3$). Dans ces conditions :

$$< \psi^0_{a_1}, v_{a_1}, J \mid H_{SO} \mid \psi^0_A, v_A, J > \simeq A\,(a^3\Pi_u)\, S_{v_a v_A} \qquad \text{(III.7)}$$

où $A\,(a^3\Pi_u)$ est l'élément diagonal de l'opérateur spin-orbite dans l'état $a^3\Pi_u$ et $S_{v_a v_A}$ le recouvrement vibrationnel.

Nous avons à distinguer deux cas de figure :

a - lorsque l'état $X^1\Sigma^+_g$ (v_X) est l'état supérieur de la transition : appliquée à la transition $X^1\Sigma^+_g$ $(v'_X) \rightarrow a^3\Pi_{u,1}$ (v''_{a_1}) l'équation (III.2) devient :

$$A\,(v'_X J', v''_{a_1} J'') = \frac{64\pi^4}{3h}\ \nu^3 \sum_M \frac{3\,|< \psi'_X v'_X J' M \mid \sum_i \mu_{Z_i} \mid \psi''_{a_1} v''_{a_1} J'' M >|^2}{(2J'+1)} \qquad \text{(III.8)}$$

En utilisant les équations (III.3, III.6, III.7) et en tenant compte de la règle de sélection $\Delta S = 0$, la probabilité d'émission d'EINSTEIN (s^{-1}) s'écrit :

$$A\,(v'_X J', v''_{a_1} J'') = \frac{64\pi^3}{3h}\ \frac{\nu^3}{(2J'+1)} \left| \sum_{v_A} \frac{A(a^3\Pi_u)\, S_{v''_{a_1} v_A} \int \psi_{v'_X}(R)\, D_{X-A}(R)\, \psi_{v_A}(R)\, dR}{E^0(a^3\Pi_{u,1}, v''_{a_1}, J'') - E^0(A^1\Pi_u, v_A, J'')} \right|^2 S_{J'J''}$$

(III.9)

où $D_{X-A}(R)$ représente le moment de transition électronique de la transition $X^1\Sigma^+_g - A^1\Pi_u$. Les coefficients $S_{J'J''}$ sont les facteurs de HÖNL-LONDON d'une

transition $^1\Sigma \rightarrow {}^1\Pi$ (KOVACS table 3.4)

$$\begin{aligned} S_{J'J''} &= J' + 1 \text{ branche P } (J' = J'' - 1) \\ S_{J'J''} &= J' \quad\quad \text{branche R } (J' = J'' + 1) \\ S_{J'J''} &= 2J' + 1 \text{ branche Q } (J' = J'') \end{aligned} \qquad \text{(III.10)}$$

b) Lorsque l'état $a^3\Pi_{u,1}$ (v'_{a_1}) est l'état supérieur de la transition la probabilité d'émission d'EINSTEIN (s^{-1}) s'obtient de la même manière que précédemment :

$$A\,(v'_{a_1}\,J'\,,v''_X\,J'') = \frac{64\pi^3}{3h}\,\frac{\nu^3}{(2J'+1)}\left|\sum_{v_A}\frac{A(a^3\Pi_u)\,S_{v''_{a_1}v_A}\int\psi_{v'_X}(R)\,D_{X-A}(R)\,\psi_{v_A}(R)\,dR}{E^0(a^3\Pi_{u,1},v'_{a_1},J') - E^0(A^1\Pi_u,v_A,J')}\right|^2 S_{J'J''}$$

(III.11)

Mais les facteurs de HÖNL-LONDON correspondent maintenant à la transition $^1\Pi \rightarrow {}^1\Sigma$ (KOVACS table 3.4)

$$\begin{aligned} S_{J'J''} &= J' \quad\quad \text{branche P} \\ S_{J'J''} &= J' + 1 \text{ branche R} \\ S_{J'J''} &= 2J' + 1 \text{ branche Q} \end{aligned} \qquad \text{(III.12)}$$

On constate que le coefficient d'EINSTEIN d'une transition reliant deux niveaux rotationnels J_X et J_a donnés (appartenant respectivement aux états $X^1\Sigma_g^+$ et $a^3\Pi_{u,1}$) ne dépend pas du sens dans lequel se fait la transition.

Nous nous sommes intéressés jusqu'à présent aux transitions mettant en jeu la composante $\Omega = 1$ de l'état $a^3\Pi_u$, seule composante nous l'avons déjà mentionné, qui est couplée directement par interaction spin-orbite à l'état $A^1\Pi_u$. En fait, les composantes $\Omega = 0$ et $\Omega = 2$ de l'état $a^3\Pi_u$ se mélangent à la composante $\Omega = 1$ de cet état par la rotation de la molécule. En particulier, dans la molécule C_2, la constante spin-orbite diagonale de l'état $a^3\Pi_u$ est faible (-15.3 cm^{-1} (AMIOT, CHAUVILLE et MAILLARD (1979)) et ce mélange devient très vite important même pour les faibles valeurs du nombre quantique de rota-

tion J. Le caractère $a^3\Pi_{u,1}$ de chaque composante Ω de l'état $a^3\Pi_u$ * peut être obtenu par diagonalisation, pour chaque valeur de J, de la matrice du hamiltonien de rotation de l'état $a^3\Pi_u$ construite sur la base des vecteurs du cas (a) de Hund. En d'autres termes, pour une situation qui évolue du cas (a) (pour les faibles valeurs de J) au cas (b) (pour les valeurs de J plus importantes), chaque fonction d'onde $\psi\ (a^3\Pi_{u,0})$, $\psi\ (a^3\Pi_{u,1})$ et $\psi\ (a^3\Pi_{u,2})$ peut s'exprimer sous la forme :

$$\psi\ (a^3\Pi_{u,\Omega}) = \sum_{k=1}^{3} C_{\Omega,k}\ \Phi\ (a^3\Pi_{u,k}) \qquad \text{(III.13)}$$

où $\Phi\ (a^3\Pi_{u,k})$ représente les fonctions du cas (a) de HUND de l'état $a^3\Pi_u$ et le coefficient $C_{\Omega,k}$ le poids de la composante k (cas a) dans la composante Ω de l'état $a^3\Pi_u$.

Les formules (III.9) et (III.11) obtenues pour les probabilités d'EINSTEIN restent applicables pour chaque composante de l'état $a^3\Pi_u$ à condition de faire apparaître dans les facteurs de HÖNL-LONDON le caractère $^3\Pi_1$ de chacune des composantes $a^3\Pi_{u,\Omega}$. Les expressions correspondantes des facteurs $S_{J'J''}$ sont données pour chaque composante Ω dans le tableau suivant :

Transition $X^1\Sigma_g^+ \rightarrow a^3\Pi_{u,\Omega}$ $J' \rightarrow J''$		Transition $a^3\Pi_{u,\Omega} \rightarrow X^1\Sigma_g^+$ $J' \rightarrow J''$
$C^2_{\Omega,1} \times (J' + 1)$	Branche P	$C^2_{\Omega,1} \times J'$
$C^2_{\Omega,1} \times J'$	Branche R	$C^2_{\Omega,1} \times (J' + 1)$
$C^2_{\Omega,1} \times (2J' + 1)$	Branche Q	$C^2_{\Omega,1} \times (2J' + 1)$

La règle de normalisation $\sum_{J''} S_{J'J''} = (2 - \delta_{0,\Lambda}\delta_{0,\Lambda''})(2S+1)(2J'+1)$ *reste valable*

---

* La pureté du nombre quantique Ω s'affaiblit progressivement lorsque J augmente.

3) Résultats

Pour calculer les intégrales de recouvrement $S_{v_a v_A}$ et les intégrales du moment dipolaire de transition qui apparaissent dans les équations (III.9) et (III.11), nous avons déterminé les fonctions d'onde de vibration des états électroniques $X^1\Sigma_g^+$, $a^3\Pi_u$ et $A^1\Pi_u$ par intégration de NUMEROV des potentiels MORSE de ces états. Ces potentiels MORSE ont été construits sur les constantes d'équilibre données par AMIOT, CHAUVILLE et MAILLARD (1979) pour l'état $a^3\Pi_u$, MARENIN et JOHNSON (1970) pour l'état $X^1\Sigma_g^+$ et BALLIK et RAMSAY (1967) pour l'état $A^1\Pi_u$. La table III.A rassemble les constantes à l'équilibre de ces états.

Le calcul de la différence d'énergie qui apparait au dénominateur des équations (III.9) et (III.11) peut être simplifié en considérant que cette différence d'énergie est indépendante de J puisque les constantes de rotation des états $A^1\Pi_u$ et $a^3\Pi_u$ sont très voisines (table III.A). Ainsi :

$$E^0(a^3\Pi_{u,1}, v_{a_1}, J) - E^0(A^1\Pi_u, v_A, J) \simeq E^0(a^3\Pi_{u,1}, v_{a_1}) - E^0(A^1\Pi_u, v_A) \quad \text{pour}$$

tout J.

Par contre, la connaissance très précise des niveaux d'énergie rovibrationnels des états $a^3\Pi_u$ et $X^1\Sigma_g^+$ est indispensable pour déterminer les fréquences ν de transition entre ces niveaux. Les niveaux $X^1\Sigma_g^+$ s'obtiennent directement à partir des constantes données par MARENIN et JOHNSON (1970), tandis que ceux de l'état $a^3\Pi_u$ ont été obtenus par diagonalisation de la matrice du hamiltonien présentée par AMIOT, CHAUVILLE et MAILLARD (1979). Rappelons que cette diagonalisation permet également de trouver le poids $^3\Pi_{u,1}$ dans chaque composante Ω de l'état $a^3\Pi_u$.

Enfin, la variation de la constante spin-orbite diagonale de l'état $a^3\Pi_u$ en fonction du nombre quantique de vibration est très faible, au moins pour les premiers niveaux vibrationnels : $A = -15.262\ cm^{-1}$ pour $v = 0$ à $A = -15.198\ cm^{-1}$ pour $v = 3$ (AMIOT, CHAUVILLE et MAILLARD (1979). Nous avons négligé cette variation dans les équations (III.9) et (III.11) en supposant pour tous les niveaux vibrationnels concernés de l'état $a^3\Pi_u$ une valeur constante

TABLE III.A : Constantes d'équilibre (cm^{-1}) des états $X^1\Sigma_g^+$, $A^1\Pi_u$ et $a^3\Pi_u$ de C_2.

	T_e	ω_e	$\omega_e x_e$	B_e	α_e	D_e	β_e
$X^1\Sigma_g^+$ [a]	0.0	1854.783	13.389	1.820013	0.017682	$6.959\ 10^{-6}$	$6.6\ 10^{-9}$
$A^1\Pi_u$ [b]	8391.00	1608.35	12.07	1.61634	0.01686	$6.44\ 10^{-6}$	
$a^3\Pi_u$ [c]	718.3181	1641.3423	11.66474	1.632532	0.016545	$6.4375\ 10^{-6}$	$5.2\ 10^{-9}$

a - MATENIN et JOHNSON (1970)

b - BALLIK et RAMSAY (1963)

c - AMIOT, CHAUVILLE et MAILLARD (1979)

de A ($^3\Pi_u$) égale à -15.26 cm^{-1}.

La table III.B donne pour les premiers niveaux vibrationnels de l'état $X^1\Sigma_g^+$ les probabilités de transition en s^{-1} sommées sur tous les niveaux inférieurs pour la transition $X^1\Sigma_g^+ \rightarrow a^3\Pi_u$. Ces probabilités sont indépendantes du nombre quantique de rotation J' de l'état $X^1\Sigma_g^+$ dès que $J' \geqslant 1$. Le cas particulier des niveaux J' = 0 donne pour chaque niveau vibrationnel une probabilité de transition plus faible que les autres niveaux rotationnels puisqu'il n'existe à partir de ces niveaux que deux raies possibles (une raie R (1) dans chacune des composantes $^3\Pi_{u,0}$ et $^3\Pi_{u,1}$ de l'état $a^3\Pi_u$). Les niveaux vibrationnels $v' \geqslant 5$ de l'état $X^1\Sigma_g^+$ se situent au dessus de certains niveaux vibrationnels de l'état $A^1\Pi_u$. Ils sont donc susceptibles de se dépeupler par transition dipolaire $X^1\Sigma_g^+ \rightarrow A^1\Pi_u$ beaucoup plus rapidement que par transition d'intercombinaison. C'est la raison pour laquelle nos résultats (Table III.B) ne sont présentés que pour les premiers niveaux vibrationnels ($v_X < 5$).

De la même manière, la table III.C rassemble pour les premiers niveaux vibrationnels de l'état $a^3\Pi_u$, les probabilités de transition en s^{-1} sommées sur tous les niveaux inférieurs lorsque l'état $a^3\Pi_u$ est l'état supérieur de la transition. Les résultats sont présentés pour chaque composante Ω de l'état $a^3\Pi_u$. Contrairement au cas où $X^1\Sigma_g^+$ est l'état supérieur, ces probabilités ne sont plus indépendantes du nombre quantique de rotation J' du niveau supérieur. La probabilité de transition augmente lorsque J croit pour les composantes $\Omega = 0$ et $\Omega = 2$ de l'état $a^3\Pi_u$ et diminue pour la composante $\Omega = 1$. Cette dépendance en J' des probabilités de transitions des différentes composantes s'explique simplement si on se souvient que la transition $a^3\Pi_{u,\Omega} \rightarrow X^1\Sigma_g^+$ est gouvernée pour chaque composante Ω par le caractère $a^3\Pi_{u,1}$ de cette composante. Pour les faibles valeurs de J' le mélange des trois composantes est faible et la plus grande partie de l'intensité se trouve dans la sous-bande $a^3\Pi_{u,1} \rightarrow X^1\Sigma_g^+$. Au fur et à mesure que J' augmente le mélange $a^3\Pi_{u,0}$, $a^3\Pi_{u,1}$ et $a^3\Pi_{u,2}$ devient plus important et l'intensité des sous-bandes $a^3\Pi_{u,0} \rightarrow X^1\Sigma_g^+$ et $a^3\Pi_{u,2} \rightarrow X^1\Sigma_g^+$ croit au détriment de l'intensité de la sous-bande $a^3\Pi_{u,1} \rightarrow X^1\Sigma_g^+$. Enfin, la dernière remarque concerne les plus bas niveaux de rotation (v', J' = 0) de la composante $\Omega = 0$ de l'état $a^3\Pi_u$: ces niveaux sont hautement métastables et ne peuvent se dépeupler que par collision.

TABLE III.B : Probabilités de transition (s^{-1}) $X^1\Sigma_g^+ \rightarrow a^3\Pi_u$ sommées sur tous les niveaux inférieurs de la transition.

v'	J'	$A_{v'J'} = \sum_{v''J''} A_{v'J',v''J''}$ notre méthode $\Sigma\|R_e\|^2$ ab-initio	Dishoeck et coll $\Sigma\|R_e\|^2$ semi-empirique
1	0	9.3×10^{-4}	
	$\neq 0$	1.4×10^{-3}	30×10^{-3}
2	0	5.7×10^{-3}	
	$\neq 0$	8.6×10^{-3}	170×10^{-3}
3	0	1.3×10^{-2}	
	$\neq 0$	2.0×10^{-2}	42×10^{-2}
4	0	2.2×10^{-2}	
	$\neq 0$	3.3×10^{-2}	75×10^{-2}

TABLE III.C : Probabilités de transition (s^{-1}) $a^3\Pi \rightarrow X^1\Sigma_g^+$ pour chaque composante de l'état $a^3\Pi_u$ sommées sur tous les niveaux inférieurs de la transition.

v'	J'	$A_{v'J'} = \sum_{v''J''} A_{v'J',v''J''}$ notre méthode $a^3\Pi_{u,0}$	$a^3\Pi_{u,1}$	$a^3\Pi_{u,2}$	Dishoeck et coll.*
0	0	0	-	-	
	1	0.49×10^{-5}	0.98×10^{-4}	-	
	2	0.11×10^{-4}	0.88×10^{-4}	0.38×10^{-5}	
	3	0.20×10^{-4}	0.73×10^{-4}	0.83×10^{-5}	
	4	0.25×10^{-4}	0.63×10^{-4}	0.13×10^{-4}	
	5	0.32×10^{-4}	0.51×10^{-4}	0.17×10^{-4}	
	6	0.35×10^{-4}	0.44×10^{-4}	0.20×10^{-4}	
1	0	0	-	-	
	1	0.19×10^{-3}	0.41×10^{-2}	-	
	2	0.43×10^{-3}	0.37×10^{-2}	0.17×10^{-3}	
	3	0.79×10^{-3}	0.31×10^{-2}	0.38×10^{-3}	1×10^{-3}—6×10^{-2}
	4	0.98×10^{-3}	0.27×10^{-2}	0.59×10^{-3}	
	5	0.13×10^{-2}	0.21×10^{-2}	0.79×10^{-3}	
	6	0.14×10^{-2}	0.19×10^{-2}	0.97×10^{-3}	
2	0	0	-	-	
	1	0.55×10^{-3}	0.12×10^{-1}	-	
	2	0.12×10^{-2}	0.10×10^{-1}	0.49×10^{-3}	
	3	0.23×10^{-2}	0.91×10^{-2}	0.11×10^{-2}	3×10^{-3}—17×10^{-2}
	4	0.28×10^{-2}	0.79×10^{-2}	0.17×10^{-2}	
	5	0.36×10^{-2}	0.64×10^{-2}	0.22×10^{-2}	
	6	0.39×10^{-2}	0.57×10^{-2}	0.28×10^{-2}	
3	0	0	-	-	
	1	0.98×10^{-3}	0.21×10^{-1}	-	
	2	0.21×10^{-2}	0.19×10^{-1}	0.88×10^{-3}	
	3	0.40×10^{-2}	0.16×10^{-1}	0.20×10^{-2}	6×10^{-3}—3×10^{-1}
	4	0.50×10^{-2}	0.14×10^{-1}	0.31×10^{-2}	
	5	0.66×10^{-2}	0.11×10^{-1}	0.41×10^{-2}	
	6	0.71×10^{-2}	0.10×10^{-1}	0.52×10^{-2}	

Van Dishoeck et Black ne donnent pour cette transition $a^3\Pi_u \rightarrow X^1\Sigma_g^+$ qu'un domaine de valeurs typiques pour chaque niveau vibrationnel v' mais ne précisent pas le niveau de rotation J' considéré. Nous avons fait figurer ces valeurs à titre de comparaison.

Nous avons fait figurer dans les tables III.B et III.C les valeurs des probabilités de transition récemment publiées par VAN-DISHOECK et BLACK (1982). La comparaison avec nos valeurs dans le cas où l'état $a^3\Pi_u$ est l'état supérieur de la transition (Table III.C) n'est pas évidente dans la mesure où VAN DISHOECK et BLACK ne donnent, pour chaque niveau vibrationnel v' de l'état supérieur, qu'un intervalle de valeurs typiques sans préciser le nombre quantique de rotation J' correspondant.

Pour ce qui est de la transition $X^1\Sigma_g^+ \rightarrow a^3\Pi_u$ (Table III.B), il apparaît clairement que nos valeurs de probabilités sont toujours beaucoup plus faibles que celles obtenues par VAN DISHOECK et BLACK. Afin d'expliquer cette différence, il est nécessaire d'exposer rapidement la méthode qu'ils ont employée.

Pour calculer les probabilités de transition, VAN DISHOECK et BLACK ont utilisé l'expression suivante :

$$A\,(v'_X J'_X,\ v''_a J''_a) = \frac{64\pi^3}{3h}\,\nu^3 \left\{ \Sigma |R_e|^2_{a-X} \Big/ N_{R_E} \right\} q_{v'_X v''_a}\, S_{J'J''} / (2J'+1) \quad \text{(III.14)}$$

Cette expression a l'avantage de se présenter sous la même forme que celle utilisée dans le cas d'une transition permise (eq (III.1)) à condition de remplacer dans l'équation III.1, le terme $|\langle \psi' | \sum_i e_i r_i | \psi'' \rangle|^2$ par le carré d'un moment de transition effectif égal à $\Sigma |R_e|^2_{a-X} / N_{R_E}$ défini par WHITING et NICHOLLS (1973), que l'on déduit des mesures expérimentales d'intensité. N_{R_E} représente le nombre de moments de transition "indépendants" obtenu en respectant la règle de sélection $\Delta\Omega = 0, \pm 1$. Ici, $N_{R_E} = 2$ pour une transition $^1\Sigma - {}^3\Pi$, $q_{v'_X v''_a}$ est le facteur de FRANCK-CONDON $X^1\Sigma_g^+ (v'_X) - a^3\Pi_u (v''_a)$ et $S_{J'J''}$ est un facteur de HÖNL-LONDON de la transition $X^1\Sigma_g^+ \rightarrow a^3\Pi_u$. La règle de normalisation des facteurs de HÖNL-LONDON dans le cas d'une transition interdite s'écrit (WHITING et NICHOLLS (1973)) :

$$\sum_{J''} S_{J'J''} = N_{R_E} (2J'+1)$$

VAN DISHOECK et BLACK ont utilisé pour les facteurs de HÖNL-LONDON les formules du cas intermédiaire cas (a) - cas (b) données par KOVACS (1969).

Par identification des équations (III.9) et (III.14) on obtient :

$$\frac{\Sigma \left|R_e\right|^2_{a-X} \; q_{v'_X v''_a}}{N_{R_E}} = \left\{ \sum_{v_A} \frac{A\,(a^3\Pi_u)\, S_{v''_a v_A} \int \psi_{v'_X}(R)\, D_{X-A}(R)\, \psi_{v_A}(R)\, dR}{E^0\,(a^3\Pi_{u,1}, v''_a) - E^0\,(A^1\Pi_u, v_A)} \right\}^2 \qquad \text{(III.15)}$$

Le calcul du carré du moment de transition $X^1\Sigma_g^+ \rightarrow a^3\Pi_u$ par l'équation (III.15) conduit à la valeur :

$$\Sigma \left|R_e\right|^2_{a-X} = 10^{-6} \text{ u.a.}$$

alors que VAN DISHOECK et BLACK avaient supposé :

$$\Sigma \left|R_e\right|^2_{a-X} = 2 \times 10^{-5} \text{ u.a.}$$

L'écart entre ces deux valeurs permet d'expliquer pourquoi nos résultats sont d'environ un facteur 20 plus faible que ceux obtenus par VAN DISHOECK et BLACK (Table III.B).

Il apparaît en conclusion que le rôle joué par la transition d'intercombinaison est beaucoup plus déterminant que celui joué par les cascades quadrupolaires dans l'équilibre des populations rotationnelles de l'état fondamental de C_2. En effet, les probabilités de transitions d'intercombinaison sont de l'ordre de 10^{-4} à 10^{-2} s^{-1} pour les premiers niveaux vibrationnels des états concernés alors que celles des cascades quadrupolaires ne sont que de 10^{-7} s^{-1}.

CONCLUSION

Nous avons dans ce chapître déterminé de manière ab-initio un certain nombre de paramètres intervenant dans les divers processus non collisionnels susceptibles d'affecter les populations de l'état fondamental de la molécule C_2.

Il convient toutefois de préciser que le bilan exposé des différents mécanismes n'est pas exhaustif. En particulier l'existence de l'état $b^3\Sigma_g^-$ situé entre l'état $a^3\Pi_u$ et l'état $A^1\Pi_u$ pourrait modifier les probabilités de la transition d'intercombinaison que nous avons présentées. En effet cet état est couplé à l'état fondamental $X^1\Sigma_g^+$ par interaction spin-orbite et peut transiter avec l'état $a^3\Pi_u$. AMIOT, CHAUVILLE et MAILLARD (1979) ont établi que l'interaction spin-orbite valait environ 6.5 cm^{-1} et COOPER et NICHOLLS (1976) ont déterminé que $\Sigma\ R_e^2\ (a^3\Pi_u - b^3\Sigma_g^-) \simeq 0.65$ a.u., valeurs à comparer à 15 cm^{-1} pour l'interaction spin-orbite $A^1\Pi_u$-$a^3\Pi_u$, et 0.27 a.u. pour $\Sigma\ R_e^2\ (A^1\Pi_u - X^1\Sigma_g^+)$. Nous avons calculé que la contribution de l'état $b^3\Sigma_g^-$ pouvait modifier les probabilités de transition données précédemment d'un facteur 2 au maximum, pour les deux premiers niveaux vibrationnels de l'état $X^1\Sigma_g^+$. Si l'on devait mesurer l'influence du $b^3\Sigma_g^-$ sur les niveaux vibrationnels supérieurs, le problème serait autrement plus compliqué car il nécessiterait la diagonalisation exacte d'une matrice construite sur tous les niveaux $X^1\Sigma_g^+$, $a^3\Pi_u$, $A^1\Pi_u$, $b^3\Sigma_g^-$ situés dans la même zone d'énergie.

Dans tous les cas prendre en compte l'influence de l'état $b^3\Sigma_g^-$ ne peut que renforcer la prépondérance de la transition d'intercombinaison sur les cascades radiatives quadrupolaires.

REFERENCES

1 - A'HEARN M.F. and FELDMAN P.D., *1980, Ap. J. (Letters)* 242, L 187

2 - AMIOT C., CHAUVILLE J. and MAILLARD J.P., *1979, J. Molec. Spectrosc.* 75, 19

3 - BAGUS P.S., LIU B., Mc LEAN A.D. and YOSHIMINE M., *1972* ALCHEMY IBM *Research Laboratory San Jose, California 95114, USA*

4 - BAGUS P.S. and WAHLGREN U.I., *1976, Comput. Chem.* 1, 95

5 - BALLIK E.A. and RAMSAY D.A., *1963, Ap. J.* 137, 84

6 - BLACK J.H. and DALGARNO A., *1977, Ap. J. Suppl.* 34, 405

7 - BLACK C.J. , HARTQVIST T.W. and DALGARNO A., *1978, Astrophys.* 224, 448

8 - BRAULT J.W., DELBOUILLE L., GREVESSE N., ROLAND G., SAUVAL A.J. and TESTERMAN L., *1982, Astr. Ap. in press*

9 - CADE P.E. and WAHL A.C., *1974, At. Data Nucl. Data Tables* 13, 339

10 - CHAFFEE F.H. and LUTZ B.L., *1978, Ap. J. (Letters)* 221, L 91

11 - CHAFFEE F.H., LUTZ B.L. and BLACK J.H., *1980, Astrophys. J.* 236, 474

12 - CLEMENTI E. and ROETTI C., *At. Data Nucl. Data Tables 1974,* 14, 282

13 - COOPER D.M. and NICHOLLS R.W., *1975, J. Quant. Spectrosc. Radiat. Transfer* 15, 139

14 - COOPER D.M. and NICHOLLS R.W., *1976, Spectrosc. Letters* 9, 139

15 - COSMOVICI C.B. and STRAFELLA F., *1981, Astr. Ap.* 98, 408

16 - CURTIS L., ENGMAN B. and ERMAN P., *1976, Phys. Scripta* 13, 270

17 - DALGARNO A. and BLACK J.H., *1973*, Ap. J. (Letters) 184, L 101

18 - DANKS A.C. and LAMBERT D.L., *in press*

19 - DUPUIS M. and LIU B., *1980*, J. Chem. Phys. 73, 337

20 - ERMAN P., LAMBERT D.L., LARSSON M. and MANNFORS B., *1982*, Astrophys. J., 253, 983

21 - HERZBERG G., LAGERQVIST A. and MALMBERG C., *1969*, Can. J. Phys. 47, 2735

22 - HOBBS L.M., *1979*, Ap. J. (Letters) 232, L 175

23 - HOBBS L.M. and CAMPBELL B., *1982*, Astrophys. J. 254, 108

24 - KIRBY K. and LIU B., *1979*, J. Chem. Phys. 70, 893

25 - KIRBY K., ROBERGE W.G., SAXON R.P. and LIU B., *1980 a*, Astrophys. J. 239, 855

26 - KIRBY K., SAXON R.P. and LIU B., *1980b*, J. Chem. Phys. 73, 1873

27 - KOVACS I., *1969*, Rotational structure in the spectra of diatomic molecules (New-York : American Elsevier)

28 - KRISHNA-SWAMY K.S. and O'DELL C.R., *1979*, Ap. J. 231, 624

29 - LAMBERT D.L. and DANKS A.C., *in press*

30 - LANG K.R., *1980*, Astrophysical Formulae (Berlin : Springer) p. 167

31 - MARENIN I.R. and JOHNSON H.R., *1970*, J. Quant. Spectrosc. Radiat. Transfer 10, 305

32 - RASEEV G., *1977*, Chem. Phys. Lett. 47, 36

33 - ROUX F., CERNY D. and D'INCAN J., *1976*, Astrophs. J. 204, 940

34 - SMITH W.H., *1969, Ap. J.* 156, *791*

35 - SOUZA S.P. and LUTZ B.L., *1977, Ap. J. (Letters)* 216, *L 49, erratum* 218, *L 31*

36 - SNOW T.P. Jr., *1978, Ap. J. (Letters)* 220, *L 93*

37 - VAN DISHOECK E. and BLACK J.H., *Astrophys. J.* 258, *533*

38 - WHITING E.E., SCHADEE A., TATUM J.B., HOUGEN J.T. and NICHOLLS R.W., *1980, J. Molec. Spectrosc.* 80, *249*

CHAPITRE IV

COLLISION $M_gO + N_2O$:

TRANSFERTS D'ENERGIE

INTRODUCTION

Les collisions réactives du type atome alcalino terreux avec un oxydant moléculaire (O_2, N_2O, NO_2, CO_2) ont depuis quelques années, fait l'objet de nombreuses études[1-7]. Trois raisons au moins peuvent expliquer l'intérêt témoigné à ce type de réactions.

- Tout d'abord, les réactions sont souvent suffisamment exothermiques pour permettre la formation des produits dans des états électroniques excités et si ces états sont radiatifs, l'étude de la chimiluminescence offre le moyen de tester l'importance relative des différentes voies réactionnelles.
- D'autre part, le développement récent des techniques laser permet la caractérisation des produits formés même dans les états électroniques non radiatifs par fluorescence induite.
- Enfin, la réactivité est considérablement accrue si les atomes réactants sont portés dans leur état métastable ; on obtient des températures vibrationnelles élevées dans les états électroniques des espèces formées et même éventuellement des inversions de population. Ce dernier point est particulièrement interessant dans la recherche des effets lasers.

Sur le plan expérimental, la réactivité du magnésium dans l'état métastable ^3P avec N_2O vient d'être étudiée par BOURGUIGNON, ROSTAS et TAIEB[4-5] dans une cellule à haute pression et flux rapide et par DAGDIGIAN et COX [2b-6] à pression plus faible dans un jet moléculaire.

Sur le plan théorique, YARKONY [63] a étudié la réactivité du magnésium dans l'état ^1S et dans l'état ^3P en réaction avec N_2O.

Il ressort de ces études, que la molécule MgO produit de la réaction Mg (^3P) + N_2O est formée principalement dans l'état fondamental $X^1\Sigma^+$ et les deux premiers états excités $a^3\Pi$ et $A^1\Pi$, situés respectivement à 2623 cm^{-1} et 3557 cm^{-1} au dessus du fondamental, contrairement à ce que laisse prévoir un diagramme de corrélation adiabatique dans lequel seul l'état $a^3\Pi$ devrait être formé. Mais des études expérimentales récentes ont révélé que la population

naissante des différents états formés dans la réaction atome d'alcalino terreux + oxydant moléculaire peut être altérée par divers processus radiatifs et collisionnels. En particulier, l'accroissement avec la pression d'oxydant de la chimiluminescence des réactions de Ca (^1S, ^3P, ^1D) et Ba (S) avec des oxydants polaires (N_2O, NO_2) [3,8-10] s'explique par la présence, par collision, de transferts de population dans les produits formés. Le même type de mécanisme peut être envisagé pour le cas particulier de MgO dont l'état non radiatif $a^3\Pi$ très proche du fondamental pourrait servir de réservoir d'énergie. Le but de notre étude est de mettre en évidence l'importance des collisions inélastiques consécutives à la réaction de formation Mg (^3P) + N_2O et qui affectent les populations des produits naissants.

Cette approche théorique repose sur le modèle dipolaire développé récemment par ALEXANDER dans l'étude de la collision CaO + N_2O [16]. L'idée de base est que le couplage collisionnel dipole-dipole qui agit à longue distance entre le produit MgO et l'oxydant polaire N_2O conduit dang MgO à des transferts d'énergie entre états électroniques différents. La probabilité de transition entre deux niveaux rovibroniques a été calculée en nous limitant au premier ordre du développement de BORN de la matrice de diffusion.

La première partie de ce travail présente quelques rappels théoriques, la seconde partie développe les calculs de sections efficaces de transfert entre les états électroniques $X^1\Sigma^+$, $a^3\Pi$ et $A^1\Pi$ de MgO et présente les résultats obtenus. Enfin, la dernière partie contient quelques commentaires et justifications des hypothèses choisies pour traiter le problème de la collision MgO + N_2O.

I - RAPPELS THEORIQUES

1) Rappels sur la théorie de perturbation semi-classique des collisions inélastiques. Approximation de Born du premier ordre

Le Hamiltonien total d'un système de deux molécules se met sous la forme :

$$H = H_{int}(\underset{\sim}{r}) - \frac{\hbar^2}{2\mu}\nabla_R^2 + V(\underset{\sim}{R}, \underset{\sim}{r}) \qquad (IV.1)$$

où $\underset{\sim}{R}$ est le vecteur qui caractérise la position relative des deux partenaires de la collision, $H_{int}(\underset{\sim}{r})$ le hamiltonien des états internes des molécules libres, $V(\underset{\sim}{R}, \underset{\sim}{r})$ le potentiel d'interaction (qui s'annule à l'infini), μ la masse réduite du système et le terme $-\frac{\hbar^2}{2\mu}\nabla_R^2$ représente l'opérateur d'énergie cinétique relative.

L'équation de SCHRÖDINGER indépendante du temps s'écrit :

$$H\,\Phi(\underset{\sim}{R}, \underset{\sim}{r}) = E\,\Phi(\underset{\sim}{R}, \underset{\sim}{r}) \qquad (IV.2)$$

$\Phi(\underset{\sim}{R}, \underset{\sim}{r})$ est la fonction d'onde totale du système.

Dans le cas où le potentiel d'interaction $V(\underset{\sim}{R}, \underset{\sim}{r})$ peut être traité comme une perturbation, il est de coutume de développer la fonction d'onde totale sur la base orthonormée des vecteurs propres $\phi_k(\underset{\sim}{r})$ du hamiltonien non perturbé $H_{int}(\underset{\sim}{r})$:

$$\Phi(\underset{\sim}{R}, \underset{\sim}{r}) = \sum_k \psi_k(\underset{\sim}{R})\,\phi_k(\underset{\sim}{r}) \qquad (IV.3)$$

C'est la formulation diabatique du problème. Cette formulation est particulièrement bien adaptée dans le cas où le temps de collision est faible par rapport à la période de rotation de la molécule.

Après intégration sur les variables internes, l'équation (IV.2) devient :

$$(\nabla_R^2 + k_i^2)\ \psi_i\ (R) \;=\; \sum_k U_{ik}\ (R)\ \psi_k\ (R) \qquad \text{(IV.4)}$$

où $k_i^2 = \frac{2\mu}{\hbar^2}\ (E - E_i)$, $U_{ik} = \frac{2\mu}{\hbar^2} \int \overset{*}{\phi}_i\ (\underset{\sim}{r})\ V\ (\underset{\sim}{R}, \underset{\sim}{r})\ \phi_k\ (\underset{\sim}{r})\ dr$

et $H_{int}\ (\underset{\sim}{r})\ \phi_i = E_i\ \phi_i$.

Dans cette équation, le terme non diagonal U_{ik} (R), qui couple deux états internes (ou voies) différents, est responsable des processus inélastiques.

Lorsque la collision n'apporte qu'une faible perturbation sur le mouvement du centre de masse du système, il est possible de recourir à une approximation semi-classique qui traite le mouvement relatif des deux partenaires de la collision de façon classique en gardant au mouvement interne son caractère quantique. Cette approximation suppose dans toute la région du couplage inélastique et pour toutes les voies, l'existence d'une trajectoire moyenne du mouvement relatif gouvernée par la présence d'un potentiel moyen. Ceci implique que les changements de la vitesse relative de la collision et du moment angulaire doivent être faibles comparés à leur valeur moyenne. Nous vérifierons qu'une telle hypothèse est parfaitement raisonnable dans le cas de la collision MgO + N_2O. La conséquence directe de ce qui précède est que l'on peut supprimer du hamiltonien total l'opérateur d'énergie cinétique à condition d'introduire un potentiel V ($\underset{\sim}{R}(t)$, $\underset{\sim}{r}$) dépendant des variables internes des molécules et du temps par l'intermédiaire de la trajectoire R(t) [64]. L'équation de SCHRÖDINGER dépendante du temps s'écrit :

$$i\hbar\ \frac{d\ \Phi\ (\underset{\sim}{r},\ t)}{dt} \;=\; \left[H_{int}\ (\underset{\sim}{r}) + V\ (\underset{\sim}{R}(t), \underset{\sim}{r}) \right]\ \Phi\ (\underset{\sim}{r},\ t) \qquad \text{(IV.5)}$$

où $$\Phi\ (\underset{\sim}{r},\ t) \;=\; \sum_n a_n\ (t)\ \phi_n\ (\underset{\sim}{r})\ e^{-iE_n t/\hbar} \qquad \text{(IV.6)}$$

Avant ($t \to -\infty$) ou après ($t \to -\infty$) la collision, le hamiltonien H(t) représente le hamiltonien des deux molécules isolées H_{int} dont les fonctions

propres ϕ_n dégagées du facteur temporel et les valeurs propres E_n satisfont à l'équation de SCHRÖDINGER indépendante du temps.

La fonction d'onde dépendante du temps Φ ($\underset{\sim}{r}$, t) permet la description complète de la dynamique de la collision. Φ ($\underset{\sim}{r}$, t) s'écrit en terme des coefficients a_n (t) (équation IV.6) et on peut définir à un instant t donné l'ensemble des coefficients a_n (t) par un vecteur colonne a (t). La transformation de l'état initial à l'état final introduit le concept de la matrice de diffusion S par l'équation matricielle :

$$a\ (\infty) \ = \ S\ a\ (-\infty) \qquad \text{(IV.7)}$$

Par une méthode d'iterations successives il est possible de développer la matrice de diffusion sous la forme [65] :

$$S \ = \ \sum_{n\,=\,0}^{\infty} \ (-\,i/\hbar)^n \ S_n \qquad \text{(IV.8)}$$

où $S_n = \lim_{t \to \infty,\, t' \to -\infty} U_n\ (t,t')$ (IV.9)

et U_n (t,t') caractérise le $(n+1)^{\text{ème}}$ terme du développement de BORN de l'opérateur d'évolution U (t,t').

Si à l'instant t' avant collision le système se trouve dans un état propre ϕ_i de H_{int}, la probabilité de le trouver à l'instant final t après collision dans un autre état propre ϕ_f est par définition :

$$P_{i \to f} \ = \ |\ <\phi_f|\ U\ (t,t')\ |\ \phi_i>\ |^2 \qquad \text{(IV.10)}$$

Le développement de BORN au premier ordre permet de l'écrire sous la forme (équation 20 de l'article)

$$P_{i \to f} = \left| \frac{i}{\hbar} <\phi_f | S_1 | \phi_i> \right|^2 = \frac{1}{\hbar^2} \left| \int_{-\infty}^{+\infty} e^{i\omega_{if}t} <\phi_f | V\ (\underset{\sim}{R}(t), \underset{\sim}{r} | \phi_i> \, dt \right|^2 \qquad \text{(IV.11)}$$

avec $\omega_{if} = \frac{1}{\hbar}\ (E_f - E_i)$

Il est nécessaire à présent de définir le potentiel intermoléculaire $V(\underset{\sim}{R}(t),\underset{\sim}{r})$.

2) Potentiel d'interaction dans le cas d'une collision entre deux partenaires polaires

Si on néglige toute contribution d'ordre magnétique, on peut écrire le potentiel d'interaction entre les deux molécules α et β sous la forme :

$$V(t) = \sum_{i_\alpha i_\beta} \left(e_{i_\alpha} e_{i_\beta} \Big/ r_{i_\alpha i_\beta}(t) \right) \qquad \text{(IV.12)}$$

où e_{i_α} (e_{i_β}) est la charge de la particule i_α (i_β) de la molécule MgO (N_2O), $r_{i_\alpha i_\beta}$ la distance entre les deux particules i_α et i_β et où la somme s'étend à toutes les particules chargées des deux molécules α et β.

La figure (IV.a) donne le système de coordonnées fixé dans l'espace et dont l'origine est choisie sur le centre de masse de la molécule α, le point de plus grande approche des deux molécules définit le paramètre d'impact b.

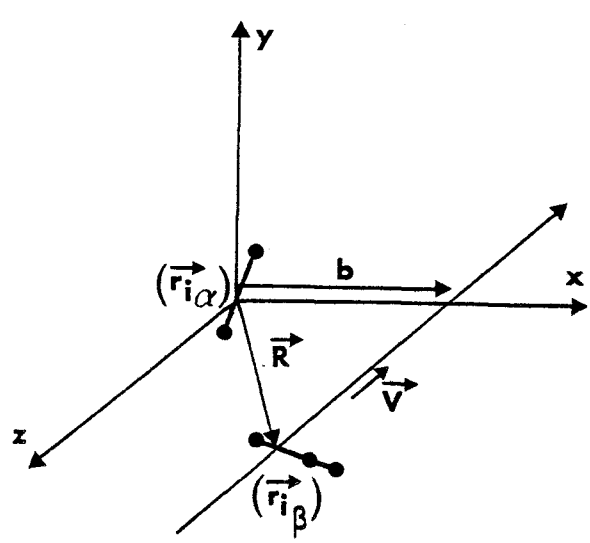

FIGURE IV.a

$\vec{r}_{i_\alpha}$ ($\vec{r}_{i_\beta}$) représente le vecteur position par rapport au centre de masse de la molécule α (β) d'une charge e_{i_α} (e_{i_β}). On peut écrire :

$\vec{r}_{i_\alpha} \equiv (r_{i_\alpha}, \hat{r}_{i_\alpha})$, $\vec{r}_{i_\beta} \equiv (r_{i_\beta}, \hat{r}_{i_\beta})$ avec $\hat{r}_{i_\alpha}$ et $\hat{r}_{i_\beta}$ des angles d'Euler des charges e_{i_α} et e_{i_β}.

$\vec{R}$ est le vecteur entre les centres de masse des deux molécules ; l'orientation de $\vec{R}$ est repérée par $\hat{R}$, $\vec{v}$ est le vecteur vitesse relative de la collision.

Chaque terme du type $r_{i_\alpha i_\beta}$ de l'équation (IV.12) s'écrit :

$$r_{i_\alpha i_\beta} = | \vec{r}_{i_\beta} + \vec{R} - \vec{r}_{i_\alpha} | \qquad \text{(IV.13)}$$

et chaque fonction $\frac{1}{r_{i_\alpha i_\beta}}$ peut alors être décomposée en produit d'harmoniques sphériques [66] :

$$\frac{1}{r_{i_\alpha i_\beta}} = \sum_{\substack{\ell_\alpha \ell_\beta \ell \\ m_\alpha m_\beta m}} A^{m_\alpha m_\beta m}_{\ell_\alpha \ell_\beta \ell}(r_{i_\alpha}, r_{i_\beta}, R)\; C_{\ell_\alpha m_\alpha}(\hat{r}_{i_\alpha})\; C_{\ell_\beta m_\beta}(\hat{r}_{i_\beta})\; C^*_{\ell m}(\hat{R}) \qquad \text{(IV.14)}$$

où les coefficients $C_{\ell m}$ sont des harmoniques sphériques non normalisées définies avec la convention de phase de CONDON et SHORTLEY [49] :

$$C_{\ell m}(\hat{R}) = \left(\frac{4\pi}{2\ell + 1}\right)^{1/2} Y_{\ell m}(\hat{R}) \qquad \text{(IV.15)}$$

Par raison d'invariance du terme $1/r_{i_\alpha i_\beta}$ par rotation simultanée de $\vec{r}_{i_\alpha}$, $\vec{r}_{i_\beta}$ et $\vec{R}$, le coefficient $A^{m_\alpha m_\beta m}_{\ell_\alpha \ell_\beta \ell}$ s'écrit :

$$A^{m_\alpha m_\beta m}_{\ell_\alpha \ell_\beta \ell}(r_{i_\alpha}, r_{i_\beta}, R) = (\ell_\alpha m_\alpha \ell_\beta m_\beta \mid \ell_\alpha \ell_\beta \ell m)\; A_{\ell_\alpha \ell_\beta \ell}(r_{i_\alpha}, r_{i_\beta}, R) \qquad \text{(IV.16)}$$

où $(\ell_\alpha m_\alpha \ell_\beta m_\beta | \ell_\alpha \ell_\beta \ell m)$ est un coefficient de CLEBSCH-GORDAN [50] et le terme $A_{\ell_\alpha \ell_\beta \ell}$ est indépendant de m_α, m_β et m.

Il est bien connu, que dans les processus de collisions inélastiques rotationnelles entre deux molécules polaires, l'inélasticité rotationnelle est dominée par la forte anisotropie du potentiel à longue distance ; c'est-à-dire encore, que les forces intermoléculaires mises en jeu dans le type de collisions se font sentir à des distances plus grandes que les distributions de charges. En d'autres termes, il est possible de considérer que les distributions de charges des deux partenaires de la collision ne se recouvrent pas ($R > r_{i_\alpha} + r_{i_\beta}$). Dans ces conditions, on peut montrer [67] que le seul terme $A_{\ell_\alpha \ell_\beta \ell}$ different de zéro est celui pour lequel $\ell = \ell_\alpha + \ell_\beta$ et que la dépendance radiale de ce coefficient est donnée par [66] :

$$A_{\ell_\alpha \ell_\beta \ell} = (-1)^{\ell_\beta} \left[\frac{(2\ell)!}{(2\ell_\alpha)!(2\ell_\beta)!} \right] \left[\frac{r_{i_\alpha}^{\ell_\alpha} \; r_{i_\beta}^{\ell_\beta}}{R^{\ell+1}} \right] \qquad \text{(IV.17)}$$

où $\ell = \ell_\alpha + \ell_\beta$.

Il en résulte que le potentiel total d'interaction V(t) de l'équation (IV.12) devient :

$$V(t) = \sum_{\substack{\ell_\alpha \ell_\beta \\ m_\alpha m_\beta m}} (-1)^{\ell_\beta + m} \left[\frac{4\pi\,(2\ell)!}{(2\ell+1)(2\ell_\alpha)!(2\ell_\beta)!} \right]^{1/2} (\ell_\alpha m_\alpha \ell_\beta m_\beta \mid \ell_\alpha \ell_\beta \ell m)$$

$$Q_{\ell_\alpha m_\alpha}(\underset{\sim}{r}_\alpha)\; Q_{\ell_\beta m_\beta}(\underset{\sim}{r}_\beta)\; R(t)^{-\ell-1}\; Y_{\ell,-m}(\hat{R}) \qquad \text{(IV.18)}$$

$\underset{\sim}{r}_\alpha$ et $\underset{\sim}{r}_\beta$ désignent respectivement l'ensemble des coordonnées de toutes les charges des molécules α et β et $Q_{\ell m}$ est l'opérateur moment multipolaire électrique d'ordre ℓ défini par [66] :

$$Q_{\ell m}(\underset{\sim}{r}) = e \left[\frac{4\pi}{2\ell+1} \right]^{1/2} \sum_i Z_i \, r_i^\ell \, Y_{\ell m}(\hat{r}_i) \qquad \text{(IV.19)}$$

L'équation (IV.18) peut se mettre sous la forme :

$$V = \sum_{\ell_\alpha, \ell_\beta = 0}^{\infty} V_{\ell_\alpha \ell_\beta} \qquad \text{(IV.20)}$$

Les termes $V_{\ell_\alpha \ell_\beta}$ représentent les interactions instantanées entre les différents multipoles des deux molécules α et β. V_{00} est l'interaction charge-charge, V_{10} l'interaction charge-dipole, V_{11} l'interaction dipole-dipole etc...

Dans le cas qui nous intéresse, le premier terme non nul de l'équation (IV.20) est celui correspondant à l'interaction dipole-dipole soit $\ell_\alpha = \ell_\beta = 1$. Nous nous sommes limités à ce seul terme dans la suite de l'étude de la collision MgO + N_2O pour deux raisons : La première est que l'interaction quadrupole-dipole est en général un ou deux ordres de grandeur plus faible que l'interaction dipole-dipole ; ensuite, son effet se fait sentir à des distances plus faibles que celles mises en jeu dans l'interaction dipole-dipole puisqu'elle varie comme R^{-4} et non plus comme R^{-3} ; or, nous le verrons dans le paragraphe suivant, l'effet des interactions à courte distance est inclus dans une procédure de coupure de la probabilité de transition.

II - CALCULS DES SECTIONS EFFICACES DE TRANSFERT D'ENERGIE ENTRE LES PLUS BAS ETATS ELECTRONIQUES DE MgO ($X^1\Sigma^+$, $a^3\Pi$, $A^1\Pi$) PAR COLLISION AVEC N_2O

CROSS SECTIONS FOR COLLISIONAL ENERGY TRANSFER BETWEEN LOW-LYING ELECTRONIC STATES OF MgO ($X^1\Sigma^+$, $a^3\Pi$, $A^1\Pi$) IN COLLISIONS WITH N_2O.

Brigitte POUILLY and Jean-Michel ROBBE
Laboratoire de Spectroscopie des Molécules Diatomiques, ERA 303
Université des Sciences et Techniques de Lille, Bât. P5,
59655 - Villeneuve d'Ascq, FRANCE

and

Millard H. ALEXANDER
Department of Chemistry, University of Maryland, College Park
MARYLAND 20742

Abstract

The dipolar model developed by Alexander [J. Chem. Phys. 76, 429 (1982)] for collision induced transfer between closely spaced rotational manifolds of different electronic states, is here extended to the ground $X^1\Sigma^+$ and low lying $A^1\Pi$ and $a^3\Pi_0$ states of MgO, in collisions with N_2O. Spin-orbit or orbit-rotation mixing of two Born-Oppenheimer states leads to substantial dipole moments between states of the full molecular Hamiltonian. These dipole moments, and their phases relative to those of the perturbation matrix elements, are determined by SCF-CI calculations. The collisional coupling of the transition dipoles between the various MgO states with the permanent dipole of the N_2O molecule is treated here within the first Born approximation. We report cross sections for transitions within and between the rotational manifolds of selected near resonant vibrational levels of the (nominally) $X^1\Sigma^+$, $A^1\Pi_{e,f}$ and $a^3\Pi_{0e}$ states of MgO. The cross sections are substantial, although not as large as those reported by Alexander for CaO, in the neighborhood of the crossings between the various rotational ladders.

I - INTRODUCTION

Although there has been much experimental interest in reactions of the heavier alkaline earth atoms (Ba, Sr, Ca) with molecular oxidants [1-3], there have been very few studies of similar reactions involving Mg, [2b, 4-7] most likely because the reactions of the ground state atoms are endoergic. Taieb, Bourguignon and Rostas [4,5] have used a fast flow system to investigate reactions of Mg atoms in the ^3P state with N_2O, a reaction also studied at lower pressures in a beam-gas system by Dagdigian and Cox [2b,6]. Recently, Breckenridge and Umemoto [7] have completed an experimental study of nascent product distributions in reactions of Mg($^1P_1$) with CO_2.

In reactions of Ca and Ba(^1S) and Ca(^3P, ^1D) with polar oxidants (typically N_2O and NO_2), several experimental studies [3, 8-10] gave evidence for an increase in the total chemiluminescence yield with increasing pressure of the oxidant gas. This was interpreted [10-12] to imply that inelastic collisions, subsequent to the initial formation of products, act to transfer population from non-radiating excited states ($^{1,3}\Pi$, $^3\Sigma^+$), as well as high vibrational levels of the ground state, [1] of the alkaline earth oxide product into the $A^1\Sigma^+$ state, [13,14] which is itself strongly radiating [15]. In subsequent work [16] one of us (MHA) developed a simple dipolar model to explain the mechanism of the observed electronic energy transfer. This model makes us of small non-Born-Oppenheimer mixings between the individual dark excited states and the radiating $A^1\Sigma^+$ state [15] which results in a substantial transition dipole between the perturbed electronic states. The interaction between this transition dipole and the permanent dipole moment of a polar partner, in particular the N_2O oxidant gas, will lead to collisional transfer between the rotational manifolds of the

two perturbed states. The transfer will be most probable for rotational levels nearest the point of greatest mixing of the Born-Oppenheimer states, where the transition moment will be largest.

Cross sections and thermal rate constants for transfer from various vibrational manifolds of the $A'^1\Pi$ states and $a^3\Pi$ of CaO into the $A^1\Sigma^+$ state were determined [16] within the standard impact parameter version of the first Born approximation [17-20], modified to ensure statistical microreversibility [21]. With these computed constants it was then possible to model [22] the pressure dependence of CaO ($A^1\Sigma^+ \rightarrow X^1\Sigma^+$) emission under the kinetic conditions typical of the beam-gas experiments carried out in Dagdigian's laboratory [2,3,6,23].

The reaction of $Mg(^3P)$ atoms with N_2O presents a different picture. Experimentally, $B^1\Sigma^+ \rightarrow X^1\Sigma^+$ chemiluminescence is not observed under single collision conditions [2b,6] although production of the $B^1\Sigma^+$ state is energetically allowed. At higher pressure Bourguignon et al. [5] observe $B \rightarrow X$ emission. However, after a careful kinetic analysis they attribute this chemiluminescence to reactions of atoms in the ^1P state, produced by an energy pooling process [24,25] involving the collision of two ^3P atoms. In contrast to the observed [3] behaviour of $Ca(^3P, ^1D)$ the MgO $B \rightarrow X$ chemiluminescence was found [5] to decrease with increasing N_2O pressure.

A major difference between the products of the reactions of $Mg(^3P, ^1P)$ on the one hand and those of $Ba(^1S)$ or $Ca(^3P, ^1D)$ is the location of the first excited Σ and Π states. In MgO the Π states lie closer to the ground $X^1\Sigma^+$ state than to the first excited $B^1\Sigma^+$ and $b^3\Sigma^+$ states [14,26-30]. It is natural then to inquire to what extent collisions will act to transfer

nascent population from the $A^1\Pi$ and $a^3\Pi$ states not into the excited $B^1\Sigma^+$ state, as in the case of the $Ca(^3P, ^1D) + N_2O$ and $Ba(^1S) + N_2O$ reactions [15], but rather into the ground $X^1\Sigma^+$ state. Since the molecular beam studies of Dagdigian [6] indicate that the $a^3\Pi$ state is the primary product in the reaction of $Mg(^3P)$ with N_2O, it may well be necessary to take into account this collisional population transfer, in constructing kinetic models for the reactions of $Mg(^3P)$ under flame or fast-flow conditions. This type of collisional process may also contribute to the anomalous populations of the Λ doublets of the $a^3\Pi$ state observed recently in flame experiments by Cross, Ip and Field [31].

In the present article, we calculate the expected magnitude of the cross-sections for inelastic transfer from rotational manifolds of the lower vibrational levels of $MgO(a^3\Pi, A^1\Pi)$ into rotational manifolds of the $X^1\Sigma^+$ state, in collision with N_2O. The dipolar model developed earlier [16] is used. It requires a knowledge of the values of the non-Born-Oppenheimer perturbation parameters, Coriolis orbit-rotation and spin-orbit, which may be taken from experiment [32], and of the necessary electronic dipole matrix elements, which we have taken either from ab initio calculations described below, or from the recent work of Diffenderfer, Yarkony and Dagdigian [33].

The organization of this paper is as follows : In the next section we describe SCF + CI ab initio calculations performed on the four lowest electronic states of MgO ($X^1\Sigma^+$, $a^3\Pi$, $A^1\Pi$ and $B^1\Sigma^+$). Particular attention is paid to the investigation of the sign of the dipole matrix elements relative to that of the perturbation parameters, so that the interference effects between the various dipole coupling terms [16] can be treated correctly. Once the phase of the electronic wave-functions are clearly defined, calculations of (i) the non-Born-Oppenheimer perturbation parameters (section III), (ii) the electronic dipole moments

(section IV) and (iii) their relative signs are discussed and compared with experimental or theoretical results. Section V reviews the formalism of the standard impact parameter Born approximation and its application to the calculation of the energy transfer cross-sections. Results are presented in Section VI. A brief conclusion follows.

II - ELECTRONIC WAVEFUNCTION CALCULATIONS

a - Method

Many theoretical calculations have been devoted to the characterization and the description of the lowest singlet and triplet states of MgO. Richards, Verhaegen and Moser [34] as well as Schamps and Lefebvre-Brion [26] performed SCF calculations and estimated the correlation energies. Configuration mixing calculations were carried out by Malrieu, Huron and Rancurel [27]. Recently, more sophisticated methods : MCSCF (Bauschlicher, Silver and Yarkony [28]), full Valence MCSCF (Bauschlicher, Lengsfield, Silver and Yarkony [29]) and State Averadged MCSCF (Diffenderfer and Yarkony [35]) have been applied and discussed.

All these authors agree that the four lowest lying states of MgO belong essentially to three configurations :

$$(1\text{-}5)\sigma^2\ 1\pi^4\ 2\pi^4\ 6\sigma^2 \qquad (1)$$

$$(1\text{-}5)\sigma^2\ 1\pi^4\ 2\pi^3\ 6\sigma^2\ 7\sigma \qquad (2)$$

$$(1\text{-}5)\sigma^2\ 1\pi^4\ 2\pi^4\ 6\sigma\ 7\sigma \qquad (3)$$

The last studies [27,28,29,35] emphasize that although the $A^1\Pi$ and $a^3\Pi$ states can be well described by the single configuration (2), the two lowest $^1\Sigma^+$ states involve strong mixing of at least the two configurations (1) and (3). This results from the necessity of accounting for the change of the ionic character of the bond between the $X^1\Sigma^+$ and $B^1\Sigma^+$ states. One way to deal with such a problem is to start from MCSCF orbitals, as was done by Yarkony et al. [28,29,35]. This method will yield good values of the energies but the additional complexity may not be essential for calculations of the matrix elements of the one-electron operators with which we are dealing in this study (spin-orbit, orbit-rotation,

dipole moment).

We chose to use an SCF-CI technique based on the "nearly empty CI method" developed by Raseev [36]. The reliability of this method has already been established [37,38] and will be further demonstrated by the calculations reported here. In a first step the molecular orbitals are partitioned into three classes :

(i) the core orbitals, composed of molecular orbitals ($1\sigma^2 \rightarrow 3\sigma^2$) which arise from Mg(1s 2s) and O(1s) atomic orbitals. These are frozen in the calculations ;

(ii) the valence orbitals which define the spectroscopic states of interest : $4\sigma \rightarrow 7\sigma$, $1\pi \rightarrow 3\pi$;

(iii) the virtual orbitals which are unoccupied in the valence states and whose space has been limited to $8\sigma \rightarrow 11\sigma$ and $4\pi \rightarrow 5\pi$.

An exploratory Full Valence CI (FVCI) including all valence CSF's generated by distributing 14 electrons among the valence orbitals, allows us to select a number of reference determinants (practically all determinants whose weight is greater than 0.1 in the FVCI wavefunction). The FVCI configuration space is then extended by adding all CSF's obtained by the excitation of one valence electron to the virtual orbitals with the constraint that each CSF must be related to the whole reference determinants space by at most 2 electron replacements. A partially filled CI matrix is built with the diagonal elements and all off-diagonal elements coupled to at least one of the reference determinants. The diagonalization of this matrix is followed by a configuration selection and a smaller full matrix is reconstructed with CSF's whose energy contribution is greater than a threshold of 1.10^{-5} hartree.

The SCF molecular orbitals used as input in the CI calculations are linear combinations of Slater type atomic orbitals taken from Clementi and Roetti [39] for the Mg(^{1}S) and O(^{3}P) atoms. Two 3p orbitals (ζ_{3p} = 0.6 and 1.7) have been added on the Mg atom to improve the flexibility of the basis set and two 3d and one 4f on each center (ζ_{3dMg} = 0.94695 and 2.0083, ζ_{4fMg} = 2.4, ζ_{3dO} = 2.5 and 1.15, and ζ_{4fO} = 2.5) to describe the distortion of the atomic orbitals upon molecule formation. All calculations were performed with the Alchemy program developed by Bagus, Liu, Mc Lean and Yoshimine [40].

b - Ab-initio energies and spectroscopic constants

$^1\Sigma^+$ states

Preliminary FVCI calculations using SCF molecular orbitals obtained from the direct energy minimization of either configuration (1) or (3) have shown that the reference determinant space must contain the CSF's arising from the electron occupations :

$$(1\text{-}5)\sigma^2\ 6\sigma^2 \qquad 1\pi^4\ 2\pi^4 \qquad (4)$$

$$(1\text{-}5)\sigma^2\ 6\sigma\ \ 7\sigma \quad 1\pi^4\ 2\pi^4 \qquad (5)$$

$$(1\text{-}5)\sigma^2\ 6\sigma^2 \qquad 1\pi^4\ 2\pi^3\ 3\pi \qquad (6)$$

$$(1\text{-}5)\sigma^2 \qquad 7\sigma^2\ 1\pi^4\ 2\pi^4 \qquad (7)$$

The importance of the first three CSF's have been previously pointed out by Yarkony et al [28]. The fourth has been added to correct a correlation defect of the SCF description. With this four-dimensional reference space, 1524 CSF's were obtained and 144 CSF's were selected by a threshold of 1.10^{-5}. CI calculations

were performed at four internuclear separation ranging from 3.1 to 3.8 bohr with molecular orbitals obtained in an SCF calculation of configuration (3).

Table I displays our CI results and deduced spectroscopic constants. Selected results of Yarkony et al [28] as well as experimental values are given for comparison. Although the CI energies are consistently higher than the MCSCF-CI values, the agreement of the spectroscopic constants is excellent.

$^3\Pi$ and $^1\Pi$ states

It is well known that in alkaline earth oxides, the lowest $^3\Pi$ and $^1\Pi$ states are pure [28,41]. Hence, it did not seem necessary to perfom CI calculations for these states and only the SCF results are given in Table I. The calculated spectroscopic constants appear to be quite accurate.

III - NON-BORN-OPPENHEIMER PERTURBATION PARAMETERS

As discussed in the Introduction, in order to model the collision dynamics we need to characterize the degree of non-Born-Oppenheimer mixings between the ground $X^1\Sigma^+$ and the $A^1\Pi$ and $a^3\Pi$ states. In Hund's case (a), the total wavefunction of each of these states may be written as [42] :

$$| J \Omega M, v S \Lambda \Sigma > = | J \Omega M > | v S \Lambda \Sigma > \qquad (8)$$

Linear combinations of these wavefunctions lead to definite parity states [43], which we label with the e/f notation of Kopp and Hougen [44]. The $^1\Pi_e$ levels are coupled to $^1\Sigma^+$ by the Coriolis orbit-rotation interaction and the $^3\Pi_{0e}$ levels

TABLE I : Energies and Spectroscopic Constants for the Lowest States of MgO [a]

	r = 3.1 [b]	r = 3.3 [b]	r = 3.5 [b]	r = 3.7 [b]	r = 3.8 [b]	T_e (cm^{-1})	ω_e (cm^{-1})	r_e [b]
$X^1\Sigma^+$	-274.47189	-274.47964	-274.47763		-274.46478	0	780.1	3.348
	(-274.63011)	(-274.63739)	(-274.63526)	(-274.62780)		0	(795)	(3.342)
exp						0	785.1 [e]	3.305 [c]
$B^1\Sigma^+$	-274.37992	-274.38617	-274.38195		-274.36541	20570	844.3	3.306
	(-274.53228)	(-274.53617)	(-274.53066)	(-274.51982)		(22289)	(796)	(3.269)
exp						19984 [c]	824.0 [c]	3.282 [c]
$a^3\Pi$ [6]	-274.45235	-274.46790	-274.47178		-274.46534	1780	721.7	3.487
			(-274.56987)				712.3 [d]	3.507 [d]
exp						2633 [e]	648 [e]	3.534 [e]
$A^1\Pi$ [6]	-274.44883	-274.46448	-274.46843		-274.46202	2515	722.0	3.488
			(-274.56493)				746.2 [d]	3.504 [d]
exp						3557 [e]	664.4 [c]	3.522 [c]

[a] In parentheses are given the SA MCSCF results of Diffenderfer and Yarkony (ref 35). [b] Distances in bohr. [c] Lagerqvist and Uhler (ref 54). [d] Bauschlicher, Lengsfield, Silver and Yarkony (MCSCF + CI results, ref 29). [e] Ikeda, Wong, Harris and Field (ref 32 [6] SCF results.

are coupled to $^1\Sigma^+$ by the spin-orbit interaction.

The coupling matrix elements are written as :

$$< J M v_A\, ^1\Pi_e \mid H_{OR} \mid J M v_X\, ^1\Sigma^+ > \;=\; -[2J(J+1)]^{1/2} < v_A \mid B \mid v_X > < ^1\Pi \mid L_+ \mid ^1\Sigma^+ > \qquad (9)$$

and

$$< J M v_a\, ^3\Pi_{0e} \mid H_{SO} \mid J M v_X\, ^1\Sigma^+ > \;=\; 2^{1/2} < v_a \mid v_X > < ^3\Pi_0 \mid \sum_i a_i \vec{\ell}_i . \vec{s}_i \mid ^1\Sigma^+ > \qquad (10)$$

where $< v_A \mid B \mid v_X >$ is an off-diagonal matrix element of the rotational operator $B(r)$ and $< v_a \mid v_X >$ is a vibrational overlap integral. The sum which appears in eq 10 is taken over all electrons.

The electronic matrix elements are usually expressed in terms of two one-electron parameters $a = < 2\pi \mid a\ell_+ \mid 7\sigma >$ and $b = < 2\pi \mid \ell_+ \mid 7\sigma >$, so that

$$< ^1\Pi \mid L_+ \mid ^1\Sigma^+ > \;=\; 2^{1/2}\, b \qquad (11)$$

$$< ^3\Pi_0 \mid \sum_i a_i \vec{\ell}_i . \vec{s}_i \mid ^1\Sigma^+ > \;=\; \frac{1}{2}\, a. \qquad (12)$$

Before calculation of the a and b parameters, it is necessary to define explicitly the phase choice for the electronic wavefunction. For this purpose, we fixed the canonical order for the molecular orbitals ($1\sigma \rightarrow 7\sigma$, $1\pi \rightarrow 3\pi$) and were careful, when these molecular orbitals appeared in different molecular states, to keep the same sign on the main LCAO coefficient. Also, we use throughout this work the conventional phase choice defined by Condon and Shortley [45] for the matrix elements of the $\ell_\pm$ and $s_\pm$ operators, namely

$$< \ell, \lambda \mid \ell_{\pm} \mid \ell, \lambda \mp 1 > \; > \; 0 \qquad (13)$$

$$< \tfrac{1}{2}, \sigma \mid s_{\pm} \mid \tfrac{1}{2}, \sigma \mp 1 > \; = \; + 1 \qquad (14)$$

With these phase definitions and starting from the electronic wavefunctions for the $X^1\Sigma^+$, $A^1\Pi$ and $a^3\Pi$ states, we have calculated the following values of the electronic matrix elements a and b at r=3.3 and 3.8 bohr using a program written by Hall [46] which calculates the matrix elements between determinants :

$$b = + 0.76 \quad \text{and} \quad a = + 98 \text{ cm}^{-1} \quad ; \quad r = 3.3 \text{ bohr} \qquad (15)$$

and

$$b = + 0.79 \quad \text{and} \quad a = + 106 \text{ cm}^{-1} \quad ; \quad r = 3.8 \text{ bohr.} \qquad (16)$$

The magnitudes are in good agreement with the experimental values [32] obtained at r = 3.8 bohr (R-centroid value of the perturbation), namely [47]

$$| b |_{exp} = 0.60 \quad \text{and} \quad | a | = 101 \text{ cm}^{-1} \qquad (17)$$

The signs of a and b are impossible to obtain experimentally, and are, of course, arbitrary. What will be important, for the dynamical model used here, [16] are the signs of a and b relative to the signs of the electronic dipole matrix elements.

IV - DIPOLE MATRIX ELEMENTS

We turn now to the calculation of these matrix elements, following Alexander's earlier notation [16].

The electronic dipole moment operator is defined in a space-fixed frame by [48] :

$$Q_{lm} = (4\pi/3)^{1/2}\, e \sum_i z_i\, r_i\, Y_{lm}(\hat{r}_i), \qquad (18)$$

where Y_{lm} is a spherical harmonic and where the sum is taken over all particles of charge ez_i. The factorization of the total wavefunction into electronic, vibrational and rotational parts allows us to write an electronic dipole moment $R_{lk}(r)$ as :

$$R_{lk}(r) = \int {}^{2S'+1}\phi_{\Lambda'}(q, \sigma; r)\, Q_{lk}(q, r)\, {}^{2S+1}\phi_{\Lambda}(q, \sigma; r)\, dq\, d\sigma \qquad (19)$$

where Q_{lk} is a dipole component with $k = \Lambda' - \Lambda$, q and σ denote collectively the space and the spin coordinates of all electrons, r is the internuclear separation and all quantities are referred to a molecule-fixed frame.

We have calculated the relevant non-vanishing values of $R_{lk}(r)$ for inter and intrastate coupling involving the X, a, and A states of MgO, using our ab initio wavefunctions with the phase choice described in Sec. III. The results, displayed in Table II, are rather encouraging. Ikeda et al. [32] have determined an experimental value of the $R_{10}^{BX} / R_{11}^{AB}$ ratio of 1.35 ± 0.07 at r = 3.3 a.u., which compares well with our values of 1.25 for this ratio. Our interstate dipole moments differ by only few percent from those given by Huron et al. [27], who also used an SCF + CI method. The discrepancy with the results of Diffenderfer et al. [35] is a little greater, but the r-dependence, which is another sensitive test of the accuracy of the wavefunctions, agrees much better.

In conclusion, all parameters needed to treat the dynamics of the collision [16] have been precisely determined and their relative sign fixed theoretically.

TABLE II : Inter and Intrastate Dipole Matrix Elements (a.u.) [a]

State,State [b] $R_{l,\Lambda'-\Lambda}$	r = 3.1 [c]	r = 3.3 [c]	r = 3.5 [c]	r = 3.8 [c]
X,X R_{10}	1.69 2.227 [d]	1.84 2.278 [d]	1.98 2.294 [d]	2.16
B,B R_{10}	2.25 2.512 [d]	2.32 2.562 [d]	2.40 2.678 [d]	2.51
a,a R_{10}	0.88	1.05	1.23	1.52
A,A R_{10}	0.80	0.98	1.17	1.47
A,X R_{11}	0.432	0.412 0.36 [e] 0.347 [f]	0.380 0.315 [f]	0.323
A,B R_{11}	0.909	0.953 0.100 [e]	0.999	1.061
B,X R_{10}	1.766 [d]	- 1.195 1.595 [d] 1.13 [e]	1.402 [d]	

[a] 1 a.u. = 2.5417 Debye. For the intrastate dipole moments a positive sign indicates Mg^+O^- polarity. For the interstate dipole moments the signs reflect the phase choices made in the text (section III). [b] Eq (19). $R_{10} = \mu_Z$, $R_{11} = -\frac{1}{\sqrt{2}}(\mu_x+i\mu_y)$ and corresponds to the matrix element : $< \Lambda=1, S=\Sigma=0 | Q_{11} | \Lambda=0, S=\Sigma=0 >$. [c] Distances in bohr. [d] ref 35. [e] ref 27. [f] ref 33.

We shall see in the next section that this last point is particularly important in the case of MgO since, in contrast with the previous CaO collisional energy transfer study [16], it is important not to neglect the contribution of the interstate dipole moment matrix element between the $A^1\Pi$ and $X^1\Sigma^+$ states.

V - COLLISION DYNAMICS

We have treated MgO + N_2O collisions within the semi-classical time-dependent first Born approximation which represents a truncation to first order in the expansion of the scattering matrix S, and which has been already employed in earlier studies of collisional energy transfer [16-20]. This approximation is justified if the time-dependent interaction potential V(t,b), where b is the impact parameter, between both molecules remains much weaker than the kinetic energy of the relative motion so that V(t,b) can be treated as a perturbation on the total Hamiltonian for the bimolecular system.

Within the first Born approximation, the probability for a transition between an initial state $|\, i>$ and a final state $|\, f>$ is given by [17-19]

$$P_{if}(b) = \hbar^{-2} \left| \int_{-\infty}^{+\infty} \exp(i\,\omega_{if}\,t) < f \,|\, V(t,b) \,|\, i > dt \right|^2 \qquad (20)$$

where $\omega_{if} = (E_{\alpha f} + E_{\beta f} - E_{\alpha i} - E_{\beta i})/\hbar$, with subscripts α and β referring to MgO

and N_2O respectively. As is usually done, we will assume a linear trajectory for the relative motion of the two collision partners.

The integral cross section for the $J_\alpha J_\beta \rightarrow J'_\alpha J'_\beta$ transition is obtained by summing and averaging $P_{if}(b)$ (eq 20) over the projection quantum numbers, and then integrating over the impact parameter. We have

$$\sigma_{J_\alpha\, J_\beta \rightarrow J'_\alpha\, J'_\beta} = 2\pi \int_0^\infty b\, P_{J_\alpha\, J_\beta \rightarrow J'_\alpha\, J'_\beta}(b)\, db \quad , \tag{21}$$

where the degeneracy averaged transition probability is given by [16,48]

$$P_{J_\alpha J_\beta \rightarrow J'_\alpha J'_\beta}(b) = \frac{2}{3\hbar^2 b^4 v^2} \frac{(J'_\alpha \Lambda'_\alpha \Omega'_\alpha v'_\alpha \| Q_1 \| J_\alpha \Lambda_\alpha \Omega_\alpha v_\alpha)^2 (J'_\beta \Lambda'_\beta \Omega'_\beta v'_\beta \| Q_1 \| J_\beta \Lambda_\beta \Omega_\beta v_\beta)^2}{(2J_\alpha + 1)(2J_\beta + 1)}$$

$$\sum_{m=-2}^{+2} \left| J_m^2(\omega_{if}, b) \right|^2 \delta(S_\alpha S'_\alpha)\, \delta(\Sigma_\alpha \Sigma'_\alpha) \tag{22}$$

Here v is the relative velocity and the reduced matrix elements of the dipole operator are defined by [16]

$$(J'\Lambda'\Omega' v' \| Q_1 \| J\Lambda\Omega v) = (-1)^{J'-M'} \begin{pmatrix} J' & 1 & J \\ -M' & M'-M & M \end{pmatrix}^{-1} (J' M' \Lambda' \Omega' v' | Q_{1m} | J M \Lambda \Omega v) \tag{23}$$

where $\begin{pmatrix} \cdot & \cdot & \cdot \\ \cdot & \cdot & \cdot \end{pmatrix}$ is a 3j symbol [49,50]. The quantities $J_m^2(\omega_{if},b)$ arise from the integration over time in eq 20. The sum in eq 22 can be well approximated by [18,51]

$$\sum_m \left| J_m^2 (\omega_{if}, b) \right|^2 = 4 \exp(-2\omega_{if} b/v) \left[A_2 + B_2 \omega_{if} b/v + C_2 \omega_{if}^2 b^2/v^2 + \ldots \right], \quad (24)$$

where values of the coefficients have been presented by several authors [18,51].

To avoid unphysically large values of the transition probability at small values of the impact parameter, we used the cutoff procedure previously defined. [16,52] It consists in rewriting the transition probability as

$$P_{J_\alpha J_\beta \to J'_\alpha J'_\beta}(b) = P^0_{J_\alpha J_\beta \to J'_\alpha J'_\beta}(b) \, (J_\alpha \Omega_\alpha \, 1 \, \Lambda'_\alpha - \Lambda_\alpha \mid J_\alpha \, 1 \, J'_\alpha \, \Omega'_\alpha)^2 \, (J_\beta \Omega_\beta \, 1 \, \Lambda'_\beta - \Lambda_\beta \mid J_\beta \, 1 \, J'_\beta \, \Omega'_\beta)^2 , \quad (25)$$

where $(J\,\Omega\,1\;\Lambda'-\Lambda \mid J\,1\,J'\,\Omega')$ is a Clebsch-Gordan coefficient [49].
Equation (21) is then written as

$$\sigma_{J_\alpha J_\beta \to J'_\alpha J'_\beta} = (J_\alpha \Omega_\alpha \, 1 \, \Lambda'_\alpha - \Lambda_\alpha \mid J_\alpha \, 1 \, J'_\alpha \, \Omega'_\alpha)^2 \, (J_\beta \Omega_\beta \, 1 \, \Lambda'_\beta - \Lambda_\beta \mid J_\beta \, 1 \, J'_\beta \, \Omega'_\beta)^2 \left[\frac{\pi b_c^2}{2} + 2\pi \int_{b_c}^{\infty} b \, P^0_{J_\alpha J_\beta \to J'_\alpha J'_\beta}(b) \, db \right] \quad (26)$$

where b_c, the cutoff impact parameter, is chosen so that $P^0 (b = b_c) = 0.5$.
We note that the contribution to the cross section arising from impact parameters greater than b_c is described identically in eqs 21 and 26. Equation 26 is to be preferred over earlier cutoff procedures [17-19] in that statistical microreversibility is ensured within the cutoff region.

If the rotational levels of the target are neither selected nor resolved then the appropriate cross section, indexed only in the initial and final rotational quantum numbers of molecule α, is obtained from eq 26 by summing over all values of J'_β and averaging over an assumed Boltzmann distribution of initial rotational levels. We then have [16]

$$\sigma_{J_\alpha \to J'_\alpha}(v) = Z_\beta^{-1}(T_r) \sum_{J_\beta} (2J_\beta + 1) \exp\left[-B_\beta J_\beta (J_\beta + 1)/k T_r\right] \sum_{J'_\beta} \sigma_{J_\alpha J_\beta \to J'_\alpha J'_\beta} \quad , \tag{27}$$

where Z_β, T_r and B_β denote the rotational partition function, the rotational temperature and the rotational constant of the target, respectively.

If two Born-Oppenheimer states are mixed by a small perturbation, then one must use in eq 22 the reduced dipole matrix elements appropriate to the mixed states [16]. For mixing between the $X^1\Sigma^+$ state of MgO and either the $A^1\Pi$ or $a^3\Pi_0$ states, the wavefunctions of the mixed states can be expressed as a linear combination of the definite parity Born-Oppenheimer wavefunctions.
In the notation of our previous work [16] we define

$$|\, J\, M\, a\rangle = A\,|\, J\, M\, v_X\, {}^1\Sigma^+\rangle + B\,|\, J\, M\, v_A\, {}^1\Pi_e\rangle \tag{28}$$

$$|\, J\, M\, b\rangle = |\, J\, M\, v_A\, {}^1\Pi_f\rangle \tag{29}$$

$$|\, J\, M\, c\rangle = C\,|\, J\, M\, v_X\, {}^1\Sigma^+\rangle + D\,|\, J\, M\, v_a\, {}^3\Pi_{0e}\rangle \tag{30}$$

where each pair of coefficients A, B or C, D is obtained by diagonalization of a 2x2 Hamiltonian matrix. Since the non-Born-Oppenheimer perturbations for MgO are small in magnitude (eqs 15-17), the mixing will be significant, with

the A, B, C and D coefficients significantly different from zero or unity, only in the neighborhood of the isoenergetic point, where the rotational manifolds of the two Born-Oppenheimer states cross. Far from these crossings the wavefunctions given by eqs 28-30 become identical to the pure $X^1\Sigma^+$, $A^1\Pi$ and $a^3\Pi_0$ wavefunctions.

In the case of these mixed states the reduced dipole matrix elements appearing in eq 22 can be written as linear combinations of reduced matrix elements between the various basis states defined by eqs 28-30. We have

$$(J+1,\ a' \| Q_1 \| J,\ a) = AA'\ R^{v_X v_X}_{10}\ (J+1)^{1/2} + BB'\ R^{v_A v_A}_{10}\ [J(J+2)/(J+1)]^{1/2} - R^{v_A v_X}_{11}\ [J^{1/2}\ A'B - (J+2)^{1/2}\ AB'] \tag{31}$$

$$(J-1,\ a' \| Q_1 \| J,\ a) = -\ AA'\ R^{v_X v_X}_{10}\ J^{1/2} - BB'\ R^{v_A v_A}_{10}\ [(J-1)(J+1)/J]^{1/2} - R^{v_A v_X}_{11}\ [(J+1)^{1/2}\ A'B - (J-1)^{1/2}\ AB'] \tag{32}$$

$$(J',\ a \| Q_1 \| J,\ b) = \delta(J'\ J)(2J+1)^{1/2} \left\{ -\ A\ R^{v_A v_X}_{11} + B\ R^{v_A v_A}_{10}\ [(J(J+1)]^{-1/2} \right. \tag{33}$$

$$(J+1,\ c' \| Q_1 \| J,\ c) = (J+1)^{1/2}\ [CC'\ R^{v_X v_X}_{10} + DD'\ R^{v_a v_a}_{10}] \tag{34}$$

$$(J-1,\ c' \| Q_1 \| J,\ c) = -\ J^{1/2}\ [CC'\ R^{v_X v_X}_{10} + DD'\ R^{v_a v_a}_{10}] \tag{35}$$

Here the quantities $R^{v'v}_{1,\Lambda'-\Lambda}$ correspond to a vibrational average of the electronic

transition moment $R^{\text{State-State}}_{1,\Lambda'-\Lambda}(r)$ (eq 19), which were calculated at various values of r, as given in Table II. We have

$$R^{v'v}_{1,\Lambda'-\Lambda} = \int \chi_{v'}(r)\, R_{1,\Lambda'-\Lambda}(r)\, \chi_{v}(r)\, dr \qquad (36)$$

where $\chi_v'(r)$ is the vibrational wavefunction with the electronic state index suppressed for simplicity.

Equations 31-35 were obtained using the following expression for the reduced dipole matrix element between Hund's case (a) functions :

$$(J'\ \Omega'\ v'\ S'\ \Lambda'\ \Sigma' \| Q_1 \| J\ \Omega\ v\ S\ \Lambda\ \Sigma) = (-1)^{-J'-\Omega'} R^{v'v}_{1,\Lambda'-\Lambda} [(2J+1)(2J'+1)]^{1/2} \begin{pmatrix} J' & 1 & J \\ -\Omega' & \Lambda'-\Lambda & \Omega \end{pmatrix} . \qquad (37)$$

In the derivation of eqs 31-35 it is also necessary to take into account that for a Σ-Π transition, the transition matrix element $R^{v_A v_X}_{11}$ is equal to the negative of the reversed quantity $R^{v_X v_A}_{11}$ [16].

There is no electric dipole coupling between Born-Oppenheimer states of differing multiplicity. Furthermore only the $^3\Pi_{0e}$ levels are mixed with the $X^1\Sigma^+$ levels by the spin-orbit perturbation. Thus in the case (a) limit neither the $^3\Pi_{0f}$, nor the $^3\Pi_{1e/f}$ nor the $^3\Pi_{2e/f}$ levels will be directly coupled by collisions with the $X^1\Sigma^+$ levels, at least within the dipolar model used here.

At high J, where a pure case (a) description of the $^3\Pi$ state is no longer appropriate, the 1e and 2e levels will become increasingly mixed with the 0e level. Collision induced transitions from the former levels into the $X^1\Sigma^+$ state will then become possible, by virtue of this mixing. More will be said about this in the next section.

V - RESULTS

Table III lists the crossings between the rotational manifolds of the v_X = 3-10 levels and those of the v_A = 0-6 and v_a = 0-8 levels [53]. We have listed only those crossings for which the rotational quantum number at the crossing is less than 100. We see for a given value of v_X the crossings with the $A^1\Pi$ and $a^3\Pi_0$ states are always energetically far apart. Thus the mixing between each of these states and the $X^1\Sigma^+$ ground state can be treated as two separate two-manifold problems (a-X and A-X). The spectroscopic constants of the $X^1\Sigma^+$, $A^1\Pi$ and $a^3\Pi_0$ states are given in Table IV. The rotational constants of the $X^1\Sigma^+$ state have been taken from Lagerqvist and Uhler [54]. Although the latter values are valid only for v = 0-2, we have verified that neglect of the slight corrections for the higher vibrational levels reported by Ikeda et al [32] does not appreciably affect either the calculated mixing coefficients or the dipole matrix elements (eq 36).

These matrix elements were computed by numerical integration of eq 36, using a spline fit to interpolate the ab initio values of $R_{1,\Lambda'-\Lambda}(r)$, determined at the points listed in Table II. The vibrational wavefunctions χ_v were themselves obtained by Numerov integration of Morse potentials used to represent the $X^1\Sigma^+$, $A^1\Pi$, and $a^3\Pi$ states

The $R^{v'v}_{1,\Lambda'-\Lambda}$ values, as well as the overlap integrals $\langle v_a | v_X \rangle$ and the matrix elements of the rotational operator $\langle v_A | B(r) | v_X \rangle$ which appear in eqs 9 and 10, are listed in Table V. For the determination of the A, B, C and D

TABLE III : Location of Crossings between the MgO $X^1\Sigma^+$ (v_X) and the $A^1\Pi$ (v_A) or a $^3\Pi_{0e}$ (v_a) Rotational Manifolds and Cross Sections for Interstate Transfer in Collisions with N_2O at v = 5.5 10^4 cm/s.

			Cross section ($\AA^2$)				Cross section ($\AA^2$)
v_X	v_A	J [a]	$^1\Pi_e \rightarrow X$	$^1\Pi_f \rightarrow X$	v_a	J	$^3\Pi_{0e} \rightarrow X$
3	... [b]				0	81	5
4	0	96	4	5	1	67	7
5	1	88	4	8	2	49	13
6	2	79	5	11	3	19	71
7	3	69	7	12	... [c]		
8	4	57	10	13	6	92	4
9	5	43	18	14	7	82	5
10	6	23	60	13	8	69	

[a] Values of J at the crossing between the rotational manifolds of the Born-Oppenheimer Π and Σ states. The $\Pi_e \rightarrow X$ cross sections correspond to R-branch ($J \rightarrow J+1$) transitions ; the $\Pi_f \rightarrow X$ cross sections, to Q-branch ($J \rightarrow J$) transitions. [b] No crossing with the v_X=3 manifold occurs for $J < 100$. [c] No crossing with the v_X=7 manifold occurs for $J < 100$.

TABLE IV : Spectroscopic Constants of the $X^1\Sigma^+$, $A^1\Pi$ and $a^3\Pi$ States of MgO (cm^{-1}).

	$X^1\Sigma^+$	$A^1\Pi$	$a^3\Pi$ [a]
T_e	0	3557.5 [a]	2623
ω_e	785.14 [a]	664.44 [b]	648
$\omega_e x_e$	5.07 [a]	3.91 [b]	3.9
B_e	0.5743 [b]	0.5056 [b]	0.5022
α_e	0.0050 [b]	0.0046 [b]	0.0042
A	-	-	-64

[a] ref 32. [b] ref 54.

TABLE V : Vibrational Matrix Elements of the Dipole Moment and Rotational Operators between the $A^1\Pi$ and $X^1\Sigma^+$ states ; and Overlap Integrals between the $X^1\Sigma^+$ and $a^3\Pi$ states [a].

v_X	v_A	v_a	$R_{11}^{v_A v_X}$ (Debye)	$< v_A \lvert B(r) \rvert v_X >$ (cm^{-1})	$< v_a \lvert v_X >$
3		0			0.325
4	0	1	0.108	0.057	0.458
5	1	2	0.192	0.102	0.495
6	2	3	0.263	0.140	0.461
7	3		0.318	0.169	
8	4	6	0.351	0.188	-0.262
9	5	7	0.369	0.197	-0.317
10	6	8	0.366	0.199	-0.329

[a] The signs of all parameters correspond to the phase choices adopted throughout this work.

coefficients (eqs 28-30) which represent the degree of mixing between the Born-Oppenheimer states, we have used the experimental values of the a (spin-orbit) and b (coriolis) perturbation parameters (eqs 11, 12 and 17) with the both signs taken as positive, as indicated by the theoretical calculations (eqs 15 and 16). The N_2O target is assumed to remain in its electronic ground state with rotational constant [55] $B_\beta = 0.4182\ cm^{-1}$ and dipole moment [56] $R_\beta = 0.167$ D. The N_2O rotational temperature T_r in eq 27 was taken to be 300 K.

Cross sections have been calculated at two values of the relative velocity of the collision partners : $v = 5.5\ 10^4$ cm/s and $1.8\ 10^5$ cm/s, which correspond to typical velocities in the experiments of, respectively, Bourguignon et al. [5] and Dagdigian [6].

For the value of J which is closest to the isoenergetic point at the crossings, Table III gives the values of the cross sections at $v = 5.5\ 10^4$ cm/s. It is obvious that the cross sections are largest when the crossing occurs at relatively low J. Similar behavior was seen in Alexander's calculations [16] on $A'\,^1\Pi \rightarrow A^1\Sigma^+$ energy transfer in the CaO + N_2O system. This decrease occurs because at high J the rotational spacings of the MgO molecule are proportionally larger. This has two effects. First, the mixing coefficients (eqs 28-30), which are obtained by solution of 2x2 secular determinants, are proportionally smaller. As a result the transition dipoles between the eigenstates of the full molecular Hamiltonian may decrease in magnitude. Secondly, due to the increase in the spacing between adjacent rotational levels, the quantity represented by the sum in eq 24 will decrease, and, consequently, so will the inelastic transition probability (eq 22) and cross section (eq 26).

Figure 1 displays the Born $J \rightarrow J+1$ cross sections at $v = 5.5\ 10^4$ cm/s for transitions between the various mixed states which lie near the crossings of the $v_A = 5$ and 6 manifolds of the (nominally) $A^1\Pi$ state with, respectively, the $v_X = 9$ and 10 manifolds of the (nominally) $X^1\Sigma^+$ state. We see that the cross

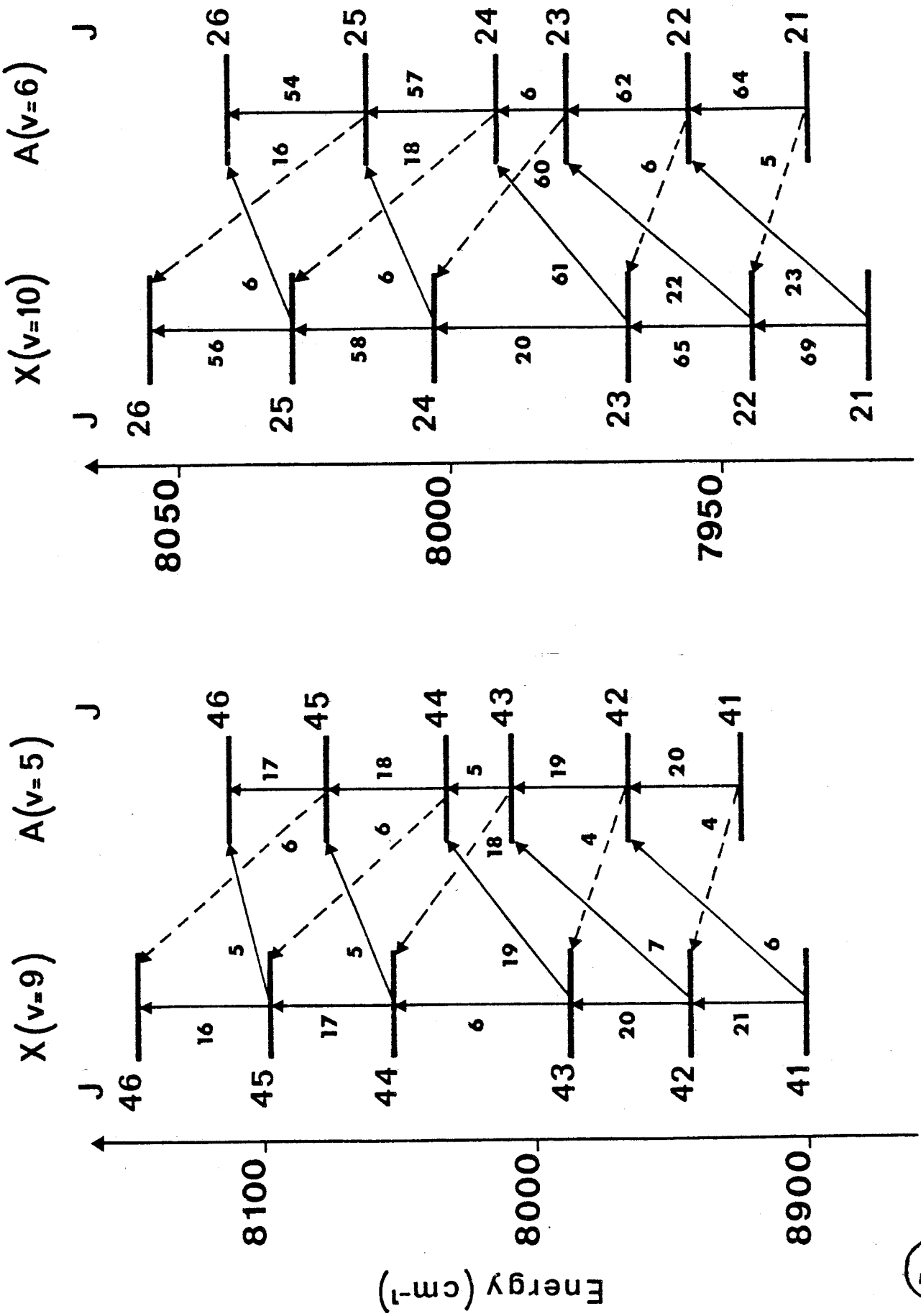

Figure I

sections for transitions in which the predominant electronic character of the state changes are comparable in size to those for transitions in which the predominant electronic character is preserved.

Figure 2 illustrates the dependence on J of the cross sections for the (nominally) $A^1\Pi_e$ (v_A, J) → (nominally) $X^1\Sigma^+$ (v_X, J + 1) transitions over a wider range of J values in the neighborhood of the crossing of the $v_A = 5$ and $v_X = 9$ manifolds. Values are graphed both for v = 5.5 10^4 cm/s and v = 1.8 10^5 cm/s. To test the sensitivity of the input values of the various electronic dipole matrix elements, we have also plotted in Fig. 2 the cross sections at v = 5.5 10^4 cm/s for the (nominally) $A^1\Pi_e$ → (nominally) $X^1\Sigma^+$ transition computed using the inter- and intrastate dipole moments of Yarkony et al [33,35]. The curves are qualitatively similar. In both cases the A→X cross section is largest at the isoenergetic point J ≃ 43 and drops swiftly as J increases or decreases from this value. The cross section actually drops to zero for J ≃ 38 with the dipole moments of the present paper and for J ≃ 28 with the dipole moments of Yarkony et al [33,35].

The shape of these curves, and, specifically, the vanishing of the cross sections, is related to the variation with J of the absolute value of an effective dipole moment defined as

$$(J+1,\ a'||\ \mu\ ||\ J,\ a) \;=\; (J+1,\ a'||\ Q_1\ ||\ J,\ a)\ \ (J+1)^{-1/2}\ , \qquad (38)$$

since the transition probabilities are proportional to the square of the reduced matrix elements (eq 22). This effective moment avoids the $J^{1/2}$ dependency of the reduced matrix elements. From eqs 31 and 32 we see that even if the dipole moments are all of the same sign, nevertheless, because the A and B coefficients will differ in sign in the mixed states of predominantly $A^1\Pi_e$ or $X^1\Sigma^+$ character [16], and because the third term in eqs 31 and 32 enters with a minus sign, a cancellation of the various terms can occur. To illustrate this point Fig. 3 displays the effective dipole moments (eq 38) between the mixed states of predominantly

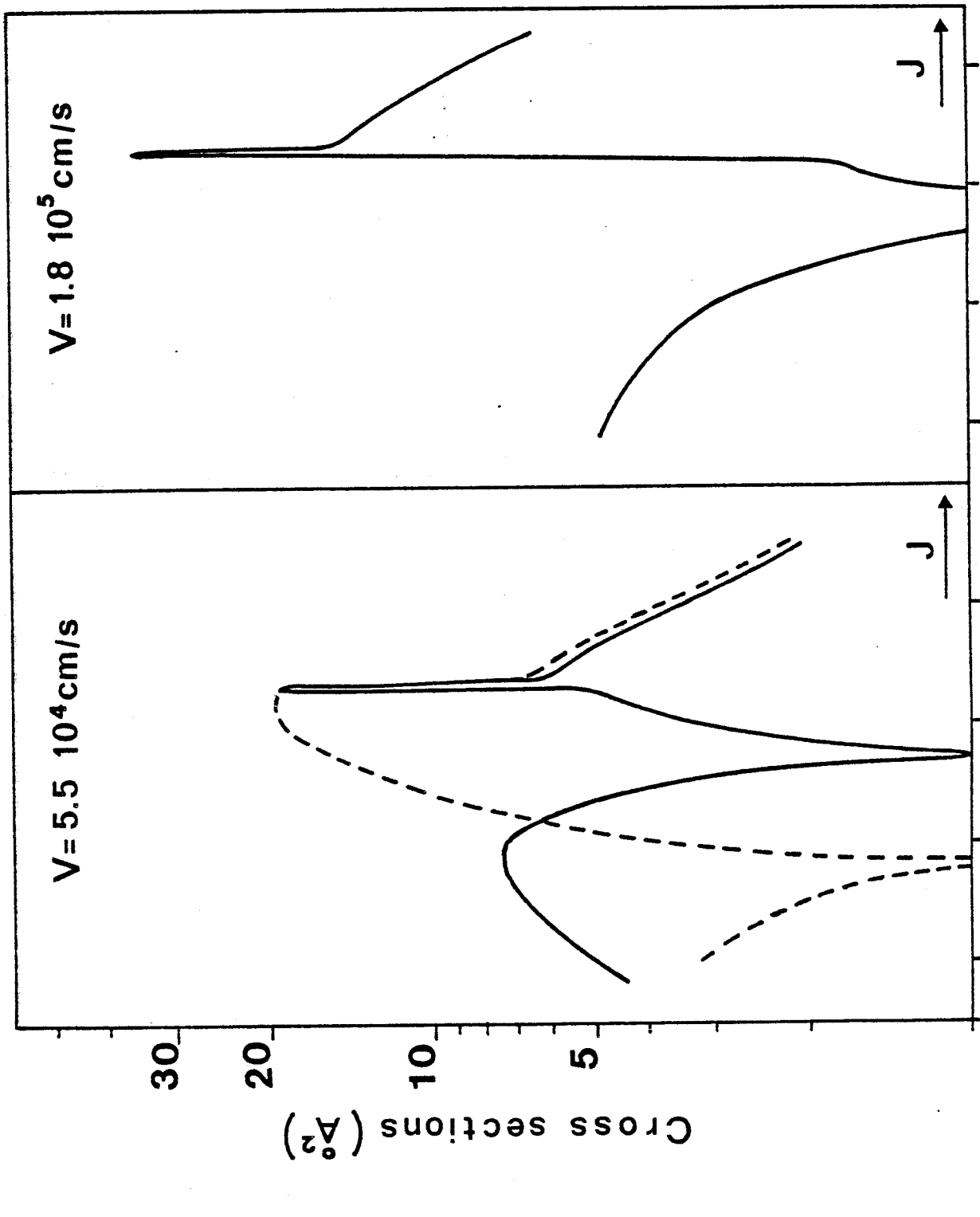

Figure 2

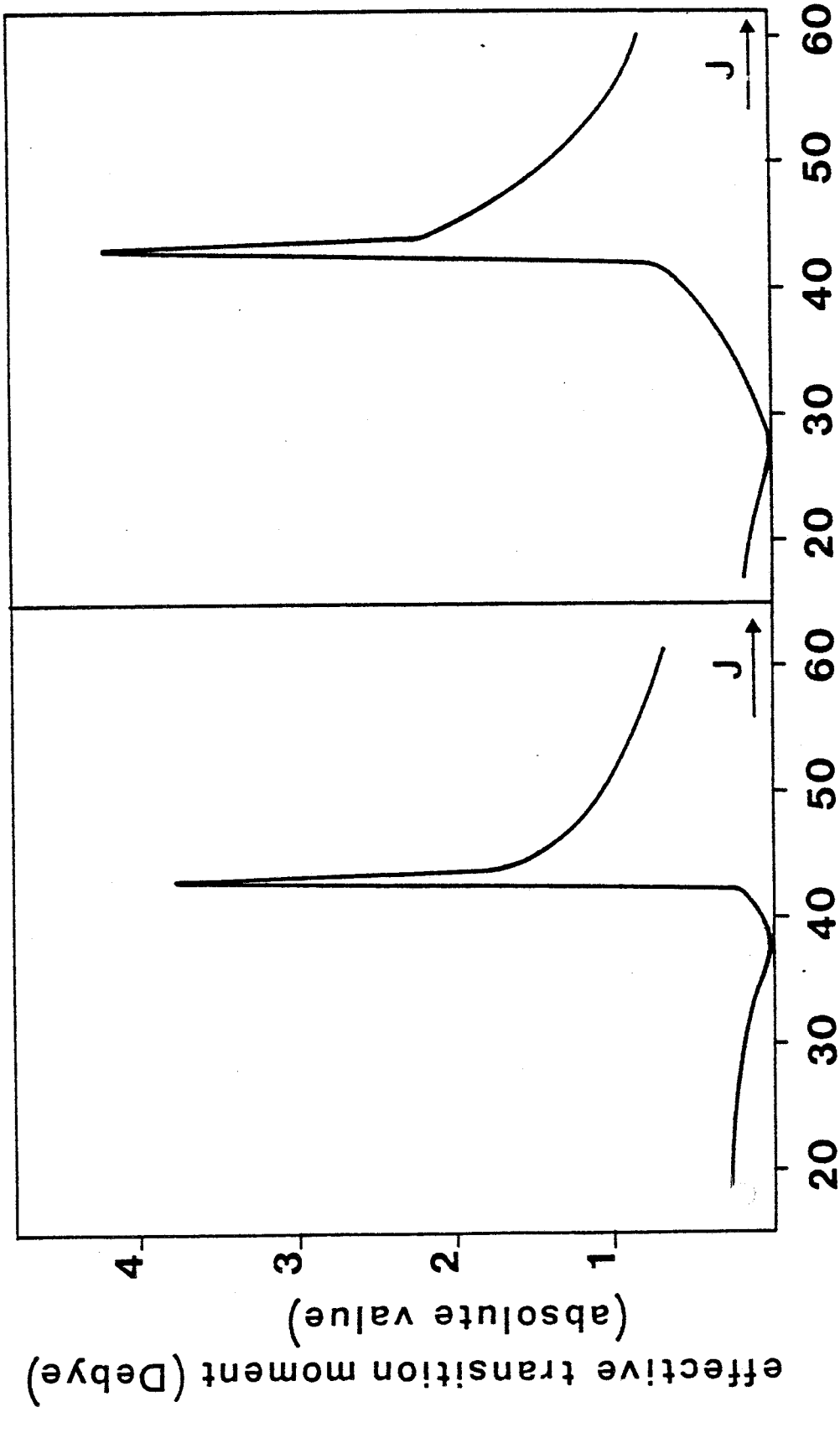
effective transition moment (Debye)
(absolute value)
4
3
2
1
20
30
40
50
60
J
20
30
40
50
60
J

Figure 3

$A^1\Pi_e$ and $X^1\Sigma^+$ character in the region of the crossing between the $v_A = 5$ and $v_X = 9$ rotational manifolds. Since the vanishing of the dipole moment occurs at lower J in the case of the electronic moments of Yarkony et al, the dependence on J of the (nominally) $A^1\Pi_e \rightarrow$ (nominally) $X^1\Sigma^+$ cross sections (Fig. 2) displays a broader maximum.

The (nominally) $A^1\Pi_e \rightarrow$ (nominally) $X^1\Sigma^+$ cross sections obtained here are somewhat smaller than the values reported by Alexander [16] in his study of transfer between the (nominally) $A'^1\Pi_e$ and (nominally) $A^1\Sigma^+$ states of CaO in collision with N_2O. This is undoubtedly because the dipole moments in CaO are ~ 2 times larger than the comparable values in MgO (Table II), which reflects the longer bond length and (presumably) more polar bond in CaO. Since the transition probabilities vary as the square of the reduced dipole matrix elements (eq 22), we anticipate that the transfer cross sections will be $\simeq 4$ times smaller than in CaO, which is what we observe.

It is informative to compare the cross sections for transitions between the mixed states of differing electronic character, with cross sections for rotationally inelastic transitions within the (nominally) $A^1\Pi_e$ and the (nominally) $X^1\Sigma^+$ levels. These are displayed in Fig. 4 for $v_A = 6$ and $v_X = 10$, calculated for a relative velocity of $5.5\ 10^4$ cm/s. Far from the isoenergetic points, these transitions correspond to rotational relaxation within the pure states. The X state cross sections are larger, because the electric dipole moment is slightly larger in this state (Table II). The total rotational relaxation cross sections can be obtained from the values shown in Fig. 4 by addition of the cross sections for the downward transitions $J \rightarrow J-1$, which can be deduced from statistical microreversibility. As in the case of CaO [16], these total cross sections are very large. We find at low rotational levels $\sigma \simeq 140$ Å^2 for the $A^1\Pi_e$ ($v_A = 6$) state and $\sigma \simeq 180$ Å^2 for the

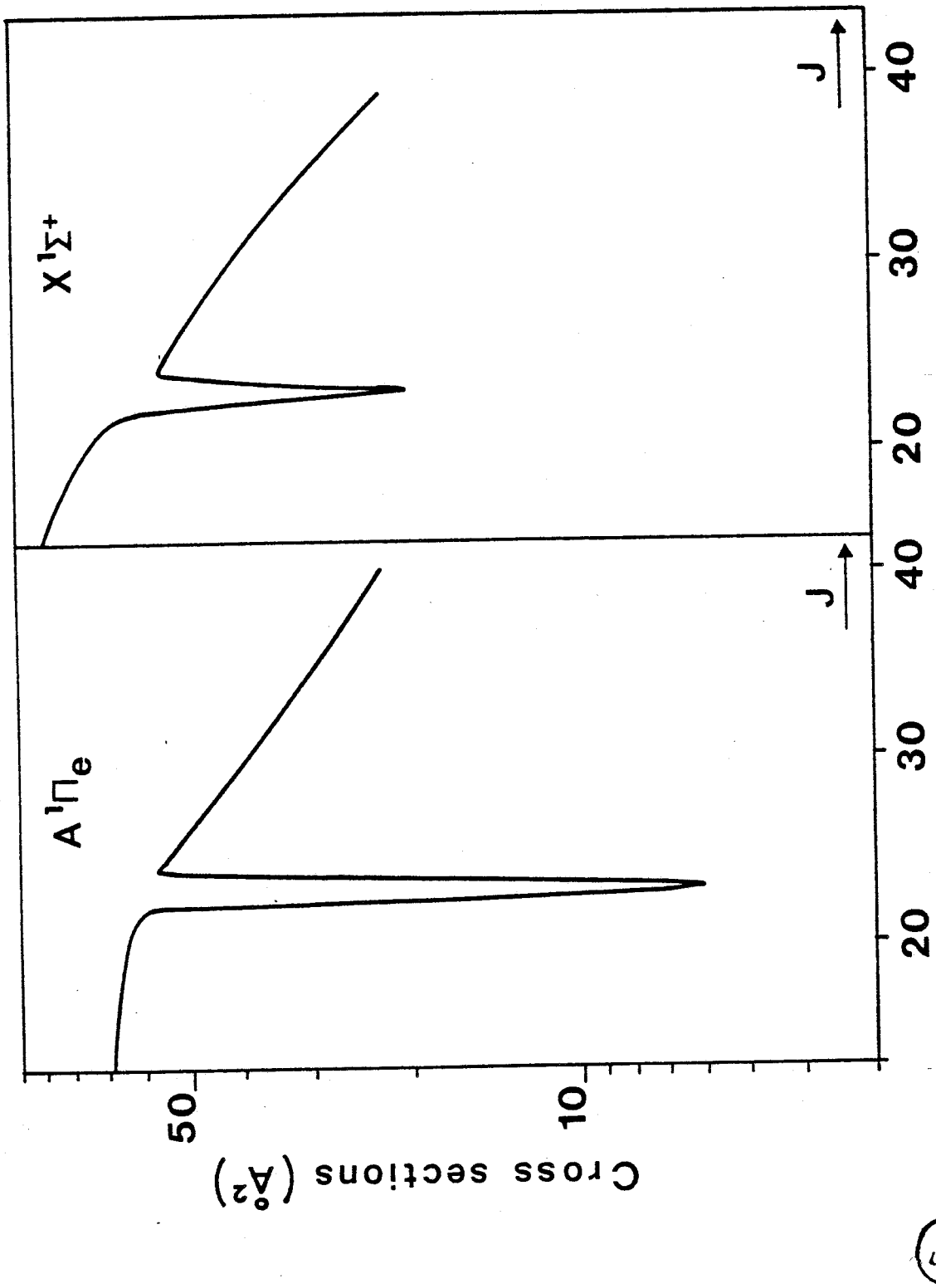

Figure 4

$X^1\Sigma^+$ (v_X = 10) state. As J increases the rotational energy spacings increase so that the cross sections decrease slowly with J. The sharp dip at the isoenergetic point reflects a decrease in the intrastate moment due to the strong mixing between the Born-Oppenheimer $A^1\Pi_e$ and $X^1\Sigma^+$ states.

The orbit-rotation term in the molecular Hamiltonian will not mix electronic states of $^1\Pi_f$ symmetry with states of $^1\Sigma^+$ symmetry. Thus collisional transfer from the rotational levels of the $^1\Pi_f$ state into the rotational levels of the (nominally) $X^1\Sigma^+$ state can take place only by means of $^1\Pi_f \rightarrow {}^1\Pi_e$ transfer involving the small $^1\Pi_e$ component in the mixed state or by direct $^1\Pi_f \rightarrow {}^1\Sigma^+$ transfer involving the A → X transition dipole, as shown in eq 33. The dipolar coupling due to the first of these mechanisms decreases inversely with J. In Fig. 5 we display cross sections at v = 5.5 10^4 cm/s for $A^1\Pi_f \rightarrow$ (nominally) $X^1\Sigma^+$ transfer in the region of the $v_A = 5$, $v_X = 9$ and $v_A = 6$, $v_X = 10$ crossings. We see that direct $^1\Pi_f \rightarrow X^1\Sigma^+$ coupling by means of the A-X transition moment is the predominant mechanism. Also the cross sections for transfer into the (nominally) $X^1\Sigma^+$ state from the $A^1\Pi_f$ state are as large as those from the (nominally) $A^1\Pi_e$ state, and the distribution in J is broader. The magnitude of the cross sections from the $A^1\Pi_f$ level, seen in Table III and Fig. 5, is unexpected. In Alexander's previous calculation on energy transfer in CaO, where the $A'^1\Pi$-$A^1\Sigma^+$ transition moment, because unknown, was taken to be zero, the analogous $A'^1\Pi_f \rightarrow A^1\Sigma^+$ cross sections were negligibly small, as in the trace in Fig. 5 corresponding to $R_{11}^{AX} = 0$.

It is possible for collisions to induce transitions between the (nominally) $A^1\Pi_e$ state and the other $A^1\Pi_f$ Λ-doublet, by a mechanism entirely similar to that discussed in the preceding paragraph. These cross sections, for $v_A = 6$ and v = 5.5 10^4 cm/s, are displayed in Fig. 6 as a function of J. The discontinuity in the slope at J = 26 reflects the mixing of the Born-Oppenheimer $A^1\Pi_e$ and

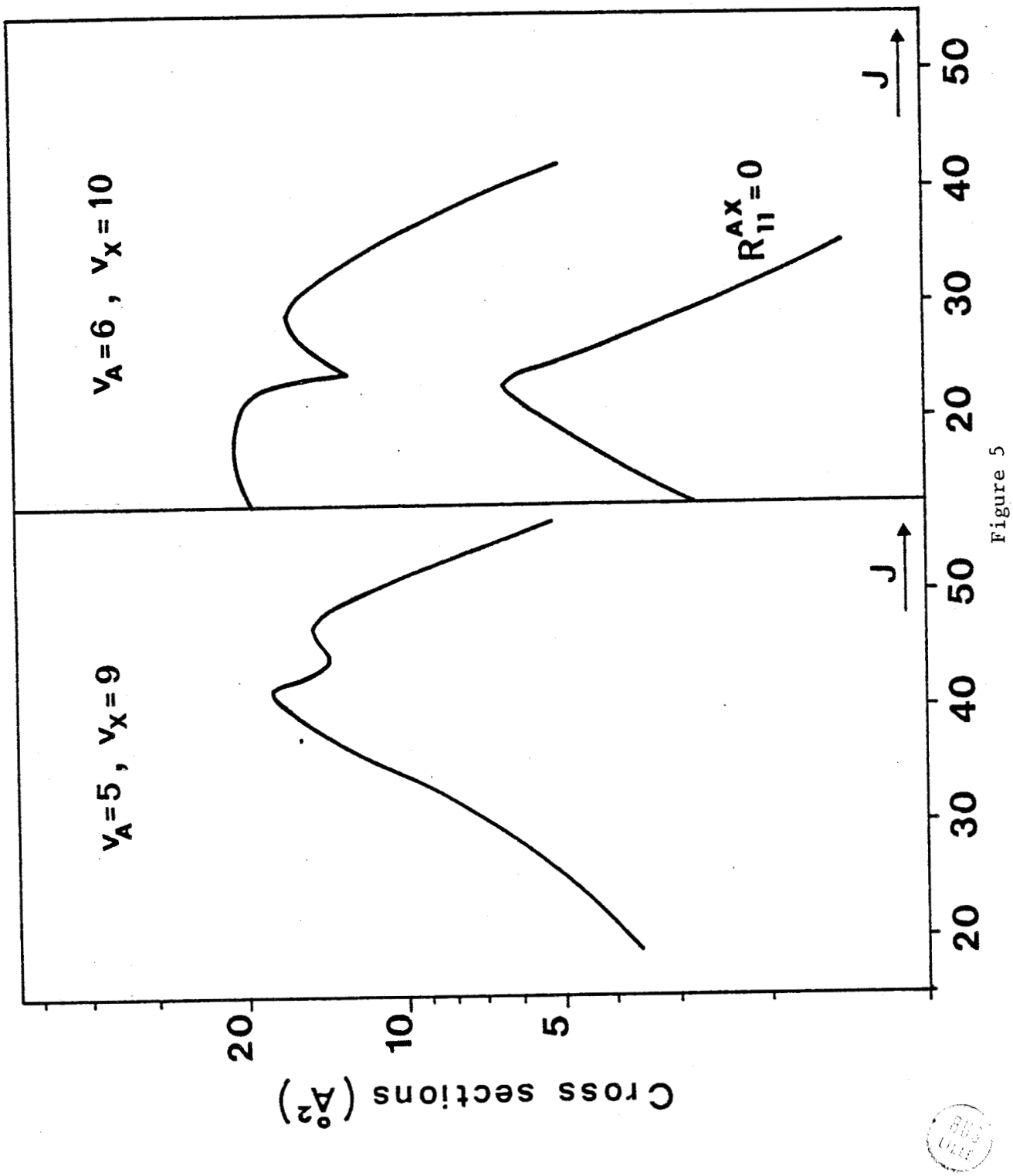

Figure 5

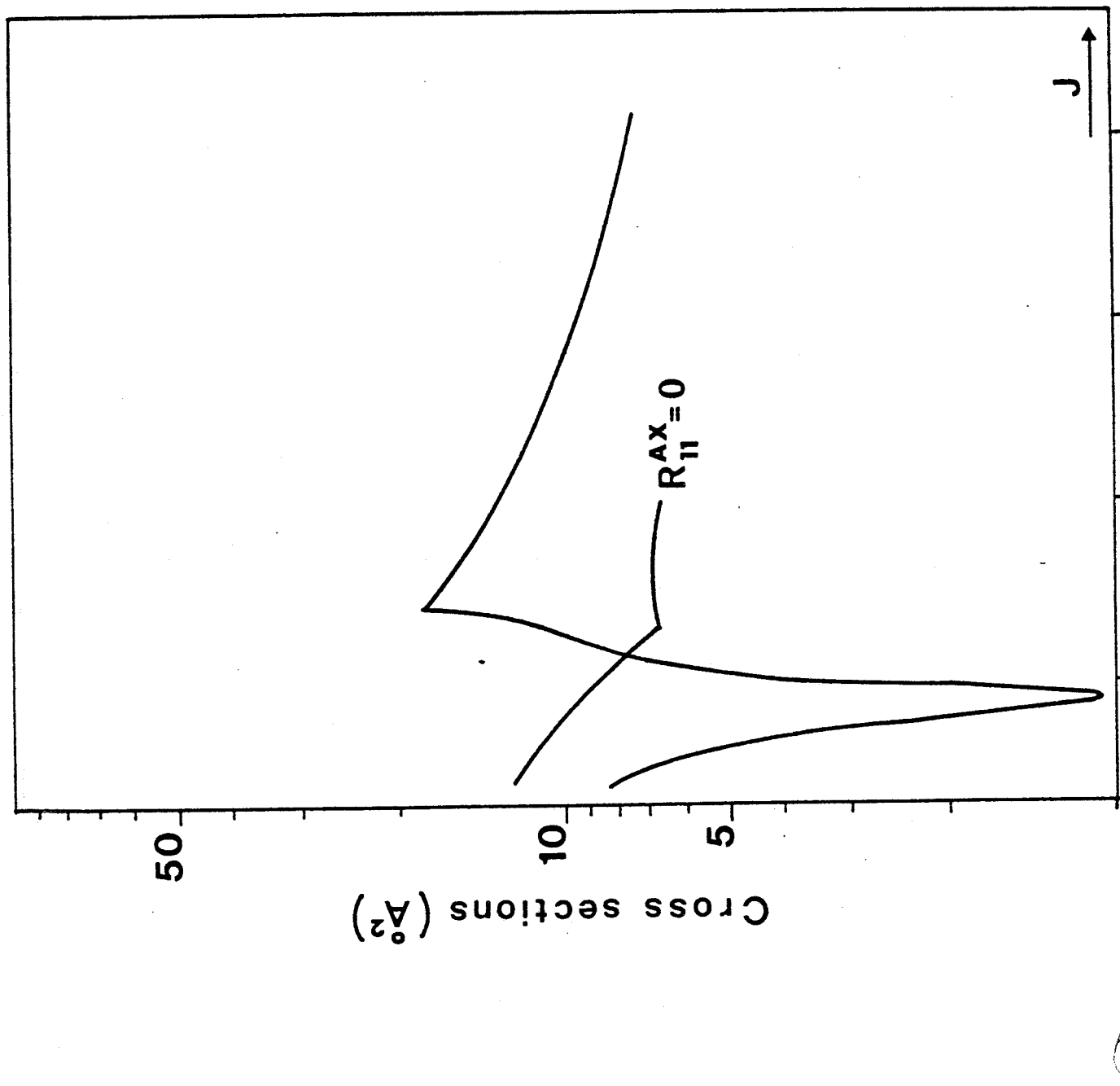

Figure 6

$X^1\Sigma^+$ states. We observe, as in the case of the $A^1\Pi_f \rightarrow$ (nominally) $X^1\Sigma^+$ transitions, that the cross sections are sensitive to the transition moment R_{11}^{AX} ; neglect of this term results in a very different dependence on J. In any case, the cross sections are small compared to $\Pi_e \rightarrow \Pi_e$ transitions (see Fig. 4), even near the isoenergetic point, demonstrating that $\Pi_e \rightarrow \Pi_f$ transitions are improbable. This is one more example of the propensity toward conservation of e/f symmetry in collisions of molecules in Π states [57,58], which was predicted by Alexander [58] for molecules in $^2\Pi$ electronic states in collisions with noble gas atoms and seen by Linton [59], Bernath et al. [60], and Nedelec and Dufayard [61] in experimental studies involving collisions of, respectively, YO, CaF, and CdH, all in the $A^2\Pi$ excited state. In a future paper [62] we shall extend this analysis to collisions within a $^3\Pi$ manifold.

Turning now to collisions between the (nominally) $a^3\Pi_{0e}$ and (nominally) $X^1\Sigma^+$ mixed states, we plot in Fig. 7 these cross sections as a function of J in the region of the $v_a = 2$, $v_X = 5$ and $v_a = 3$, $v_X = 6$ crossings. From Table III we see that these correspond to the $a^3\Pi$-$X^1\Sigma^+$ crossings at lowest J, where the transfer cross sections are largest. There is considerable qualitative similarity between Figs. 2 and 7, although there is no evidence of the coincidental cancellation of the cross sections in the case of transfer from the (nominally) $a^3\Pi_{0e}$ state. As discussed in the preceding section, at high J the orbit-rotation coupling will mix strongly the Ω = 0, 1, and 2 levels of a $^3\Pi$ state, so that a case (a) description will no longer be appropriate. By virtue of this mixing transfer into the $X^1\Sigma^+$ state will take place from all the Ωe levels of the $a^3\Pi$ state. Actual calculations of the mixing coefficients, using known expressions for the coupling matrix elements [42], indicates that the nominally Ω = 0 levels is 96 % pure at J = 19 (the $v_a = 3$, $v_X = 6$ crossing), and still 80 % pure at J = 49 (the $v_a = 2$, $v_X = 5$ crossing). For higher values of J which characterize the other $a^3\Pi$-$X^1\Sigma^+$ crossings (Table III), it might be more accurate to use the intermediate coupling molecular wavefunctions in the treatment of the collision dynamics.

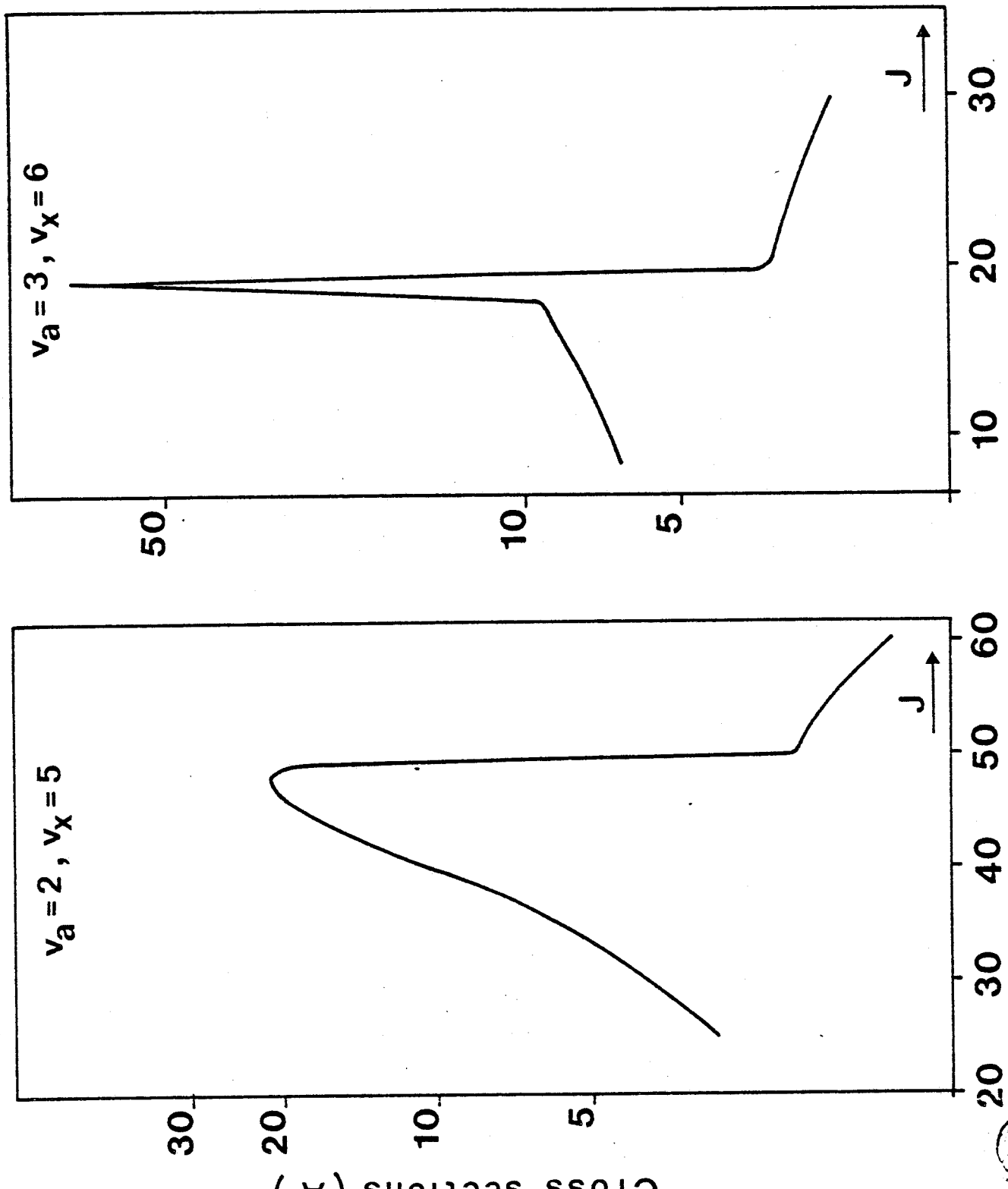

Figure 7

VII - CONCLUSIONS

In the present paper we have extended the dipolar model developed by Alexander [16] to treat inelastic collisions within and between the rotational manifolds of the (nominally) $X^1\Sigma^+$, $A^1\Pi_{e/f}$, and $a^3\Pi_{0e}$ electronic states of MgO in collisions with N_2O. The necessary matrix elements of the electric dipole operator were determined by SCF-CI calculations. Careful attention was devetod to determining the phases of the off-diagonal dipole matrix elements relative to the phases of the orbit-rotation matrix element, which mixes the Born-Oppenheimer $A^1\Pi_e$ and $X^1\Sigma^+$ wavefunctions. The relevant inelastic cross sections were calculated using a first-order Born treatment of the collision dynamics modified [16,52] to ensure statistical microreversibility. Our main conclusions are as follows :

1) Near the points where two rovibrational manifolds of different Born-Oppenheimer states cross, substantial cross sections (on the order of 10-20 $\mathring{A}^2$) may occur for transitions between mixed states of predominantly different electronic character.

2) The magnitudes of the maximum transfer cross sections decrease as the value of the rotational quantum number J at the crossing increases.

3) The breadth of the transfer cross section distribution is a sensitive function of the assumed dipole matrix elements, in particular the off-diagonal element between the Born-Oppenheimer $A^1\Pi_e$ and $X^1\Sigma^+$ states.

4) The presence of this matrix element results in substantial cross sections for transitions from rotational levels of the $A^1\Pi_f$ state into the (nominally) $X^1\Sigma^+$ state.

We see from Table III that sizeable cross sections exist for collisional transfer into a subset of rotational levels of the (nominally) $X^1\Sigma^+$ state for each vibrational level of this state with $v_X > 5$. Obviously, as in the case of CaO ($A^1\Sigma^+$) + N_2O collisions [16], this type of collisional transfer process, could result in pressure dependent changes in the populations of the $X^1\Sigma^+$, $A^1\Pi$, and $a^3\Pi_{0e}$ states of nascent MgO products, in reactions of Mg atoms with N_2O under oxidant rich conditions.

If a Boltzmann distribution of the nascent product rotational levels is assumed, with rotational temperature T, then the fraction of the nascent population with δJ of a crossing at $J = J_c$ can be written as

$$P(J_c, \delta J) = \sum_{J = J_c - \delta J}^{J_c + \delta J} f(J) \; / \; \sum_J f(J), \qquad (39)$$

where $f(J) = (2J+1) \exp[-B\,J(J+1)/kT]$. In the limit of closely spaced rotational levels the sums may be replaced by integrals to give

$$P(J_c, \delta J) \simeq \exp[-B\,(J_c + 1/2 - \delta J)^2 / kT] - \exp[-B\,(J_c + 1/2 + \delta J)^2 / kT] \qquad (40)$$

If, we take $\delta J = 10$ and $J_c = 50$ (see Table III and Figs 2 and 5 and 7), $B = 0.5\ cm^{-1}$ (the values for the A and a states), T = 1000 K, as suggested by Dagdigian's experiments [6], we calculate $P(J_c, \delta J) = 0.19$. This indicates that typically 10-20 % of the nascent population in a particular vibrational level of the $X^1\Sigma^+$, $A^1\Pi$ or $a^3\Pi_{0e}$ states would lie close enough to one of the rotational "windows" for efficient population transfer to occur either into or out of the $X^1\Sigma^+$ state.

Alexander and Osmolovsky [22] have used the dipolar model cross sections and rate constants for the CaO-N_2O system generated by Alexander [16] to model, under steady-state conditions, the pressure dependence of the population of

the $A^1\Sigma^+$ state of CaO subsequent to the reaction of Ca (^3P) with N_2O. The cross sections calculated here could be used to carry out a similar analysis of the pressure dependence of the MgO $X^1\Sigma^+$, $A^1\Pi$ and $a^3\Pi_{0e}$ populations in reactions of Mg atoms with N_2O. In contrast to the CaO molecule, it is the ground $^1\Sigma^+$ state which in MgO is directly coupled with the low-lying Π states, so that no radiative relaxation will occur. Thus rotational relaxation within the (nominally) Σ^+ state, for which the cross sections (Fig. 4) are much larger than those for the (nominally) $\Pi \rightarrow$ (nominally) Σ transitions, will compete strongly with population transfer.

As Alexander has discussed before [16], use of the Born approximation and the inclusion of only dipole-dipole coupling may introduce considerable error into the predicted cross sections. Specifically, we neglect the short-range contributions to the intermolecular potential, which could lead to additional inelastic flux at small impact parameters. Also the dipole selection rules implicit in the reduced matrix elements ($\Delta J = \pm 1$ for $\Pi_e \rightleftharpoons \Sigma$, $\Pi_e \rightleftharpoons \Pi_e$ and $\Sigma \rightleftharpoons \Sigma$ transitions and $\Delta J = 0$ for $\Pi_e \rightleftharpoons \Pi_f$ transitions) may not provide a truly accurate picture of the distribution of flux among the final rotational states. We feel that the calculations are, however, accurate enough to provide a reasonable picture of the magnitude of the cross sections for transfer within and between the low-lying states of MgO and of the variation of these cross sections with rotational quantum number. The structure present in Figs 2 and 5-7 indicates that an experimental study, with rotational state resolution, of energy transfer among the $X^1\Sigma^+$, $A^1\Pi$, and $a^3\Pi_{0e}$ states of MgO could provide a sensitive test of the dynamical model presented here. Hopefully, continued investigations of Mg + N_2O reactions will provide the information to fully understand the dynamics of these reactions and the subsequent energy transfer pathways.

Acknowledgment. The authors are grateful for partial support of the research reported here, to the Centre National de la Recherche Scientifique, ATP : "Dynamique réactionnelle des états excités" ; to NATO, grant 232.81 ; to the U.S. Army Research Office, grant DAAG 29-81 K-0102 ; to the Computer Science Center of the University of Maryland and to the Centre Inter Régional de Calcul Electronique at Orsay, France.

We are indebted to our experimentalist colleagues, Paul Dagdigian and Guy Taieb, for helpful discussion of the dynamics of the reactions of Mg with N_2O.

Figure Captions

Figure 1. Cross sections for upward ($J \rightarrow J+1$) transitions between the various states arising from the mixing of the $A^1\Pi_e$ and $X^1\Sigma^+$ Born-Oppenheimer states of MgO near the crossings between the $v_X = 9,10$ and $v_A = 5,6$ vibrational manifolds. The relative velocity is 5.5 10^4 cm/s. The indicated energies correspond to the mixed (perturbed) states. The zero of energy refers to the $v_X = 0$, $J = 0$ level of the $X^1\Sigma^+$ state. The levels are denoted X or A depending on their predominant character.

Figure 2. Cross sections of two relative velocities, for upward ($J \rightarrow J+1$) transitions from the rotational levels of the (nominally) $A^1\Pi_e$ ($v_A = 5$) manifold to the (nominally) $X^1\Sigma^+$ ($v_X = 9$) manifold in the neighborhood of the crossing between the two vibrational manifolds. For clarity the cross sections have been drawn as continuous curves, although they are defined only for integer values of J. The solid curves were obtained using the dipole moments computed here and reported in Table III and V ; the dashed curves, using the dipole moments reported by Yarkony et al (refs 33 and 35).

Figure 3. Variation with rotational quantum number of the absolute effective dipole matrix element $(J+1, a' || \mu || J, a)$ (eq 38) for transitions in which the $|a'>$ state is (nominally) $X^1\Sigma^+$ ($v_X = 9$) and the $|a>$ state, (nominally) $A^1\Pi_e$ ($v_A = 5$). The left hand panel was determined from the dipole moments computed here and reported in Tables III and V, the right hand panel, from the dipole moments reported by Yarkony et al. (refs 33 and 35).

Figure 4. Cross sections for upward ($J \rightarrow J+1$) transitions within the (nominally) $X^1\Sigma^+$ ($v_X = 10$) and the (nominally) $A^1\Pi_e$ ($v_A = 6$) manifolds in the neighborhood of the crossing between the two rovibrational manifolds. The relative velocity is 5.5 10^4 cm/s. For clarity the cross sections have been drawn as continuous curves, although they are defined only for integer values of J.

Figure 5. Cross sections for transitions into the (nominally) $X^1\Sigma^+$ ($v_X = 9,10$) rotational manifolds from the $v_A = 5,6$ rotational manifolds of the $A^1\Pi_f$ state. Because of symmetry only Q-branch ($J \rightarrow J$) processes contribute (eq 33). The relative velocity is 5.5 10^4 cm/s. For clarity the cross sections have been drawn as continuous curves, although they are defined only for integer values of J. The lower trace in the right hand panel illustrates the effect of neglecting the A - X transition moments in eq 33.

Figure 6. Cross sections for transfer from the f-symmetry Λ-doublet of the $A^1\Pi$ state ($v_A = 6$) into the e-symmetry mixed state rotational level of predominant $A^1\Pi$ character. The relative velocity is 5.5 10^4 cm/s. One of the traces illustrates the effect of neglecting the A - X transition moment in eq 33. For clarity the cross sections have been drawn as continuous curves, althouth they are defined only for integer values of J.

Figure 7. Cross sections for upward ($J \rightarrow J+1$) transitions from the rotational levels of the (nominally) $a^3\Pi_{0e}$ ($v_a = 2,3$) manifolds to rotational levels of the (nominally) $X^1\Sigma^+$ ($v_X = 5,6$) manifolds, in the neighborhood of the crossings. The relative velocity is 5.5 10^4 cm/s. For clarity the cross sections have been drawn as continuous curves, although they are defined only for integer values of J.

III - COMMENTAIRES

1) Hypothèse d'une trajectoire linéaire

L'équation (IV.18) détermine le potentiel d'interaction V(t) et fait apparaître le terme R(t) qui caractérise la trajectoire relative des deux partenaires de la collision. Nous avons déjà mentionné au § I l'hypothèse d'une trajectoire moyenne gouvernée par la présence d'un potentiel moyen $\bar{V}(R)$. Nous avons choisi de traiter le problème par la méthode du paramètre d'impact [68,69] qui consiste à choisir le cas particulier d'une trajectoire définie par un potentiel moyen $\bar{V}(R)$ nul. C'est-à-dire encore que la trajectoire est supposée linéaire et décrite à vitesse constante $\vec{v}$. En d'autres termes, on veut que la collision ne perturbe que faiblement le mouvement du centre de masse du système. Ceci peut se traduire par les inégalités suivantes :

$$\Delta E / kT_{TR} \ll 1 \qquad \Delta J / L \ll 1 \qquad \text{(IV.21)}$$

où ΔE et ΔJ représentent respectivement l'énergie transférée du mouvement de translation au mouvement de rotation et le moment angulaire transféré du mouvement orbital au mouvement de rotation.

T_{TR} est la température de translation et

L le moment angulaire orbital du mouvement relatif

L'hypothèse d'une trajectoire linéaire se justifie à grand paramètre d'impact parce que les forces qui régissent la trajectoire (forces de VAN DER WAALS et forces répulsives) se font sentir à des distances plus courtes que celles mises en jeu dans l'interaction dipole-dipole.

Dans le cas particulier d'une transition $J_\alpha \to J_\alpha + 1$, $J_\beta \to J_\beta - 1$ par exemple les deux relations précédentes (IV.21) deviennent :

$$\frac{\Delta E}{k\,T_{TR}} = \frac{1}{(5.036 \times 10^{22})} \frac{B_\alpha\,[2J_\alpha + 2] - 2\,B_\beta J_\beta}{k\,T_{TR}} \quad ; \quad \frac{\Delta J}{L} = \frac{\hbar}{m\,v\,b} \qquad (IV.22)$$

où B_α et B_β s'expriment en cm^{-1}, m est la masse du système MgO + N_2O. Dans le cas des expériences de DAGDIGIAN et COX par exemple, T_{TR} vaut 4100 K $v = 1.8 \times 10^5$ cm/s. Avec un paramètre d'impact égal à 5 Å on obtient :

$$\frac{\Delta E}{k\,T_{TR}} \leqslant 0.03 \quad \text{et} \quad \frac{\Delta J}{L} \leqslant 0.04$$

Ce qui justifie parfaitement l'emploi d'une trajectoire moyenne.

A faible paramètre d'impact, le problème est tout autre. Tout d'abord, le potentiel d'interaction V (R(t),t) qui agit, rappelons-le, sur les variables internes des molécules devient trop important pour justifier l'emploi d'une approximation basée sur la théorie des perturbations au premier ordre. D'autre part, il n'est plus fondé de négliger les interactions autres que dipole-dipole qui apparaissent dans le développement du potentiel (eq. IV.20). Les forces répulsives de courte portée deviennent importantes et dans l'hypothèse du modèle des sphères dures, la trajectoire se composerait de deux demi-droites En fait, on peut considérer que l'utilisation de la probabilité de coupure englobe de manière implicite tous les effets à faible paramètre d'impact dont nous venons de parler.

2) Fonction de résonance

L'expression de la probabilité de transition non polarisée déduite de $P_{i \to f}$ est donnée par : (équation 22)

$$P_{J_\alpha J_\beta \to J'_\alpha J'_\beta}(b) = \frac{2}{3\hbar^2 b^4 v^2} \frac{(J'_\alpha \Lambda'_\alpha \Omega'_\alpha v'_\alpha \| Q_1 \| J_\alpha \Lambda_\alpha \Omega_\alpha v_\alpha)^2 (J'_\beta \Lambda'_\beta \Omega'_\beta v'_\beta \| Q_1 \| J_\beta \Lambda_\beta \Omega_\beta v_\beta)^2}{(2J_\alpha + 1)(2J_\beta + 1)}$$

$$\sum_{m=-2}^{+2} \left| J_m^2 (\omega_{if}, b) \right|^2 \delta(S_\alpha S'_\alpha) \delta(\Sigma_\alpha \Sigma'_\alpha) \qquad (22)$$

dans laquelle le terme $\sum_{m=-2} |J_m^2 (\omega_{if}, b)|^2$ correspond à un facteur $\frac{4}{3}$ près à la fonction de résonance du premier ordre $R_2^1 (\omega_{if}\, b/v)$ définie par CROSS et GORDON [51]. Cette fonction donne la distribution en fréquences de la transformée de Fourier de la perturbation et détermine le comportement de la probabilité de transition.

Elle peut être développée sous la forme :

$$R_2^1 (x) = \exp(-2x)\,(A + Bx + Cx^2 + Dx^3 + \ldots) \qquad (IV.23)$$

où $x = \omega_{if}\, b/v$

et les coefficients A, B, C et D ont été calculés par CROSS et GORDON [51] puis par SCHARMA et BRAU [18].

La figure IV.b représente la variation de la fonction de résonance en fonction de x.

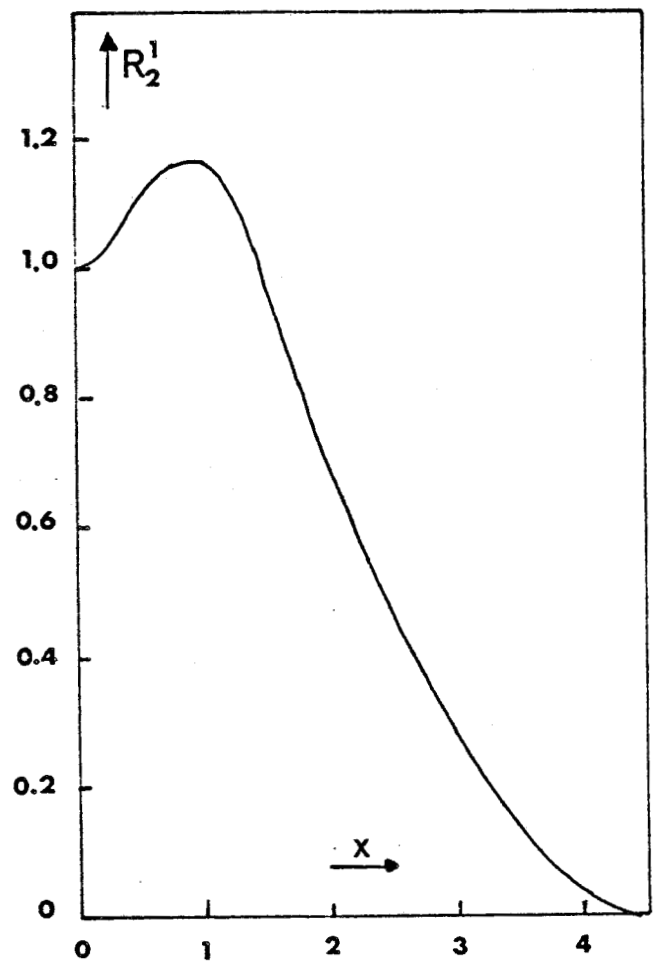

Figure IV.b

La valeur $\omega_{if} = 0$ correspond à une collision résonante c'est-à-dire pour laquelle il n'existe pas de transfert d'énergie ΔE du mouvement de translation au mouvement de rotation. Nous venons de voir que la fonction R_2^1 (X) est proportionnelle à $\exp\left(-\frac{2\,\omega_{if}.b}{v}\right)$: en conséquence, pour une valeur donnée du paramètre d'impact b et à une vitesse donnée v, la transition sera plus efficace si ΔE est faible (transfert résonant), c'est-à-dire si les fréquences de rotation des deux molécules sont proches.

On justifie ainsi le fait que la section efficace de tranfert à l'intérieur d'un même état diminue quand le nombre quantique de rotation J augmente (Fig. 4). En effet, lorsque J_α augmente, les niveaux de rotation de la molécule MgO sont de plus en plus espacés ; or, les sections efficaces sont calculées pour une température de rotation de la cible N_2O égale à 300 K. Avec cette température de rotation, le nombre quantique de rotation maximum J_β de la cible est $J_\beta = 62$. Puisque la constante de rotation de N_2O est proche de celle de MgO les transferts résonants correspondent à $J_\beta \simeq J_\alpha$. Lorsque J_α augmente le nombre de molécules-cibles susceptibles de conduire à des transferts résonants diminue et donc la section efficace de transfert diminue. De la même manière, dans les transferts $A^1\Pi_e \rightarrow X^1\Sigma_e^+$ et $a^3\Pi_{0e} \rightarrow X^1\Sigma_e^+$, les sections efficaces maximales sont atteintes quand les croisements se produisent à J faible (Table III de l'article).

En contre partie, pour ΔE grand et à vitesse donnée, la transition sera plus efficace dans le domaine des faibles paramètres d'impact. A titre d'illustration, la figure IV.c représente en fonction du nombre quantique de rotation J_β de la cible, le paramètre d'impact permettant d'obtenir une probabilité de transition constante (choisie ici égale à 0.5) dans le cas de la transition $(A^1\Pi_e,\ v_A=6,\ J_\alpha=23) \rightarrow (X^1\Sigma_e^+,\ v_X=10,\ J'_\alpha=24)$. On constate que le paramètre d'impact passe par un maximum dans la région où l'échange est le plus résonant c'est-à-dire entre $J_\beta \simeq 24$ et $J_\beta \simeq 36$ et que sa valeur décroit nettement de part et d'autre de ce maximum afin de conserver constante la quantité $\frac{\omega_{if} b}{v}$ caractéristique de la fonction de résonance.

3) Choix de la probabilité de coupure P_c^0

La notion de probabilité de coupure a été introduite afin d'éviter les valeurs excessives de la probabilité de transition qui pourraient être atteintes

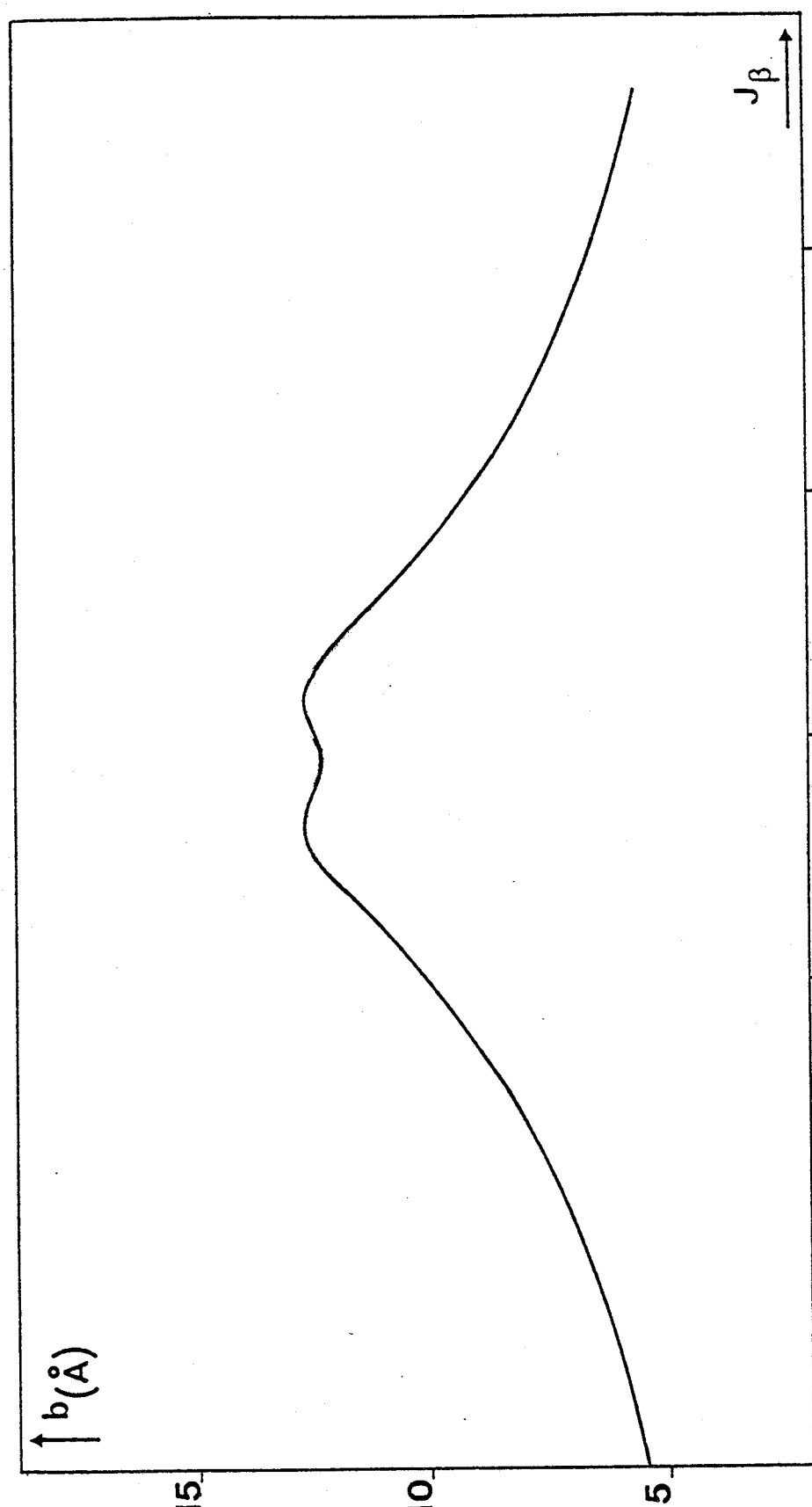

FIGURE IV.c

Paramètre d'impact en fonction du nombre quantique de rotation de la cible N_2O pour une probabilité de transition égale à 0.5.

quand le paramètre d'impact tend vers zéro (cf. eq. 22). Il est bien évident que la valeur maximum que peut atteindre la probabilité de transition est égale à l'unité. L'idée immédiate est donc d'imposer $P_c^0 = 1$.

Des études de processus analogues [16,52] ont révélé que l'approximation de BORN du premier ordre utilisée avec $P_c^0 = 1$ majore les valeurs de sections efficaces calculées d'environ 30 % et que la valeur la mieux adaptée pour la probabilité de coupure était $P_c^0 = 0.5$. Nous avons constaté dans notre cas que si nous imposions $P_c^0 = 1$ les valeurs calculées du paramètre d'impact pouvaient atteindre 2 Å. Dans ces conditions, les principales hypothèses de base de notre modèle étaient mises en défaut.

References and Notes

(1) For reactions of Ba, see Y.C. Hsu and J.G. Pruett, *J. Chem. Phys.* 76, 5849 (1982) ; and references contained therein.

(2) For reactions of Sr, see (a) B.E. Wilcomb and P.J. Dagdigian, *J. Chem. Phys.* 69, 1779 (1978) ; (b) J.W. Cox and P.J. Dagdigian, *J. Phys. Chem.* 86, 3738 (1982) ; and references contained therein.

(3) For reactions of Ca, see J.A. Irvin and P.J. Dagdigian, *J. Chem. Phys.* 74, 6178 (1981) ; and references contained therein.

(4) G. Taieb, *J. Phys.* (Paris) 42, 537 (1981).

(5) B. Bourguignon, J. Rostas and G. Taieb, *J. Chem. Phys.* 77, 2979 (1982).

(6) P.J. Dagdigian, *J. Chem. Phys.* 76, 5375 (1982).

(7) W.H. Breckenridge and H. Unemoto, in press.

(8) C.R. Dickson, S.M. George and R.N. Zare, *J. Chem. Phys.* 67, 1024 (1977).

(9) E.S. Fleming and H.B. Palmer, in "Electronic Transition Lasers", edited by J.I. Steinfeld, M.I.T., Cambridge, Mass., 1976, p. 70 ; J.J. Reuther and H.B. Palmer, *J. Chem. Phys.* 77, 83 (1982).

(10) R.W. Field, R.A. Gottscho, J.G. Pruett and J.J. Reuther, in "Proceedings of the 14th International Conference on Free Radicals, Sanda, Japon 1979.

(11) C.R. Jones and H.P. Broida, *J. Chem. Phys.* 60, 4369 (1974) ; R.W. Field C.R. Jones and H.P. Broida, ibid. 70, 4377 (1974).

(12) C.J. Hsu, W.D. Krugh and H.B. Palmer, *J. Chem. Phys.* 60, 5118 (1974).

(13) R.W. Field, *J. Chem. Phys.* 60, 2400 (1974).

(14) K.P. Huber and G. Herzberg, "Constants of Diatomic Molecules (Van Nostrand Reinhold, New York, 1979).

(15) In the case of MgO, the four excited states in question are designated $a^3\Pi$, $A^1\Pi$, $b^3\Sigma^+$ and $B^1\Sigma^+$ (ref 14).

(16) M.H. Alexander, *J. Chem. Phys.* 76, 429 (1982).

(17) C.G. Gray and J. Van Kranendonk, *Can. J. Phys.* 44, 2411 (1966).

(18) R.D. Sharma and C.A. Brau, *J. Chem. Phys.* 50, 924 (1969).

(19) H.A. Rabitz and R.G. Gordon, *J. Chem. Phys.* 53, 1815, 1831 (1970).

(20) For an excellent review, see G.G. Balint-Kurti in "International Review of Science Physical Chemistry)(Butterworth, London 1975) *Series 2, Vol. 1.*

(21) P.J. Dagdigian and M.H. Alexander, *J. Chem. Phys.* 72, 6513 (1980).

(22) M.H. Alexander and M.G. Osmolovsky, *J. Chem. Phys.* 77, 839 (1982).

(23) P.J. Dagdigian, *Chem. Phys. Lett.* 55, 239 (1978) ; L. Pasternack and P.J. Dagdigian, *Chem. Phys.* 33, 1 (1978) ; J.A. Irvin and P.J. Dagdigian *J. Chem. Phys.* 73, 176 (1980).

(24) G. Taieb and H.P. Broida, *J. Chem. Phys.* 65, 2914 (1976).

(25) W.J. Breckenridge, W.L. Nikolai and J. Stewart, *J. Chem. Phys.* 74 2073 (1981).

(26) J. Schamps and H. Lefebvre-Brion, *J. Chem. Phys.* 56, 573 (1972).

(27) B. Huron, J.P. Malrieu and P. Rancurel, *Chem. Phys.* 3, 277 (1976) ; B. Huron and P. Rancurel, *Chem. Phys. Lett.* 13, 515 (1976) ; B. Huron, J.P. Malrieu and P. Rancurel, *J. Chem. Phys.* 58, 5745 (1973).

(28) C.W. Bauschlicher, JR., D.M. Silver and D.R. Yarkony, *J. Chem. Phys.* 73, 2867 (1980).

(29) C.W. Bauschlicher, JR., B.H. Lengsfield III, D.M. Silver and D.R. Yarkony, *J. Chem. Phys.* 74, 2379 (1981).

(30) C.W. Bauschlicher et al. (ref 29) predict that the as yet unobserved $b^3\Sigma^+$ state lies much farther below the $B^1\Sigma^+$ than would be expected by extrapolation from the level spacings of Ca and Ba.

(31) K. Cross, P.C.F. Ip, and R.W. Field, private communication (1982).

(32) T. Ikeda, N.B. Wong, D.O. Harris and R.W. Field, *J. Mol. Spectrosc.* 68 452 (1977).

(33) R.N. Diffenderfer, D.R. Yarkony and P.J. Dagdigian, *J. Quant. Spectrosc. Radiat. Transf.*, in press.

(34) W.G. Richards, G. Verhaegen and C.M. Moser, *J. Chem. Phys.* 45, 3226 (1966).

(35) R.N. Diffenderfer and D.R. Yarkony, in press.

(36) G. Raseev, *Chem. Phys. Lett.* 47, 36 (1977).

(37) B. Pouilly, J.M. Robbe, J. Schamps and E. Roueff, *J. Phys. B*, in press.

(38) J.M. Robbe and H. Lefebvre-Brion, *J. Mol. Spectrosc.* 90, 439 (1981).

(39) E. Clementi and C. Roetti, *At. Data, Nucl. Data,* Tables 14, (1974).

(40) P.S. Bagus, B. Liu, A.D. McLean and M. Yoshimine, "Alchemy", I.B.M. Research Laboratories, San Jose, California 95114, 1972.

(41) C.W. Bauschlicher and D.R. Yarkony, *J. Chem. Phys.* 78, 3990 (1977).

(42) J.T. Hougen, *Nat. Bur. Stand. U.S. Monograph.* 115 (1970).

(43) J.M. Brown, J.T. Hougen, K.P. Huber, J.W.C. Johns, I. Kopp, H. Lefebvre-Brion, A.J. Merer, D.A. Ramsay, J. Rostas and R.N. Zare, *J. Mol. Spectrosc.* 55, 500 (1975).

(44) I. Kopp and J.T. Hougen, *Canad. J. Phys.* 45, 2581 (1967).

(45) E.U. Condon and G.H. Shortley, "Theory of Atomic Spectra", Cambridge University Press, Cambridge, England, 1957.

(46) J.A. Hall, J. Schamps, J.M. Robbe and H. Lefebvre-Brion, *J. Chem. Phys.* 59, 3271 (1973).

(47) R.W. Field, private communication (1981). The values which appear in the paper of Ikeda et al. (ref 32) (0.85 and 71.7) must be respectively divided and multiplied by the missing factor $\sqrt{2}$ in eqs 36 and 45a of ref 32, which define the perturbation parameters.

(48) Equation (22) is eq 64 of ref 16 with $\ell_a = \ell_b = 1$; $\ell = 2$.

(49) D.M. Brink and G.R. Satchler, "Angular Momentum", Oxford University, Oxford, 1975, 2nd edition.

(50) A.R. Edmonds, "Angular Momentum in Quantum Mechanics", Princeton University, Princeton, 1960.

(51) R.J. Cross, Jr. and R.G. Gordon, *J. Chem. Phys.* 43, 3571 (1966).

(52) P.J. Dagdigian and M.H. Alexander, *J. Chem. Phys.* 72, 6513 (1980).

(53) The qualitative picture of the crossings between the various rovibrational manifolds is similar to that shown in Fig. 1 of ref 16.

(54) A. Lagerqvist and U. Uhler, *Ark. Fys.* 1, 459 (1949).

(55) G. Herzberg, "Infrared and Raman Spectra of Polyatomic Molecules", Van Nostrand, Princeton, 1968.

(56) R.D. Nelson, D.R. Lide, Jr., and A.A. Maryott, Natl. Stand. Ref. Data Ser., *Natl. Bur. Stand.* 10 (1967).

(57) R.A. Gottscho, *Chem. Phys. Lett.* 81, 66 (1981).

(58) M.H. Alexander, *J. Chem. Phys.* 76, 5974 (1982).

(59) C. Linton, *J. Mol. Spectrosc.* 69, 351 (1978).

(60) P.F. Bernath and R.W. Field, *J. Mol. Spectrosc.* 82, 339 (1980) ; P.C.F. Ip, P.F. Bernath and R.W. Field, ibid. 89, 53 (1981).

(61) O. Nedelec and J. Dufayard, *Chem. Phys.* 71, 279 (1982).

(62) M.H. Alexander and B. Pouilly, to be published.

(63) D.R. Yarkony, in press.

(64) L. Landau et E. Lifchitz "Physique Théorique" Tome III "Mécanique Quantique" (Eds MIR Moscou (1966)).

(65) A. Messiah, "Mécanique Quantique" (Eds. Dunod (1964)).

(66) C.G. Gray, *Can. J. Phys.* 54, 505 (1976).

(67) R.J. Buehler and J.O. Hirschfelder, *Phys. Rev.* 83, 628 (1951).

(68) N.F. Mott, *Proc. Camb. Phil. Soc. Math. Phys. Sci.* 27, 553 (1931).

(69) D.R. Bates, "Atomic and Molecular Processes, chap. 4, Academic Press (1962).

CONCLUSION

Plutôt que rappeler les résultats obtenus au cours de ce travail, il nous semble préférable, à titre de conclusion, de montrer quelles perspectives s'offrent désormais à nous dans le domaine de la dynamique collisionnelle.

Afin de compléter le bilan radiatif présenté dans ce travail, l'étude de l'excitation rotationnelle de la molécule C_2 par collision avec H_2 a été entreprise car il est bien connu que les collisions inélastiques avec les espèces abondantes du milieu interstellaire (en particulier H et H_2) modifient sensiblement l'équilibre des populations rotationnelles de la molécule C_2.

L'étude d'un processus analogue à celui présenté dans le dernier chapître est actuellement engagée sur la collision CN + N_2O. Ce mécanisme pourrait peut être expliquer l'inversion de population importante sur les niveaux vibrationnels de l'état fondamental $X^2\Sigma^+$ de CN produit de la réaction C + N_2O observée par COSTES à l'Université de Bordeaux.

Mais il doit être entendu, que l'orientation vers les problèmes de dynamique que nous avons choisie, ne doit pas être considérée comme figée mais qu'elle est l'amorce d'une évolution vers les problèmes passionnants du domaine des collisions réactives.

APPENDICE

APPENDIX 2: OBSERVED AND CALCULATED FREQUENCIES IN THE BeS $A^1\Pi$–$X^1\Sigma^+$ TRANSITION (UNITS: cm^{-1}) (FROM C. J. CHEETHAM'S THESIS)

A 1 PI V= 5 - X 1 SIG V= 0 TRANSITION R(J) BRANCH

J	EXPT	CALC	EXPT-CALC
3	11534.610	11534.628	-0.018
4	11534.610	11534.593	0.017
5	11534.280	11534.236	0.044
6	11533.650	11533.557	0.093
7	11532.580	11532.556	0.024
8	11531.240	11531.232	0.008
10	11527.630	11527.619	0.011
11	11525.310	11525.329	-0.019
12	11522.740	11522.717	0.023
13	11519.790	11519.783	0.007
14	11516.500	11516.526	-0.026
16	11509.060	11509.045	0.015
17	11504.820	11504.821	-0.001
18	11500.250	11500.275	-0.025
19	11495.390	11495.406	-0.016
20	11490.230	11490.215	0.015
21	11484.730	11484.702	0.028
22	11478.850	11478.866	-0.016
23	11472.660	11472.708	-0.048
24	11466.210	11466.227	-0.017
25	11459.390	11459.424	-0.034
26	11452.270	11452.298	-0.028
27	11444.860	11444.850	0.010
28	11437.060	11437.080	-0.020
29	11428.970	11428.987	-0.017
30	11420.590	11420.571	0.019
31	11411.880	11411.833	0.047
32	11402.790	11402.773	0.017
33	11393.460	11393.390	0.070
34	11383.640	11383.685	-0.045

A 1 PI V= 5 - X 1 SIG V= 0 TRANSITION Q(J) BRANCH

J	EXPT	CALC	EXPT-CALC
4	11528.360	11528.332	0.028
5	11526.770	11526.724	0.046
6	11524.740	11524.794	-0.054
7	11522.540	11522.543	-0.003
9	11517.070	11517.075	-0.005
10	11513.840	11513.859	-0.019
12	11506.440	11506.462	-0.022
13	11502.280	11502.281	-0.001
14	11497.770	11497.779	-0.009
15	11492.950	11492.955	-0.005
16	11487.810	11487.810	-0.000
17	11482.340	11482.344	-0.004
18	11476.550	11476.556	-0.006
19	11470.440	11470.446	-0.006
20	11464.020	11464.016	0.004
21	11457.250	11457.264	-0.014
22	11450.170	11450.191	-0.021
23	11442.800	11442.796	0.004
24	11435.080	11435.081	-0.001
25	11427.050	11427.044	0.006
26	11418.670	11418.686	-0.016
27	11410.010	11410.007	0.003
28	11401.020	11401.007	0.013
29	11391.730	11391.686	0.044
30	11382.060	11382.045	0.015
31	11372.090	11372.082	0.008
32	11361.800	11361.798	0.002
33	11351.190	11351.194	-0.004

APPENDIX 2—*Continued*

A 1 PI V= 2 - X 1 SIG V= 0 TRANSITION P(J) BRANCH

J	EXPT	CALC	EXPT-CALC
6	11518.840	11517.276	10.564
7	11513.840	11513.772	0.068
8	11509.920	11509.946	-0.026
9	11505.780	11505.798	-0.018
10	11501.320	11501.330	-0.010
11	11496.550	11496.540	0.010
12	11491.420	11491.429	-0.009
13	11485.980	11485.997	-0.017
14	11480.220	11480.244	-0.024
15	11474.170	11474.170	0.000
16	11467.760	11467.775	-0.015
17	11461.060	11461.059	0.001
18	11453.990	11454.022	-0.032
19	11446.620	11446.665	-0.045
20	11438.960	11438.987	-0.027
21	11430.980	11430.988	-0.008
22	11422.650	11422.669	-0.019
23	11414.050	11414.030	0.020
24	11405.120	11405.071	0.049
25	11395.850	11395.791	0.059

A 1 PI V= 0 - X 1 SIG V= 0 TRANSITION R(J) BRANCH

J	EXPT	CALC	EXPT-CALC
4	12247.510	12247.460	0.050
5	12247.020	12247.035	-0.015
6	12246.250	12246.276	-0.026
7	12245.160	12245.183	-0.023
8	12243.750	12243.757	-0.007
9	12242.040	12241.997	0.043
10	12239.960	12239.904	0.056
11	12237.560	12237.477	0.083
12	12234.780	12234.716	0.064
13	12231.660	12231.622	0.038
14	12228.230	12228.194	0.036
15	12224.460	12224.432	0.028
16	12220.370	12220.337	0.033
17	12215.890	12215.908	-0.018
18	12211.170	12211.145	0.025
19	12206.040	12206.048	-0.008
20	12200.610	12200.617	-0.007
21	12194.830	12194.853	-0.023
22	12188.760	12188.755	0.005
23	12182.340	12182.323	0.017
24	12175.560	12175.558	0.002
25	12168.430	12168.459	-0.029
26	12161.040	12161.026	0.014
27	12153.270	12153.259	0.011
28	12145.160	12145.159	0.001
29	12136.720	12136.725	-0.005
30	12127.980	12127.958	0.022
31	12118.870	12118.856	0.014
32	12109.390	12109.422	-0.032
33	12099.720	12099.653	0.067
34	12089.560	12089.552	0.008
35	12079.110	12079.117	-0.007
36	12068.380	12068.348	0.032
37	12057.240	12057.246	-0.006
38	12045.810	12045.811	-0.001
39	12034.050	12034.043	0.007
40	12021.960	12021.942	0.018
41	12009.500	12009.508	-0.008
42	11996.740	11996.740	-0.000
43	11983.640	11983.641	-0.001

APPENDIX 2—*Continued*

A 1 PI V= 0 - X 1 SIG V= 0 TRANSITION R(J) BRANCH			
J	EXPT	CALC	EXPT-CALC
44	11970.270	11970.208	0.062
45	11956.480	11956.443	0.037
46	11942.350	11942.346	0.004
47	11927.850	11927.917	-0.067
48	11913.030	11913.156	-0.126
49	11898.010	11898.064	-0.054
50	11882.580	11882.640	-0.060
51	11866.830	11866.886	-0.056
52	11850.770	11850.802	-0.032
53	11834.360	11834.388	-0.028
54	11817.640	11817.646	-0.006
55	11800.550	11800.575	-0.025
56	11783.160	11783.179	-0.019
57	11765.420	11765.458	-0.038
58	11747.340	11747.416	-0.076
59	11728.980	11729.055	-0.075
60	11710.290	11710.381	-0.091
61	11691.320	11691.402	-0.082
62	11672.120	11672.130	-0.010
63	11652.560	11652.587	-0.027
64	11632.740	11632.812	-0.072
65	11612.780	11612.882	-0.102

APPENDIX 2—*Continued*

A 1 PI V= 0 - X 1 SIG V= 0 TRANSITION Q(J) BRANCH

J	EXPT	CALC	EXPT-CALC
2	12243.650	12243.588	0.062
3	12242.610	12242.588	0.022
4	12241.280	12241.256	0.024
5	12239.600	12239.591	0.009
6	12237.650	12237.592	0.058
7	12235.300	12235.260	0.040
8	12232.640	12232.596	0.044
9	12229.630	12229.598	0.032
10	12226.280	12226.267	0.013
11	12222.620	12222.603	0.017
12	12218.630	12218.607	0.023
13	12214.300	12214.277	0.023
14	12209.610	12209.614	-0.004
15	12204.640	12204.619	0.021
16	12199.280	12199.290	-0.010
17	12193.630	12193.629	0.001
18	12187.620	12187.635	-0.015
19	12181.310	12181.308	0.002
20	12174.640	12174.649	-0.009
21	12167.630	12167.656	-0.026
22	12160.320	12160.331	-0.011
23	12152.660	12152.674	-0.014
24	12144.660	12144.683	-0.023
25	12136.350	12136.361	-0.011
26	12127.720	12127.705	0.015
27	12118.710	12118.718	-0.008
28	12109.390	12109.398	-0.008
29	12099.720	12099.745	-0.025
30	12089.720	12089.761	-0.041
31	12079.430	12079.444	-0.014
32	12068.790	12068.795	-0.005
33	12057.810	12057.813	-0.003
34	12046.480	12046.500	-0.020
35	12034.850	12034.855	-0.005
36	12022.880	12022.878	0.002
37	12010.550	12010.569	-0.019
38	11997.920	11997.928	-0.008
39	11984.940	11984.955	-0.015
40	11971.630	11971.651	-0.021
41	11958.000	11958.016	-0.016
42	11944.020	11944.048	-0.028
43	11929.730	11929.750	-0.020
44	11915.130	11915.120	0.010
45	11900.150	11900.159	-0.009
46	11884.910	11884.866	0.044
47	11869.270	11869.243	0.027
48	11853.240	11853.288	-0.048
49	11837.010	11837.003	0.007
50	11820.380	11820.387	-0.007
51	11803.390	11803.440	-0.050
52	11786.150	11786.162	-0.012
53	11768.520	11768.554	-0.034
54	11750.590	11750.615	-0.025
55	11732.410	11732.346	0.064
56	11713.700	11713.747	-0.047
57	11694.760	11694.817	-0.057
58	11675.500	11675.557	-0.057
59	11655.880	11655.968	-0.088
60	11636.000	11636.048	-0.048
61	11615.790	11615.799	-0.049
62	11595.140	11595.219	-0.079
63	11574.240	11574.310	-0.070
64	11553.010	11553.072	-0.062
65	11531.440	11531.504	-0.064
66	11509.510	11509.606	-0.096

APPENDIX 2—*Continued*

A 1 PI V= 0 - X 1 SIG V= 0 TRANSITION P(J) BRANCH

J	EXPT	CALC	EXPT-CALC
5	12233.360	12233.382	-0.022
6	12230.120	12230.142	-0.022
7	12226.730	12226.569	0.161
8	12222.620	12222.663	-0.043
9	12218.450	12218.425	0.025
10	12213.860	12213.853	0.007
11	12208.960	12208.949	0.011
12	12203.680	12203.712	-0.032
13	12198.100	12198.143	-0.043
14	12192.270	12192.241	0.029
15	12185.990	12186.007	-0.017
16	12179.460	12179.441	0.019
17	12172.500	12172.542	-0.042
18	12165.310	12165.311	-0.001
19	12157.670	12157.748	-0.078
20	12149.800	12149.853	-0.053
21	12141.630	12141.627	0.003
22	12133.060	12133.068	-0.008
23	12124.140	12124.178	-0.038
24	12114.930	12114.956	-0.026
25	12105.380	12105.403	-0.023
26	12095.470	12095.518	-0.048
27	12085.290	12085.302	-0.012
28	12074.740	12074.755	-0.015
29	12063.870	12063.877	-0.007
30	12052.640	12052.668	-0.028
31	12041.090	12041.128	-0.038
32	12029.260	12029.257	0.003
33	12016.910	12017.056	-0.146
34	12004.530	12004.524	0.006
35	11991.690	11991.662	0.028
36	11978.460	11978.470	-0.010
37	11964.920	11964.948	-0.028
38	11951.100	11951.096	0.004
39	11936.910	11936.914	-0.004
40	11922.420	11922.403	0.017
41	11907.540	11907.562	-0.022
42	11892.320	11892.393	-0.073
43	11876.910	11876.894	0.016
44	11861.030	11861.066	-0.036
45	11844.900	11844.910	-0.010
46	11828.450	11828.426	0.024
47	11811.600	11811.613	-0.013
48	11794.440	11794.473	-0.033
49	11776.990	11777.005	-0.015
50	11759.220	11759.210	0.010
51	11741.080	11741.089	-0.009
52	11722.620	11722.641	-0.021
53	11703.830	11703.867	-0.037
54	11684.710	11684.768	-0.058
55	11665.300	11665.345	-0.045
56	11645.560	11645.599	-0.039
58	11605.090	11605.141	-0.051
59	11584.390	11584.432	-0.042
60	11563.210	11563.407	-0.197
61	11542.050	11542.070	-0.020
62	11520.350	11520.425	-0.075

APPENDIX 2—*Continued*

A 1 PI V= 7 - X 1 SIG V= 0 TRANSITION R(J) BRANCH			
J	EXPT	CALC	EXPT-CALC
7	12949.530	12949.519	0.011
8	12948.010	12947.991	0.019
9	12946.070	12946.118	-0.048
10	12943.890	12943.900	-0.010
11	12941.350	12941.338	0.012
12	12938.410	12938.430	-0.020
13	12935.200	12935.177	0.023
14	12931.590	12931.580	0.010
15	12927.630	12927.637	-0.007
16	12923.340	12923.350	-0.010
17	12918.710	12918.717	-0.007
18	12913.730	12913.740	-0.010
19	12908.400	12908.417	-0.017
20	12902.730	12902.749	-0.019
21	12896.650	12896.737	-0.087
22	12890.410	12890.379	0.031
23	12883.670	12883.677	-0.007
24	12876.620	12876.630	-0.010
25	12869.220	12869.237	-0.017
26	12861.490	12861.500	-0.010
27	12853.420	12853.418	0.002
28	12844.990	12844.992	-0.002
29	12836.230	12836.220	0.010
30	12827.100	12827.104	-0.004
31	12817.640	12817.644	-0.004
32	12807.830	12807.839	-0.009
33	12797.700	12797.689	0.011
34	12787.190	12787.196	-0.006
35	12776.390	12776.358	0.032
36	12765.180	12765.176	0.004
37	12753.630	12753.651	-0.021
38	12741.790	12741.782	0.008
39	12729.570	12729.570	0.000
40	12717.040	12717.015	0.025
41	12704.110	12704.118	-0.008
42	12690.880	12690.879	0.001
43	12677.290	12677.299	-0.009
44	12663.390	12663.379	0.011
45	12649.190	12649.121	0.069
46	12634.550	12634.526	0.024
47	12619.620	12619.597	0.023
48	12604.360	12604.337	0.023
49	12588.760	12588.753	0.007
50	12572.830	12572.854	-0.024
51	12556.640	12556.656	0.004
52	12540.210	12540.189	0.021
53	12523.480	12523.513	-0.033
54	12506.700	12506.765	-0.065
55	12490.300	12490.295	0.005

APPENDIX 2—*Continued*

A 1 PI V= 7 - X 1 SIG V= 0 TRANSITION			Q(J) BRANCH
J	EXPT	CALC	EXPT-CALC
3	12947.270	12947.264	0.006
4	12945.890	12945.886	0.004
5	12944.190	12944.163	0.027
6	12942.120	12942.096	0.024
7	12939.680	12939.685	-0.005
8	12936.920	12936.929	-0.009
9	12933.840	12933.829	0.011
10	12930.410	12930.385	0.025
11	12926.620	12926.596	0.024
12	12922.390	12922.463	-0.073
13	12918.010	12917.985	0.025
14	12913.160	12913.163	-0.003
15	12907.980	12907.997	-0.017
16	12902.470	12902.487	-0.017
17	12896.650	12896.632	0.018
18	12890.410	12890.433	-0.023
19	12883.900	12883.890	0.010
20	12877.000	12877.003	-0.003
21	12869.730	12869.772	-0.042
22	12862.200	12862.197	0.003
23	12854.280	12854.277	0.003
24	12846.010	12846.014	-0.004
25	12837.410	12837.407	0.003
26	12828.460	12828.456	0.004
27	12819.180	12819.161	0.019
28	12809.510	12809.523	-0.013
29	12799.540	12799.541	-0.001
30	12789.230	12789.215	0.015
31	12778.570	12778.545	0.025
32	12767.530	12767.532	-0.002
33	12756.190	12756.176	0.014
34	12744.480	12744.476	0.004
35	12732.460	12732.432	0.028
36	12720.060	12720.046	0.014
37	12707.310	12707.316	-0.006
38	12694.250	12694.243	0.007
39	12680.820	12680.827	-0.007
40	12667.060	12667.067	-0.007
41	12652.950	12652.965	-0.015
42	12638.530	12638.520	0.010
43	12623.750	12623.732	0.018
44	12608.610	12608.601	0.009
45	12593.130	12593.128	0.002
46	12577.310	12577.311	-0.001
47	12561.160	12561.153	0.007
48	12544.630	12544.651	-0.021
49	12527.750	12527.807	-0.057
50	12510.580	12510.621	-0.041
51	12493.060	12493.092	-0.032
52	12475.220	12475.221	-0.001
53	12457.020	12457.008	0.012
55	12419.570	12419.553	0.017
56	12400.320	12400.312	0.008
57	12380.780	12380.758	0.022
58	12360.820	12360.802	0.018
59	12340.560	12340.532	0.028
60	12319.950	12319.919	0.031
61	12298.960	12298.962	-0.002
62	12277.670	12277.659	0.011
63	12256.040	12256.010	0.030
64	12234.040	12234.011	0.029
65	12211.660	12211.661	-0.001
66	12188.940	12188.951	-0.011
67	12165.820	12165.871	-0.051
68	12142.340	12142.398	-0.07
69	12118.460	12118.481	-0.021
70	12094.030	12094.002	0.028
71	12068.790	12068.703	0.087
72	12042.290	12042.315	-0.025

APPENDIX 2—*Continued*

A 1 PI V= 7 - X 1 SIG V= 0 TRANSITION P(J) BRANCH			
J	EXPT	CALC	EXPT-CALC
11	12913.160	12913.071	0.089
12	12907.720	12907.710	0.010
13	12901.980	12902.006	-0.026
14	12895.940	12895.957	-0.017
15	12889.560	12889.565	-0.005
16	12882.800	12882.829	-0.029
17	12875.700	12875.749	-0.049
18	12868.310	12868.327	-0.017
19	12860.530	12860.561	-0.031
20	12852.440	12852.451	-0.011
21	12844.000	12843.999	0.001
22	12835.190	12835.203	-0.013
23	12826.060	12826.065	-0.005
24	12816.540	12816.584	-0.044
25	12806.760	12806.760	-0.000
26	12796.580	12796.594	-0.014
27	12786.090	12786.085	0.005
28	12775.240	12775.234	0.006
29	12764.120	12764.040	0.080
30	12752.500	12752.505	-0.005
31	12740.630	12740.628	0.002
32	12728.410	12728.409	0.001
33	12715.860	12715.848	0.012
34	12702.940	12702.946	-0.006
35	12689.690	12689.703	-0.013
36	12676.090	12676.120	-0.030
37	12662.200	12662.195	0.005
38	12647.930	12647.930	0.000
39	12633.340	12633.325	0.015
40	12618.400	12618.380	0.020
41	12603.100	12603.096	0.004
42	12587.450	12587.472	-0.022
43	12571.510	12571.511	-0.001
44	12555.190	12555.212	-0.022
45	12538.610	12538.576	0.034
46	12521.640	12521.604	0.044
47	12504.250	12504.298	-0.048
48	12486.620	12486.660	-0.040
49	12468.660	12468.692	-0.032
51	12431.820	12431.785	0.035
52	12412.860	12412.862	-0.002
53	12393.640	12393.645	-0.005
54	12374.180	12374.164	0.016
55	12354.490	12354.478	0.012
56	12334.710	12334.727	-0.017
57	12315.270	12315.258	0.012

APPENDIX 2—*Continued*

A 1 PI V= 0 - X 1 SIG V= 1	TRANSITION	R(J)	BRANCH

J	EXPT	CALC	EXPT-CALC
4	12662.790	12662.795	-0.005
5	12662.330	12662.301	0.029
6	12661.480	12661.464	0.016
7	12660.290	12660.285	0.005
8	12658.750	12658.763	-0.013
9	12656.900	12656.899	0.001
11	12652.160	12652.142	0.018
12	12649.190	12649.249	-0.059
13	12646.010	12646.014	-0.004
14	12642.440	12642.436	0.004
15	12638.530	12638.515	0.015
16	12634.260	12634.252	0.008
17	12629.650	12629.646	0.004
18	12624.720	12624.697	0.023
19	12619.410	12619.406	0.004
20	12613.800	12613.773	0.027
21	12607.770	12607.797	-0.027
22	12601.510	12601.479	0.031
23	12594.810	12594.820	-0.010
24	12587.810	12587.818	-0.008
25	12580.480	12580.475	0.005
26	12572.830	12572.790	0.040
27	12564.770	12564.765	0.005
28	12556.390	12556.399	-0.009
29	12547.680	12547.694	-0.014
30	12538.610	12538.649	-0.039
31	12529.220	12529.268	-0.048
32	12519.500	12519.550	-0.050
33	12509.300	12509.499	-0.199
34	12499.080	12499.119	-0.039
35	12488.390	12488.414	-0.024
36	12477.370	12477.395	-0.025
37	12466.080	12466.079	0.001
38	12454.550	12454.496	0.054
39	12442.780	12442.713	0.067
40	12430.890	12430.882	0.008
41	12419.370	12419.380	-0.010
42	12397.730	12397.766	-0.036
43	12386.130	12386.129	0.001
44	12373.200	12373.177	0.023
45	12359.450	12359.441	0.009
46	12345.180	12345.155	0.025
47	12330.450	12330.416	0.034
48	12315.270	12315.266	0.004
49	12299.740	12299.724	0.016
50	12283.820	12283.794	0.026
51	12267.480	12267.472	0.008
52	12250.770	12250.735	0.035
53	12233.560	12233.533	0.027
54	12215.730	12215.754	-0.024
55	12197.160	12197.213	-0.053

APPENDIX 2—*Continued*

A 1 PI V= 0 - X 1 SIG V= 1 TRANSITION Q(J) BRANCH

J	EXPT	CALC	EXPT-CALC
4	12656.730	12656.702	0.028
5	12654.990	12654.990	-0.000
6	12652.950	12652.936	0.014
7	12650.550	12650.539	0.011
8	12647.800	12647.800	-0.000
9	12644.720	12644.719	0.001
10	12641.280	12641.296	-0.016
11	12637.540	12637.530	0.010
12	12633.430	12633.422	0.008
13	12628.970	12628.971	-0.001
14	12624.160	12624.179	-0.019
15	12619.040	12619.044	-0.004
16	12613.570	12613.567	0.003
17	12607.770	12607.748	0.022
18	12601.590	12601.586	0.004
19	12595.080	12595.083	-0.003
20	12588.230	12588.237	-0.007
21	12581.040	12581.050	-0.010
22	12573.500	12573.520	-0.020
23	12565.640	12565.649	-0.009
24	12557.420	12557.435	-0.015
25	12548.850	12548.880	-0.030
26	12539.940	12539.983	-0.043
27	12530.680	12530.744	-0.064
28	12521.120	12521.163	-0.043
29	12511.180	12511.240	-0.060
30	12500.910	12500.975	-0.065
31	12490.300	12490.369	-0.069
32	12479.370	12479.421	-0.051
33	12468.160	12468.131	0.029
34	12456.500	12456.500	0.000
35	12444.560	12444.527	0.033
36	12432.210	12432.212	-0.002
37	12419.570	12419.555	0.015
38	12406.550	12406.557	-0.007
39	12393.200	12393.216	-0.016
40	12379.520	12379.534	-0.014
41	12365.500	12365.509	-0.009
42	12351.140	12351.142	-0.002
43	12336.440	12336.433	0.007
44	12321.390	12321.379	0.011
45	12305.990	12305.983	0.007
46	12290.250	12290.241	0.009
47	12274.160	12274.152	0.008
48	12257.740	12257.716	0.024
49	12240.940	12240.907	0.033
50	12223.800	12223.780	0.020
51	12206.290	12206.267	0.023
52	12188.380	12188.367	0.013
53	12170.050	12170.046	0.004
54	12151.240	12151.230	0.010
55	12131.820	12131.779	0.041
55	12136.930	12136.922	0.008
56	12111.570	12111.531	0.039
56	12116.780	12116.708	0.072
57	12090.480	12090.470	0.010
57	12096.640	12096.589	0.051
58	12068.790	12068.745	0.045
58	12076.420	12076.418	0.002
59	12046.500	12046.490	0.010
59	12055.920	12056.062	-0.142
60	12035.460	12035.449	0.011
61	12014.560	12014.543	0.017
62	11993.330	11993.325	0.005
64	11949.940	11949.922	0.018
65	11927.700	11927.728	-0.028
68	11859.180	11859.147	0.033

APPENDIX 2—*Continued*

A 1 PI V= 8 - X 1 SIG V= 1	TRANSITION	P(J)	BRANCH

J	EXPT	CALC	EXPT-CALC
6	12645.780	12645.625	0.155
7	12642.000	12642.010	-0.010
9	12633.750	12633.755	-0.005
10	12629.120	12629.115	0.005
11	12624.160	12624.133	0.027
12	12618.810	12618.809	0.001
13	12613.170	12613.144	0.026
14	12607.160	12607.137	0.023
15	12600.810	12600.788	0.022
16	12594.090	12594.099	-0.009
17	12587.080	12587.068	0.012
18	12579.690	12579.696	-0.006
19	12571.970	12571.984	-0.014
20	12563.920	12563.930	-0.010
21	12555.520	12555.536	-0.016
22	12546.770	12546.801	-0.031
23	12537.680	12537.727	-0.047
24	12528.250	12528.312	-0.062
25	12518.510	12518.557	-0.047
26	12508.550	12508.463	0.087
27	12498.000	12498.030	-0.030
28	12487.230	12487.258	-0.028
29	12476.100	12476.148	-0.048
30	12464.640	12464.701	-0.061
31	12453.000	12452.916	0.084
32	12440.840	12440.796	0.044
33	12428.380	12428.341	0.039
34	12415.570	12415.553	0.017
35	12402.430	12402.435	-0.005
36	12389.000	12388.991	0.009
37	12375.210	12375.226	-0.016
38	12361.160	12361.151	0.009
39	12346.790	12346.781	0.009
40	12332.160	12332.149	0.011
41	12317.350	12317.320	0.030
42	12302.440	12302.448	-0.008
43	12287.880	12287.908	-0.028
44	12263.220	12263.261	-0.041
45	12248.630	12248.595	0.035
46	12232.640	12232.618	0.022
47	12215.890	12215.860	0.030
48	12198.570	12198.558	0.012
49	12180.820	12180.807	0.013
50	12162.660	12162.650	0.010
51	12144.080	12144.106	-0.026
52	12125.180	12125.179	0.001
53	12105.820	12105.864	-0.044
54	12086.110	12086.139	-0.029
55	12065.820	12065.955	-0.135
56	12045.140	12045.199	-0.059
57	12023.590	12023.686	-0.096

APPENDIX 2—*Continued*

A 1 PI V= Y - X 1 SIG V= 1 TRANSITION R(J) BRANCH

J	EXPT	CALC	EXPT-CALC
18	13307.820	13307.813	0.007
19	13303.390	13303.406	-0.016
20	13298.090	13298.091	-0.001
21	13292.120	13292.142	-0.022
22	13285.700	13285.710	-0.010
23	13278.890	13278.858	0.032
24	13271.640	13271.612	0.028
25	13263.970	13263.986	-0.016
26	13256.000	13255.983	0.017
27	13247.660	13247.605	0.055
28	13238.860	13238.847	0.013
29	13229.690	13229.701	-0.011
30	13220.150	13220.144	0.006
31	13210.160	13210.138	0.022
32	13199.630	13199.609	0.021
32	13203.410	13203.337	0.073
33	13188.470	13188.465	0.005
33	13192.210	13192.106	0.104
34	13180.830	13180.777	0.053
34	13176.600	13176.669	-0.069
35	13169.300	13169.290	0.010
36	13157.590	13157.566	0.024
37	13145.530	13145.553	-0.023
38	13133.240	13133.224	0.016
39	13120.560	13120.564	-0.004
40	13107.530	13107.564	-0.034
41	13094.230	13094.220	0.010
42	13080.540	13080.529	0.011
43	13066.500	13066.489	0.011
44	13052.120	13052.099	0.021
45	13037.380	13037.359	0.021
46	13022.260	13022.267	-0.007
47	13006.860	13006.823	0.037
48	12991.060	12991.028	0.032
49	12974.890	12974.880	0.010
50	12958.380	12958.380	-0.000
51	12941.560	12941.528	0.032
52	12924.330	12924.323	0.007
53	12906.760	12906.766	-0.006
54	12888.830	12888.856	-0.026
55	12870.610	12870.594	0.016
56	12851.990	12851.979	0.011
57	12833.010	12833.012	-0.002
58	12813.680	12813.693	-0.013
59	12793.990	12794.022	-0.032
60	12773.960	12773.998	-0.038
61	12753.630	12753.622	0.008

APPENDIX 2—*Continued*

A 1 PI V= Y - X 1 SIG V= 1 TRANSITION Q(J) BRANCH

J	EXPT	CALC	EXPT-CALC
5	13343.130	13343.107	0.023
6	13341.020	13340.984	0.036
7	13338.480	13338.506	-0.026
8	13335.670	13335.674	-0.004
9	13332.480	13332.488	-0.008
10	13328.930	13328.948	-0.018
11	13325.070	13325.054	0.016
12	13320.770	13320.806	-0.036
13	13316.170	13316.204	-0.034
14	13311.250	13311.248	0.002
15	13305.930	13305.938	-0.008
16	13300.280	13300.273	0.007
17	13294.270	13294.255	0.015
18	13287.860	13287.881	-0.021
19	13281.140	13281.154	-0.014
20	13274.070	13274.071	-0.001
21	13266.630	13266.633	-0.003
22	13258.870	13258.840	0.030
23	13250.710	13250.691	0.019
24	13242.220	13242.184	0.036
25	13233.350	13233.320	0.030
26	13224.120	13224.095	0.025
27	13214.540	13214.507	0.033
28	13204.590	13204.552	0.038
29	13194.250	13194.222	0.028
30	13183.550	13183.502	0.048
31	13172.420	13172.366	0.054
32	13160.860	13160.766	0.094
32	13164.880	13164.899	-0.019
33	13148.770	13148.622	0.148
33	13152.280	13152.342	-0.062
34	13139.610	13139.663	-0.053
35	13126.800	13126.867	-0.067
36	13113.840	13113.886	-0.046
37	13100.610	13100.652	-0.042
38	13087.090	13087.122	-0.032
39	13073.250	13073.274	-0.024
40	13059.060	13059.094	-0.034
41	13044.560	13044.577	-0.017
42	13029.710	13029.718	-0.008

APPENDIX 2—*Continued*

A 1 PI Vm 9 - X 1 SIG Vm 1 TRANSITION Q(J) BRANCH

J	EXPT	CALC	EXPT-CALC
43	13014.520	13014.513	0.007
45	12983.080	12983.064	0.016
46	12966.820	12966.818	0.002
47	12950.220	12950.222	-0.002
48	12933.310	12933.278	0.032
49	12916.000	12915.984	0.016
50	12898.350	12898.341	0.009
51	12880.340	12880.348	-0.012
52	12862.010	12862.005	0.005
53	12843.350	12843.313	0.037
54	12824.290	12824.271	0.019
55	12804.800	12804.880	-0.080
56	12785.130	12785.139	-0.009
57	12765.070	12765.049	0.021
58	12744.620	12744.609	0.011
59	12723.870	12723.820	0.050
60	12702.710	12702.681	0.029
61	12681.190	12681.194	-0.004
62	12659.360	12659.357	0.003
63	12637.180	12637.172	0.008
64	12614.650	12614.638	0.012
65	12591.750	12591.755	-0.005
66	12568.520	12568.523	-0.003
67	12544.900	12544.943	-0.043
68	12520.970	12521.015	-0.045
69	12496.720	12496.738	-0.018
70	12472.070	12472.113	-0.043
73	12396.120	12396.149	-0.029
74	12370.120	12370.131	-0.011
75	12343.770	12343.766	0.004
76	12317.060	12317.052	0.008
77	12290.010	12289.991	0.019
78	12262.550	12262.582	-0.032
79	12234.780	12234.825	-0.045
80	12206.740	12206.719	0.021
81	12178.290	12178.265	0.025
82	12149.360	12149.463	-0.103
84	12090.860	12090.811	0.049
85	12060.950	12060.960	-0.010

APPENDIX 2—*Continued*

A 1 PI V= 9 - X 1 SIG V= 1	TRANSITION	P(J)	BRANCH

J	EXPT	CALC	EXPT-CALC
20	13247.020	13247.046	-0.026
21	13239.520	13239.535	-0.015
22	13231.110	13231.120	-0.010
23	13222.070	13222.072	-0.002
24	13212.530	13212.542	-0.012
25	13202.570	13202.595	-0.025
26	13192.210	13192.258	-0.048
27	13181.490	13181.541	-0.051
28	13170.400	13170.451	-0.051
29	13158.950	13158.989	-0.039
30	13147.130	13147.149	-0.019
31	13134.920	13134.923	-0.003
32	13122.250	13122.290	-0.040
33	13109.200	13109.211	-0.011
34	13095.630	13095.612	0.018
35	13081.400	13081.401	-0.001
36	13099.380	13099.339	0.041
35	13085.160	13085.042	0.118
36	13066.500	13066.542	-0.042
36	13070.680	13070.649	0.031
37	13056.110	13056.102	0.008
38	13041.330	13041.321	0.009
39	13026.270	13026.256	0.014
40	13010.890	13010.877	0.013
42	12979.140	12979.130	0.010
43	12962.850	12962.748	0.102
44	12946.070	12946.023	0.047
45	12929.010	12928.954	0.056
46	12911.560	12911.539	0.021
47	12893.800	12893.778	0.022
48	12875.700	12875.670	0.030
49	12857.240	12857.215	0.025
50	12838.390	12838.412	-0.022
51	12819.180	12819.262	-0.082
52	12799.750	12799.764	-0.014
53	12779.880	12779.919	-0.039
54	12759.730	12759.727	0.003
55	12739.190	12739.187	0.003
56	12718.330	12718.301	0.029
57	12697.050	12697.067	-0.017
58	12675.430	12675.486	-0.056
59	12653.540	12653.558	-0.018
60	12631.260	12631.283	-0.023
61	12608.610	12608.662	-0.052
62	12585.720	12585.695	0.025

APPENDIX 2—*Continued*

A 1 PI V=1U - X 1 SIG V= 2 TRANSITION R(J) BRANCH

J	EXPT	CALC	EXPT-CALC
10	13048.880	13048.862	0.018
11	13046.190	13046.187	0.003
13	13039.770	13039.779	-0.009
14	13036.040	13036.047	-0.007
16	13027.620	13027.527	0.093
17	13022.750	13022.738	0.012
18	13017.590	13017.598	-0.008
19	13012.130	13012.105	0.025
22	12993.540	12993.514	0.026
23	12986.600	12986.613	-0.013
24	12979.380	12979.359	0.021
25	12971.760	12971.754	0.006
26	12963.780	12963.796	-0.016
27	12955.480	12955.487	-0.007
28	12946.840	12946.825	0.015
29	12937.770	12937.812	-0.042
30	12928.470	12928.447	0.023
31	12918.710	12918.729	-0.019
32	12908.660	12908.660	-0.000
33	12898.170	12898.240	-0.070
34	12887.430	12887.467	-0.037
36	12864.880	12864.867	0.013
37	12853.050	12853.039	0.011
38	12840.850	12840.860	-0.010
39	12828.330	12828.329	0.001
40	12815.430	12815.447	-0.017
41	12802.230	12802.213	0.017
42	12788.620	12788.628	-0.008
43	12774.700	12774.692	0.008
44	12760.410	12760.404	0.006
45	12745.790	12745.765	0.025
46	12730.780	12730.775	0.005
47	12715.440	12715.434	0.006
48	12699.740	12699.741	-0.001
49	12683.760	12683.698	0.062
50	12667.280	12667.304	-0.024
51	12650.550	12650.559	-0.009
52	12633.430	12633.463	-0.033
53	12616.030	12616.016	0.014
54	12598.220	12598.218	0.002
55	12580.060	12580.070	-0.010
56	12561.560	12561.571	-0.011
57	12542.670	12542.721	-0.051
58	12523.480	12523.521	-0.041
59	12503.930	12503.970	-0.040
60	12484.020	12484.068	-0.048
63	12422.280	12422.261	0.019
64	12400.940	12400.957	-0.017
65	12379.320	12379.302	0.018
66	12357.280	12357.297	-0.017
67	12334.900	12334.941	-0.041
69	12289.220	12289.175	0.045
70	12265.770	12265.766	0.004
71	12242.040	12242.004	0.036
72	12217.930	12217.891	0.039

APPENDIX 2—*Continued*

A 1 PI V=10 - X 1 SIG V= 2 TRANSITION Q(J) BRANCH

J	EXPT	CALC	EXPT-CALC
4	13051.530	13051.548	-0.018
5	13049.900	13049.793	0.107
6	13047.770	13047.687	0.083
7	13045.210	13045.229	-0.019
9	13039.200	13039.260	-0.060
10	13035.740	13035.749	-0.009
11	13031.910	13031.887	0.023
12	13027.620	13027.674	-0.054
13	13023.100	13023.109	-0.009
14	13018.190	13018.194	-0.004
15	13012.920	13012.927	-0.007
16	13007.290	13007.309	-0.019
18	12994.990	12995.019	-0.029
19	12988.340	12988.348	-0.008
20	12981.310	12981.325	-0.015
21	12973.950	12973.952	-0.002
22	12966.230	12966.228	0.002
23	12958.140	12958.152	-0.012
24	12949.730	12949.726	0.004
25	12940.940	12940.949	-0.011
26	12931.840	12931.821	0.019
27	12922.390	12922.343	0.047
28	12912.510	12912.514	-0.004
29	12902.330	12902.334	-0.004
30	12891.800	12891.804	-0.004
31	12880.940	12880.924	0.016
32	12869.730	12869.693	0.037
33	12858.110	12858.112	-0.002
34	12846.180	12846.181	-0.001
35	12833.910	12833.900	0.010
36	12821.270	12821.269	0.001
37	12808.280	12808.288	-0.008
38	12794.960	12794.957	0.003
39	12781.280	12781.276	0.004
40	12767.250	12767.246	0.004
41	12752.870	12752.867	0.003
42	12738.130	12738.138	-0.008
43	12723.070	12723.059	0.011
44	12707.630	12707.632	-0.002
45	12691.850	12691.855	-0.005

APPENDIX 2—*Continued*

A 1 PI V=10 - X 1 SIG V= 2 TRANSITION Q(J) BRANCH			
J	EXPT	CALC	EXPT-CALC
46	12675.710	12675.730	-0.020
47	12659.260	12659.255	0.005
48	12642.440	12642.432	0.008
49	12625.270	12625.260	0.010
50	12607.770	12607.739	0.031
51	12589.870	12589.870	-0.000
52	12571.650	12571.653	-0.003
53	12553.060	12553.087	-0.027
54	12534.120	12534.173	-0.053
55	12514.870	12514.912	-0.042
56	12495.270	12495.302	-0.032
57	12475.300	12475.344	-0.044
59	12434.390	12434.385	0.005
60	12413.400	12413.384	0.016
61	12392.030	12392.035	-0.005
62	12370.360	12370.339	0.021
63	12348.300	12348.295	0.005
64	12325.920	12325.904	0.016
65	12303.160	12303.165	-0.005
66	12280.120	12280.079	0.041
67	12256.690	12256.645	0.045
68	12232.890	12232.864	0.026
69	12208.750	12208.735	0.015
70	12184.260	12184.258	0.002
71	12159.520	12159.434	0.086
72	12134.250	12134.261	-0.011
73	12108.700	12108.734	-0.034
74	12082.710	12082.863	-0.153
75	12056.640	12056.643	-0.003
76	12030.070	12030.073	-0.003
77	12003.020	12003.152	-0.132

APPENDIX 2—*Continued*

A 1 PI V=10 - X 1 SIG V= 2 TRANSITION P(J) BRANCH

J	EXPT	CALC	EXPT-CALC
7	13036.890	13036.841	0.049
9	13028.460	13028.473	-0.013
10	13023.700	13023.762	-0.062
11	13018.620	13018.700	-0.080
12	13013.320	13013.287	0.033
13	13007.530	13007.522	0.008
15	12994.990	12994.941	0.049
16	12988.160	12988.124	0.036
17	12980.940	12980.957	-0.017
19	12965.590	12965.570	0.020
20	12957.340	12957.351	-0.011
21	12948.800	12948.782	0.018
22	12939.850	12939.863	-0.013
23	12930.610	12930.593	0.017
24	12920.990	12920.974	0.016
25	12911.010	12911.004	0.006
26	12900.690	12900.685	0.005
27	12890.000	12890.017	-0.017
28	12879.000	12878.999	0.001
29	12867.620	12867.631	-0.011
30	12855.920	12855.914	0.006
31	12843.860	12843.849	0.011
32	12831.450	12831.434	0.016
33	12818.670	12818.670	-0.000
34	12805.570	12805.558	0.012
35	12792.120	12792.097	0.023
36	12778.320	12778.287	0.033
37	12764.120	12764.129	-0.009
38	12749.620	12749.624	-0.004
39	12734.770	12734.770	0.000
40	12719.610	12719.568	0.042
41	12704.110	12704.018	0.092
42	12688.110	12688.121	-0.011
43	12671.860	12671.876	-0.016
44	12655.280	12655.284	-0.004
45	12638.360	12638.345	0.015
46	12621.070	12621.059	0.011
47	12603.440	12603.426	0.014
48	12585.470	12585.446	0.024
49	12567.120	12567.120	0.000
50	12548.410	12548.447	-0.037
51	12529.400	12529.428	-0.028
52	12510.010	12510.063	-0.053
53	12490.300	12490.352	-0.052
54	12470.310	12470.295	0.015
56	12429.170	12429.145	0.025
57	12408.020	12408.051	-0.031
58	12386.620	12386.612	0.008
59	12364.820	12364.829	-0.009
60	12342.540	12342.700	-0.160
61	12320.250	12320.226	0.024
62	12297.450	12297.407	0.043
63	12274.160	12274.244	-0.084
64	12250.770	12250.737	0.033
67	12178.150	12178.147	0.003
68	12153.250	12153.261	-0.011
69	12127.970	12128.031	-0.061

APPENDIX 2—*Continued*

A 1 PI V=11 - X 1 SIG V= 2 TRANSITION R(J) BRANCH			
J	EXPT	CALC	EXPT-CALC
30	13594.660	13594.668	-0.008
31	13584.650	13584.594	0.056
32	13574.160	13574.155	0.005
33	13563.310	13563.354	-0.044
34	13552.170	13552.189	-0.019
35	13540.640	13540.660	-0.020
36	13528.730	13528.768	-0.038
37	13516.470	13516.512	-0.042
38	13503.850	13503.892	-0.042
39	13490.850	13490.909	-0.059
40	13477.530	13477.562	-0.032
41	13463.830	13463.851	-0.021
42	13449.720	13449.776	-0.056
43	13435.300	13435.336	-0.036
44	13420.490	13420.533	-0.043
45	13405.400	13405.365	0.035
46	13389.800	13389.832	-0.032
47	13373.880	13373.935	-0.055
48	13357.660	13357.672	-0.012
49	13341.020	13341.044	-0.024
50	13324.090	13324.051	0.039
51	13306.750	13306.691	0.059
53	13270.890	13270.870	0.020
54	13252.440	13252.408	0.032
55	13233.640	13233.577	0.063
56	13214.540	13214.377	0.163
57	13194.810	13194.805	0.005
58	13174.860	13174.851	0.008
59	13154.520	13154.532	-0.012

APPENDIX 2—*Continued*

A 1 PI V=11 - X 1 SIG V= 2 TRANSITION			Q(J) BRANCH
J	EXPT	CALC	EXPT-CALC
27	13589.880	13589.832	0.048
28	13579.720	13579.690	0.030
29	13569.180	13569.186	-0.006
30	13558.310	13558.321	-0.011
31	13547.060	13547.093	-0.033
32	13535.500	13535.504	-0.004
33	13523.530	13523.553	-0.023
34	13511.260	13511.241	0.019
35	13498.560	13498.566	-0.006
36	13485.510	13485.530	-0.020
37	13472.120	13472.132	-0.012
38	13458.360	13458.373	-0.013
39	13444.200	13444.251	-0.051
40	13429.750	13429.768	-0.018
41	13414.920	13414.923	-0.003
42	13399.710	13399.717	-0.007
43	13384.120	13384.148	-0.028
44	13368.200	13368.217	-0.017
45	13351.950	13351.925	0.025
46	13335.290	13335.270	0.020
47	13318.300	13318.253	0.047
48	13300.920	13300.873	0.047
49	13283.160	13283.131	0.029
50	13265.070	13265.025	0.045
51	13246.610	13246.556	0.054
52	13227.710	13227.724	-0.014
53	13208.540	13208.527	0.013
54	13188.980	13188.966	0.014
55	13169.050	13169.040	0.010
56	13148.770	13148.747	0.023
57	13128.090	13128.087	0.003
58	13107.060	13107.050	0.009
59	13085.650	13085.652	-0.002
60	13063.870	13063.883	-0.013
61	13041.660	13041.741	-0.081
62	13019.080	13019.224	-0.144

APPENDIX 2—*Continued*

A 1 PI V=11 - X 1 SIG V= 2 TRANSITION P(J) BRANCH			
J	EXPT	CALC	EXPT-CALC
23	13599.600	13599.517	0.083
24	13589.880	13589.643	0.237
26	13568.860	13568.811	0.049
27	13557.870	13557.854	0.016
28	13546.580	13546.535	0.045
29	13534.900	13534.856	0.044
30	13522.810	13522.817	-0.007
31	13510.410	13510.417	-0.007
32	13497.680	13497.656	0.024
33	13484.520	13484.535	-0.015
34	13471.050	13471.053	-0.003
35	13457.230	13457.212	0.018
36	13443.010	13443.010	0.000
37	13428.450	13428.448	0.002
38	13413.510	13413.526	-0.016
39	13398.240	13398.243	-0.003
40	13382.610	13382.601	0.009
41	13366.610	13366.599	0.011
42	13350.300	13350.237	0.063
43	13333.740	13333.515	0.225
44	13316.430	13316.433	-0.003
45	13299.000	13298.991	0.009
46	13281.140	13281.189	-0.049
47	13263.010	13263.027	-0.017
48	13244.540	13244.505	0.035

RESUME

Ce travail présente quelques applications des méthodes de calcul de la chimie quantique à la spectroscopie moléculaire et se compose de trois parties.

La première est l'étude des perturbations observées dans le système $A^1\Pi - X^1\Sigma^+$ de la molécule BeS. Les calculs ab-initio des fonctions d'onde des états mis en jeu, des paramètres de perturbation (spin-orbite et coriolis) ont été une aide essentielle dans l'interprétation des données expérimentales et ont permis de conclure que les perturbations étaient dues à un état $^3\Pi$ de même configuration que l'état $A^1\Pi$.

La seconde partie concerne la molécule C_2 et présente la détermination ab-initio des paramètres nécessaires à l'établissement du bilan des divers processus radiatifs susceptibles d'affecter les populations rotationnelles de l'état fondamental $X^1\Sigma_g^+$:

- photodissociation
- cascades quadrupolaires et forces d'oscillateur
- transitions d'intercombinaison $X^1\Sigma_g^+ - a^3\Pi_u$

Enfin la dernière partie est l'étude des transferts d'énergie dans les plus bas états électroniques de la molécule MgO ($X^1\Sigma^+$, $a^3\Pi$ et $A^1\Pi$) par collision avec N_2O. Cette étude est basée sur le couplage dipole-dipole entre les moments de transition de MgO et le moment dipolaire permanent de la cible N_2O.

MOTS CLES

- Molécule Diatomique
- Couplage spin-orbite
- Force oscillateur
- Photodissociation
- Moment transition
- Interaction intermoléculaire
- Interaction dipolaire (couplage dipolaire)